Interaction between the Alzheimer's peptide, beta-amyloid and lipid membrane

Rahul Saurabh

M.Res (Medicine)

Submitted in accordance with the requirements for the degree of

PhD (Medicinal Chemistry)

Department of Chemistry

University of Hull

March 2015

Risk Assessment

All experiments were carried out in accordance with the University of Hull's Health and Safety guidelines. A full COSHH and risk assessment was carried out for each new experiment, signed by the undertaking student, supervisor, Dr Mark Lorch and the departmental safety officer (Dr T. McCreedy) before any practical work started. The COSHH forms carry the reference numbers RSML01-RSML06.

Acknowledgements

I would like to thank my supervisors Prof. Mark Lorch and Prof S. J. Archibald, for giving me the opportunity to work on this project.

My sincere thanks go to Prof. Mark Lorch for his friendly guidance, encouragement and advice during my study. I would like to thanks Prof. S. J. Archibald for his advice and helpful suggestions.

I am very grateful to my colleagues and staff and students of biomedical science and medicinal chemistry for their assistance, friendship and help.

Most importantly, I would like to give my heartiest thanks to my sisters (Swati Verma, Shweta Suman), family (Ritul Priya, Ritwik Rishu, Rishit Ranjan, Keertika Kanchan, Kanishka Kanchan), laws (Kuldeep Kumar, Kanchan Saxena), uncle (Dhaneshwar Jha), and friends (Yasir Alnaam, Saeed Alqarni, Othamn Alfahad, Jari Algethani, Hamza Alshehari, Mohammad Algamdi) for their love, support, advice and encouragement. Last of all I would like to thanks my beloved wife (Kanika Kanchan), whose encouragement, advice and support has proved invaluable throughout my thesis writing.

This thesis is dedicated to my

Father (Papa ji) and mother (Maa)

Sushil Kumar Verma and Sudha Shrivastwa

Abstract

Alzheimer's disease (AD) is a neurodegenerative disorder. The patho-physiological effects of amyloid beta (Aβ) may be mediated by Aβ-membrane interaction. However, the molecular mechanism of interaction between Aβ and neuronal membrane remains unknown. The aim of the study was to investigate the interaction of a toxic fragment of amyloid beta, $A\beta_{25-35}$ with the lipid membrane model using model lipid bilayers and beta breaker peptide, KLVFF.

Liquid ^{1}H NMR assay was used to investigate the aggregation properties of $A\beta_{25-35}$. The sharp NMR peaks of $A\beta_{25-35}$ appeared immediately after sample preparation and these peaks were lost after 24 hrs incubation. However, on addition of KLVFF to $A\beta_{25-35}$, the amyloid peptide peaks remain unchanged even after long period of incubation. The data suggest that KLVFF has ability to inhibit the aggregation of $A\beta_{25-35}$.

Magic angle spinning solid state NMR were used to investigate the location and interaction of $A\beta_{25-35}$ to lipid bilayers. NOESY cross-relaxation rates suggest that the soluble form of $A\beta_{25-35}$ may interact predominantly with the lipid chains near glycerol region. The cholesterol molecules did not exhibit direct interaction with soluble $A\beta_{25-35}$. However, cross relaxation rate data suggest that cholesterol may push the soluble $A\beta_{25-35}$ towards the head region of lipid bilayers. The data indicates that soluble form of $A\beta_{25-35}$ may enter into lipid bilayers and interact with phospholipids.

^{2}H NMR was used to analyse the effect of $A\beta_{25-35}$ on lipid phase behaviour. M_1 analysis and methyl splitting data were used to observe the phase transitions. $A\beta_{25-35}$ lowers the lipid phase transitions temperature in presence and absence of cholesterol. The data suggest that the insoluble form of $A\beta_{25-35}$ may develop the lipid order (stiffness) and thus lowers the phase transition temperature. The $A\beta_{25-35}$ plus KLVFF with cholesterol may also significantly raise the phase transition temperature and also elongate the phase transition boundaries, indicating that cholesterol molecules may enhance the lipid order parameter.

In conclusion, KLVFF may stop the amyloid beta aggregation either in solution or in the lipid bilayers. Cholesterol molecules may not interact directly with amyloid beta and it may also affect the location of amyloid beta in the lipid bilayers. The results of the study may be important to understand the interactions between Aβ and lipid bilayers which may act as new therapeutic strategies for the development of new drugs for amyloid diseases.

Contents

List of Figures

List of tables

Abbreviations

Aβ	Amyloid beta
$A\beta_2M$	β2-microglobulin
AANF	Artrial natriuretic factor
AD	Alzheimer's disease
ADAM	A disintegrin and metalloproteinase
ADC	Analogue to digital converter
AFM	Atomic force microscopy
APF	Annular protofibril
APP	Amyloid precursor protein
APrP	Prion protein
ATTR	Transthyretin
BACE	Beta-site APP cleaving enzyme
BBB	Blood brain barrier
BSE	Bovine spongiform encephalopathies
CCPN	Collaborative computing project for NMR
CD	Circular dichroism spectroscopy
COSY	Correlation spectroscopy
CTM	central terminal methyl
DAG	Diacylglycerol
DCM	Dichloromethane
DIG	Detergent-insoluble glycolipid-rich domain
DIPEA	N, N-Diisopropylethylamine
DMF	Dimethylformamide
DMPC	1, 2- dimyristoylphosphatidylcholine
DMSO	Dimethyl sulfoxide
DOPC	1, 2-dioleoyl-*sn*-glycero-3-phosphocholine
DSC	Differential scanning calorimetry
ECD	Electron-capture dissociation
EDTA	Ethylene diamine tetra acetic acid

EM	Electron microscopy
ESI	Electrospray ionisation
FAP	Familial amyloid polyneuropathy
FID	Free induction decay
FTIR	Fourier transform infrared spectroscopy
GUVs	Giant unilamellar vesicles
HFIP	Hexafluoroisopropyl alcohol
HTT	Huntingtin
IAPP	Islet amyloid polypeptide
IR	Infra-red
LUVs	Large unilamellar vesicles
MAS	Magic angle spinning
MRI	Magnetic resonance imaging
MTS	3-[(4,5-dimethylthiazol-2-yl)-5,3-carboxymethoxyphenyl]-2-(4-sulfophenyl)-2H tetrazolium salt
NFTs	Neurofibrillary tangles
NMR	Nuclear magnetic resonance
NOESY	Nuclear Overhauser effect spectroscopy
PC	Phosphatidylcholine
PE	Phosphatidylethanolamine
PEN-2	Persenilin enhancer-2
PFOs	Prefibrillary oligomers
PFT	Pore-forming bacterial toxins
PG	Phosphatidylglycerol
PI	Phosphatidylinositol
ppm	Parts per million
PS	Phosphatidylserine
PS1	Presenilin-1
PS2	Presenilin-2
Rf	Radio-frequency
sAPPα	Secreted amyloid precursor protein alpha
SDS	Sodium dodecyl sulfate

SM	Sphingomyelin
ssNMR	Solid state nuclear magnetic resonance
STEM	Scanning transmission electron microscopy
SUVs	Small unilamellar vesicles
TBL	Total brain lipid
TFA	Trifluoroacetic acid
TFE	Trifluoroethanol
TIS	Triisopropylsilane
TMS	Tetramethylsilane
TOCSY	Total correlation spectroscopy
TRIS	Tris (hydroxymethyl) aminomethane
VCD	Vibrational circular dischroism
XRD	X-ray fibre diffraction

Chapter 1
Introduction

1.1 Amyloid diseases

Amyloidosis is a diverse group of extracellular protein depositions or protein misfolding complications promoting neurodegenerative diseases (Alzheimer's disease, Huntington's disease and Parkinson's disease), autosomal disorders (familial amyloid polyneuropathy), dialysis-related amyloidosis and transmissible spongiform encephalopathies[1-4]. Numerous experimental studies from various biomedical branches, such as, molecular medicine, medicinal biophysics, medicinal biochemistry and neuropathology suggest that amyloidosis is generally recognized by the assembly of amyloid fibrils deposition on the extracellular surfaces[4-9]. The amyloid peptides and proteins form insoluble fibrils having almost common morphological features which are identified by electron and atomic force microscopy[11, 12]. Electron microscopic studies of amyloidogenic fibrils suggest that the fibrils are elongated, undivided and straight with an identical diameter (~10 nm)[4]. However, the pathogenesis of amyloidosis remains unknown [6-9].

Table1 List of some amyloid diseases[1]

Amyloid Proteins/ Peptides	Amyloid disease
Amyloid Beta (Aβ1-42/1-40)	Alzheimer's disease
Amylin	Diabetes types 2
Huntingtin (HTT)	Huntington's disease
α-synuclein	Parkinson's disease
Artrial natriuretic factor (AANF)	Cardiac arrhythmias
Prion protein (APrP)	Transmissible spongiform encephalopathy
β2-microglobulin ($A\beta_2M$)	Dialysis-related amyloidosis
Medin (AMed)	Aortic medial amyloid
Transthyretin (ATTR)	Familial amyloid polyneuropathy

Many experimental studies and hypothesis suggest that amyloid fibrils deposition may be responsible for more than one hundred amyloid diseases in human beings[4-6]; some of them are listed in Table 1. Hence, it is essential to know about the core structure of amyloid fibers to understand the mechanisms behind their formation and deposition on the outer surface of

tissues during amyloidosis. Amyloid fibrils are insoluble, non-crystalline and heterogeneous having high molecular weight[4]. Thus, it is not possible to determine their structures by common structural biochemistry or biophysical methods such as X-ray crystallography and liquid NMR[4, 10]. X-ray fiber diffraction is a useful alternative method to examine the structure of insoluble amyloid fibers[10-11]. X-ray fiber diffraction analysis of amyloid fibers suggest that amyloidogenic peptides assemble into a cross-β fibrillar pattern[4]. This amyloid fibrillar structural pattern is also supported by solid state nuclear magnetic resonance (SS-NMR), Fourier transform infrared spectroscopy (FTIR) and cryo-electron microscopy[12]. The formation and structure of amyloid fibrils are common in all amyloid diseases[12]. The underlying molecular mechanisms of amyloid peptides aggregation and fibrils formation from soluble peptides and their toxicity in amyloidosis are poorly understood[11]. Therefore, it is important to understand the inhibitory mechanism of amyloid fibril formation and aggregation. It is also important to understand the amyloid peptides interaction with lipid bilayers in amyloidosis, which may be a vital breakthrough to develop a new therapeutic strategy for amyloid diseases.

Amyloid beta causing Alzheimer's disease may be an excellent amyloidogenic peptide fragment model system to understand the mechanisms of amyloid aggregation, interactions with lipid bilayers, fibril formation and toxicity for many reasons: (a) aggregation and toxicity causing Aβ species are easily obtainable[13,14]; (b) amyloidogenic aggregation, fibrillation and toxicity can easily develop *in vivo* or *in vitro* from Aβ species[15]; (c) toxic fragments of Aβ may be very useful to collect significant structural data to understand amyloidosis[16-18].

1.2 Alzheimer's disease

Alzheimer's disease (AD) is a neurodegenerative disorder characterized by functional failure and death of neuronal cells[19]. The degeneration of neurons may cause mental abnormalities such as memory retardation and learning disabilities[19-21]. Neuronal degeneration is one of the leading causes of dementia, accounting for the mental deterioration around 50 to 60% of adults over 65 years[22]. Globally, about 44.35 million cases of dementia were reported in 2013 and it is predicted that AD will affect more than 65 million population by 2030[13, 23].

In healthy aging, the neuronal degeneration occurs slowly but in AD, neurons degenerate rapidly in the memory controlling parts of the brain, especially the hippocampus and cerebral cortex[24, 25]. The degeneration of neurons occur due to the fast damage of brain cells and synapses, assembly of amyloid plaques on the outer surface of neurons and deposition of

neurofibrillary tangles inside the neurons[26, 27]. The gradual degradation of neurons develop the symptoms of AD such as mental and behavioural irregularities including anger, violent behaviour and depression[26, 27].

In 1907, AD was first reported by a German psychiatrist and neuropathologist Dr. Alois Alzheimer during the treatment of a middle aged woman who had acute memory loss and linguistic problems[28], [29]. Dr. Alzheimer examined her postmortem brain using silver staining technique and observed the deposition of thick fibrillar materials throughout the cerebral cortex region[30]. Later these deposited materials were recognized as plaques and tangles[29, 30]. Further, several histopathological examinations of AD brains suggest that there are two main serious lesions; neurofibrillary tangles (NFTs) and neuritic plaques or senile plaques, which are responsible to cause AD[31] as shown in Figure 1.1.

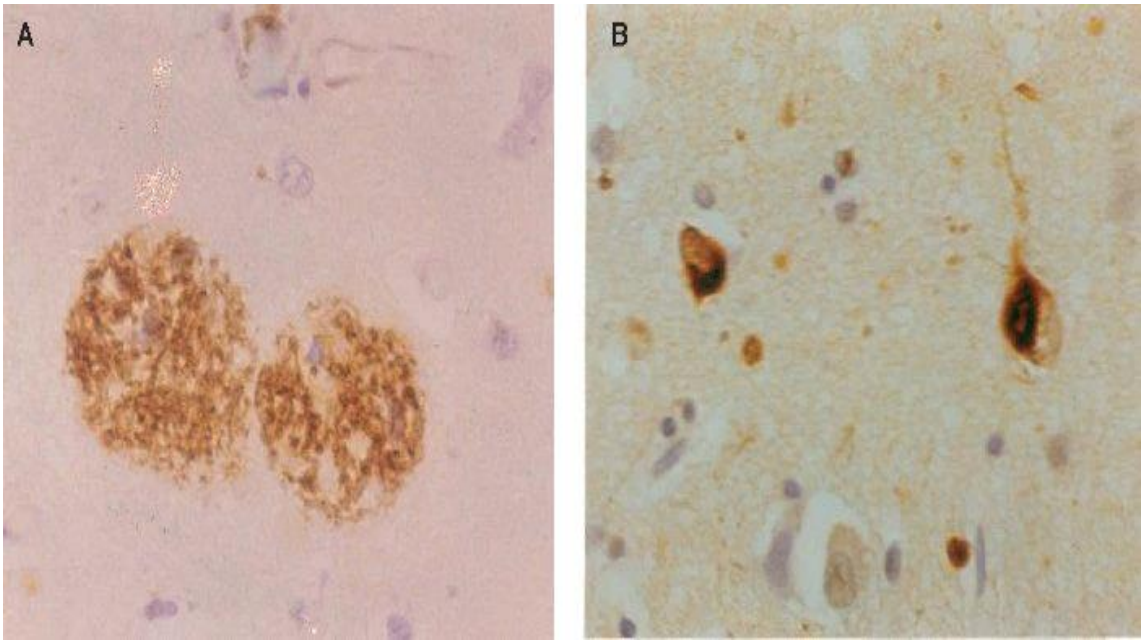

Figure 1.1 The cerebral cortex region of AD brain showing (A) neuritic plaques and (B) neurofibrillary tangles[34]. Neuritic plaques are extracellular deposition of Aβ and neurofibrillary tangles are inner deposition of microtubule-associated tau proteins of neuron and both are the main characteristics of AD.

NFTs are microtubule-associated tau proteins. Insoluble twisted fibrils of NFTs are found inside the neurons[32]. Generally, neurofibrillary tangles are not visible under traditional morphological stain such as hematoxylin (it forms hematein with metal ions, a strong colour

complexes, use to stain cellular nuclei)[31]. NFTs are observed using thioflavin S, as stain under the fluorescence microscope because it binds to the phosphorylated tau proteins[31]. Neuritic or senile plaques are assemblies of amyloid fibrils composed of beta-pleated sheet proteins, called amyloid beta (Aβ)[31]. Aβ is a small fragment of amyloid precursor protein. After aqueous contact, Aβ transforms from a soluble α helical structure into an insoluble fibrillar structure. Amyloid fibrils are dense structures deposited as cellular material outside and around the neurons[31, 33].

In the AD brain, the sulci (depression in brain surface) become enlarged. The gyri (ridge in the brain surface) also become broaden. These features are clearly observed through magnetic resonance imaging (MRI)[35-37] as shown in Figure 1.2. Clinton *et al.* (1993) explained the occupancy of amyloid peptides in the sulci and gyri of AD brain[38]. They reported that the distribution pattern of beta-amyloid in the frontal cortex gyri was different from frontal sulci[38]. MRI studies of AD brain also suggest that the volume of AD brains reduce in the hippocampus and cortex regions of the brain[39].

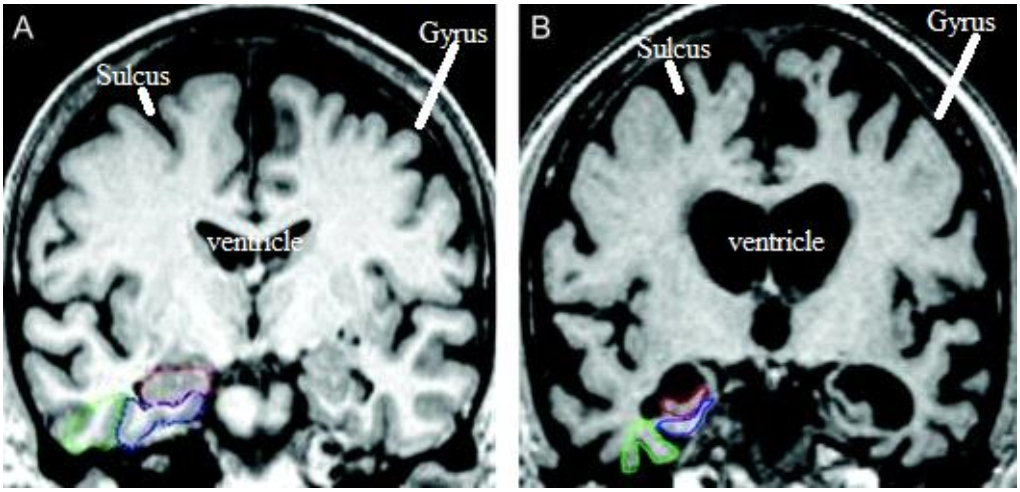

Figure 1.2 MRI comparing (A) normal and (B) Alzheimer's disease brain[37]. Enlarged sulcus and widened gyrus found in the AD brain. Ventricles are enlarged in AD brains. Hippocampus (red outline), Entorhinal cortex (blue outline) and Perirhinal cortex (green outline) are the memory centre reduced in size of AD brains[37].

1.3 Amyloid precursor protein

Amyloid beta peptide is composed of 39-43 amino acid residues, which is a part of type I trans-membrane glycoprotein, amyloid precursor protein (APP)[40, 41].The specific physiological role of APP is still unclear. However, recent studies suggest that the overexpression of APP promotes significant growth in transgenic mice[42]. The transfected cell line experiments suggest that APP may modulate cell growth and motility[43]. It is reported that APP can help in the progression of the neuronal and synaptic functions[44, 45]. The high expression of APP is found in the cortex frontal lobe of the human brain[46]. APP has mainly two main domains: a large extracellular NH_3-terminal domain and a small intracellular cytoplasmic COOH-terminal domain[47]. APP exists in eight isoforms and five common isoforms are APP563, APP695, APP714, APP770 and APP751[40, 47].

1.3.1 APP proteolytic cleavage

APP770 is found in both neuronal and non-neural cells throughout the human body[47-49]. The residues of APP770 are arranged in three different locations on the membrane. APP residues from 1 to 699 are located outside the membrane domain, residues 700 to723 form a transmembrane domain and residues 724 to 770 are situated in the cytoplasmic region of the cell[49] as shown in Figure 1.3.1.

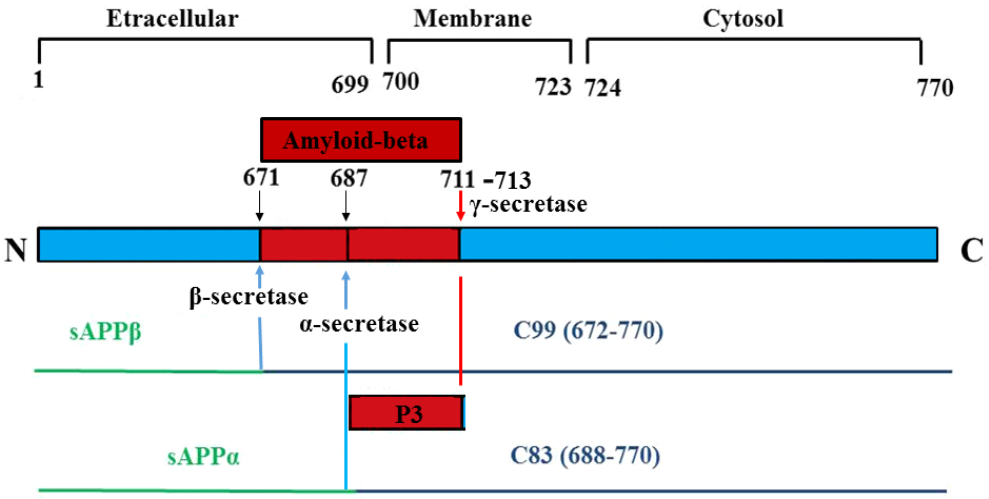

Figure 1.3.1 Schematic diagram of the cleavage of APP770 at different residue linkages. The proteolytic enzymes (α-, β- and γ-secretase) cleave APP770 and generate fragments such as P3 and toxic Aβ[49].

APP is cleaved by three proteolytic enzymes β-, α- and γ-secretase at different residue linkages towards the NH_2-terminal. β-Secretase cleaves residues between 671(Met) and 672(Asp) whereas α-secretase cleaves residues between 687(Lys) and 688 (Leu) and release the fragments in the extracellular domain[49]. The residual of APP towards COOH-terminal, commonly called C-terminal fragment (CTF) remain tethered to the membrane. CTFs, C99 (99 amino acid residues towards COOH terminal of APP) and C83 (83 amino acid residues towards COOH terminal of APP) are formed by the proteolytic action of β- and α- secretase, respectively[49]. γ-Secretase cleaves APP770 between three different peptide linkages: 711(Val) and 712 (Ile); 713 (Ala) and 714 (Thr); 720 (Leu) and 721 (Val) and produces non-toxic P3 and toxic Aβ peptide[49].

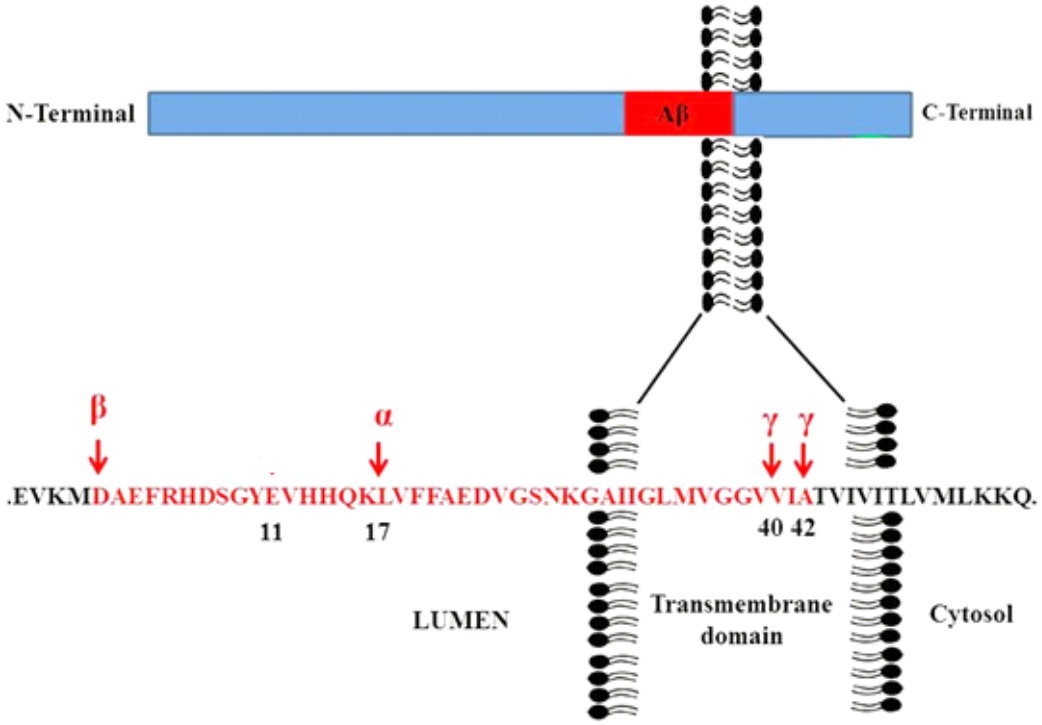

Figure 1.3.2 Schematic diagram of the position of Aβ fragment in APP transmembrane protein. N-terminal of APP has large biologically active outer domain found at the lumen and small C-terminus found in the cytosol. The peptide, Aβ lies from lumen to the transmembrane region (red)[47].

Generally, proteolytic cleavage of APP occurs in two separate paths: (i) non-amyloidogenic or α-secretase pathway, and (ii) amyloidogenic or β-secretase pathway[50, 51].

1.3.1.1 Non-amyloidogenic pathway

In the non-amyloidogenic pathway, the proteolytic enzyme α-secretase cleaves APP between 16 (Lys) and 17 (Leu) residues of Aβ fragment producing secreted amyloid precursor protein alpha (sAPPα), which is released in lumen. The remaining fragment, P3 resides in the membrane. sAPPα may help to promote neuronal outgrowth, synaptogenesis and cell adhesion[52, 53]. *In vivo* studies suggest that sAPPα may enhance the learning and memory[52, 53]. P3 is later released by the action of γ-secretase[50, 51] as shown in figure1.3.1.1. The biological role of P3 is still unknown[52].

α-Secretase belongs to a disintegrin and metalloproteinase (ADAM) group and are found mainly on the cell surface[54, 55]. Hopper and Turner (2002) reported that α- secretase activity of APP develop in post trans-Golgi complex[56]. The stimulation of protein kinase C signaling

system regulates the proliferation of α- secretase on the cell surface to cleave APP[57-59]. α-secretase cleavage occurs within the Aβ sequences of APP and hence it may stop the further generation of toxic Aβ fragment[47]. Donmez *et al.* (2010) and Postina *et al.* (2004) reported that high expression of ADAM-10 in AD mouse model substantially decreased the deposition of Aβ[60, 61].

γ-secretase is a multiprotein complex consisting of nicastrin, anterior pharynx-defective 1, PS1, PS2 and persenilin enhancer 2 (PEN-2)[62]. This proteolytic complex is important for the progressive cleavage of intramembranous transmembrane proteins. Presenilin comprises two aspartyl residues which are very important for intramembranous cleavage[63, 64]. The biological roles of γ-secretase are still not fully discovered[65].

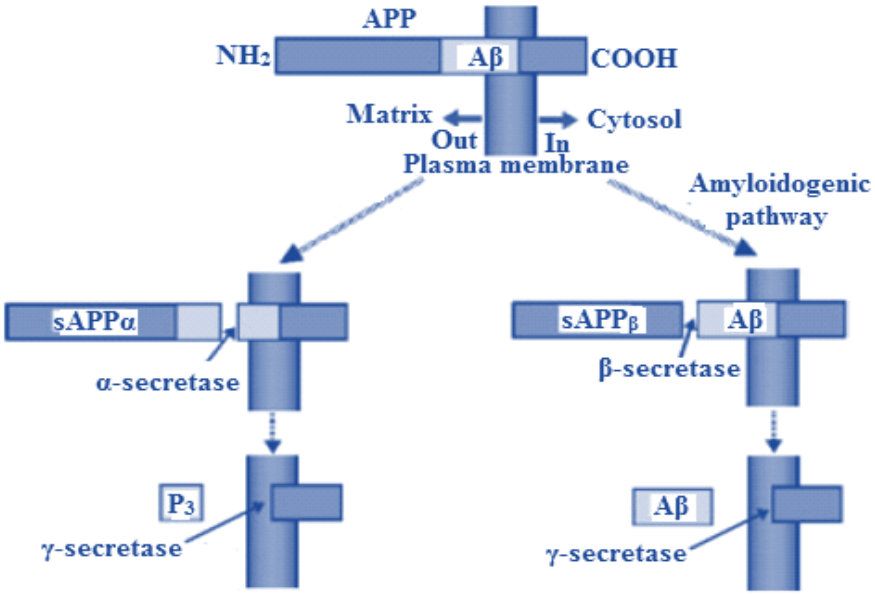

Figure 1.3.1.1 Illustration of Aβ non-amyloidogenic and amyloidogenic pathways[66]. In non-amyloidogenic pathway, sAPPα and P3 fragment is released by the action of α-secretase by γ-secretase, respectively. (ii) In amyloidogenic pathway; sAPPβ and Aβ are released by β-secretase and γ-secretase, respectively[66].

1.3.1.2 Amyloidogenic pathway

In the amyloidogenic pathway, APP is first cleaved by β-secretase and later cleaved by γ-secretase[67]. The β-secretase enzymes such as beta-site APP cleaving enzyme (BACE) and memapsin (membrane-associated aspartic protease) initiate cleavage at the NH_2-terminal of APP. Later γ-secretase cleaves Aβ fragments from APP and releases these fragments on the outer surface of the neuronal cells[67] as shown in Figure1.3.1.1.

BACE are aspartic protease enzymes. BACE1 cleaves APP at NH_2-terminus and releases soluble sAPPβ. It is associated in the looping of synapses during the growth of both central and peripheral neurons[52, 53]. A similar protein, BACE2, may also perform β-secretase activity[68]. However, the expression of BACE2 is very low in the brain and mostly found in glial cells[69]. It is reported that the expression of BACE may increase during cellular stress, hypoxia, ischemia and oxidative stress[52].

1.4 Amyloid beta

Amyloid beta (Aβ) is the main causative factor for the development of neuronal degeneration and its lethality leads to dementia and AD[26, 27]. Many scientific reports strengthen the hypothesis that Aβ peptide plays a significant role in AD[26, 27]. It is reported that Aβ peptide plaques are the main reason for AD[26, 27].

1.4.1 The structure of Aβ peptide

The structural studies of Aβ peptide (1-42) suggest that Aβ peptide residues from 1(Asp) to 27(Asn) are located in extracellular aqueous domain and remaining residues from 28(Lys) to 42(Ala) lie in the transmembrane domain[70, 71] as shown in Figure 1.4.1. Aβ peptide contains six negatively and six positively charged residues, which are mostly found in the hydrophilic domain (Aβ1-28). The Aβ residues from 17(Leu) to 21(Ala) of extracellular domain and residues from 32(Ile) to 42(Ala) of transmembrane domain are the hydrophobic regions of Aβ. The Aβ peptide sequence analysis using Garnier-Osguthorpe-Robson and Chou-Fasman methods indicate that the probability of β-sheet structure is very high from residue 28(Lys) onwards. Aβ residues from 9(Gly) to 21(Ala) have low probability to form β-sheet structure[72]. The amyloid fragment (9-21) may adopt either α-helix or β-strand conformation. Two possible β-turns are predicted between residue 6(His) and 8(Ser) as well as 2(Asp) and 29 (Asn) of Aβ[73] as shown in Figure 1.4.1.

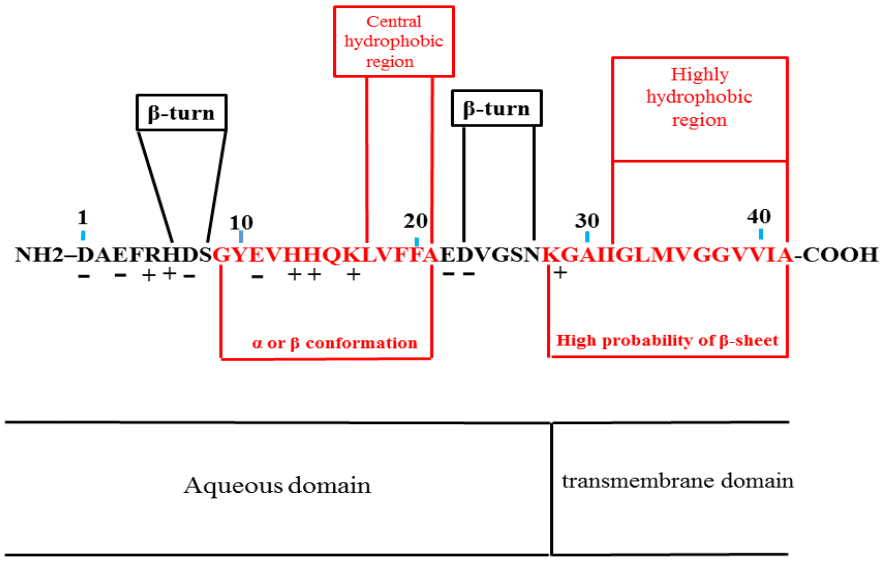

Figure 1.4.1 Schematic diagram of Aβ structure. The transmembrane region of Aβ residues are highly hydrophobic and possess β-sheet structure. Aβ residues of extracellular region are mostly hydrophilic except Aβ (17-21). Aβ (9-21) possess both α- or β- conformation. Aβ (6-8) and Aβ (23-27) are predicted as β-turn regions.

Structural studies of Aβ peptides have been investigated by various experimental methods such as, circular dichroism (CD) spectroscopy, electron microscopy (EM), NMR, Fourier transform infrared spectroscopy (FTIR), X-ray fiber diffraction (XRD) under different conditions such as pH, temperature and organic solvents (Dimethyl sulfoxide (DMSO), Trifluoroethanol (TFE) and hexafluoroisopropanol (HFIP)[18].

Zagorski and Barrow (1992) reported that the conformational changes of Aβ (1-28) are influenced by pH and temperature[74]. At pH range (1-4) and TFE (60%, a membrane mimic organic solvent, similar to SDS micelles and phospholipid vesicles), Aβ (1-28) may adopt random coil/monomeric α- helix structure whereas at pH range (<4 and >7), it may adopt oligomeric β-sheet structure[74]. NMR study suggests that Aβ (1-28) may exhibit monomeric α-helix structure at low temperature (10°C) and it may form β-sheet structure at high temperature (35°C)[74]. Lee *et al* (1995) examined Aβ in different ranges of pH (2-11) using ^{1}H NMR. They suggested that Aβ (1-28) is not able to form fibrils and is not capable to adopt α-helical conformation in water[75]. However, Aβ (10-35) and Aβ (1-40) may form plaques at pH range (5-9) and these fragments are unable to form plaques at pH <4 in water[75]. These results contradict the previous NMR studies that Aβ may adopt α-helix structure in micelle models

and low pH[74, 75]. Zhang *et al.* (1998) analysed the structure of Aβ (12-28) in water using 2D NMR. They reported a hydrophobic region between amyloid residues 17 (Leu) and 21(Ala)[76].

Talafous *et al* (1994) examined the structure of Aβ (1-28) peptide in aqueous TFE solution using 2D NMR[77]. They found that Aβ (1-28) may fold into two right handed α-helices between residues 2-11 and 13-27. These α-helices may be joined by a loop at residue 12(Val)[77]. They also reported that the side chains of residues 13(His) and 16(Lys) are very close to each other at the same side of α-helices. This closeness of residues may hinder the transition of α-helix to β sheet during initial stages of amyloidosis[77].

Fraser *et al*., (1991) examined the structure of Aβ fragments (1-28, 19-28, 17-28, 15-28, 13-28, 11-28, and 9-28) using EM, FT-IR, and X-ray diffraction[78]. They found that these fragments may acquire amyloid fibrillar structures at pH range (3-10)[78]. They reported that the ionization of side chains of amyloid fragments may be important to develop fibrils[78]. They also suggested that the electrostatic interaction between amyloid residue 13(His) and 23(Asp) and hydrophobic interactions between 17(Leu) and 21(Ala) may promote the amyloid fibril formation[78].

Using CD and ^{1}H NMR spectroscopy, Danielsson *et al*. (2005) suggested that temperature may influence the structural transitions of Aβ[79]. They reported that Aβ (1-40) may adopt α-helix structure at 0°C and a random coil structure at 60°C and pH 7[79]. Below 20°C, Aβ(12−28) may form a β-strand-like conformation. Aβ (1-9) may form a β-strand at 20°C and transform into a random coil confirmation at 60°C[79]. Using CD spectroscopy, Barrow *et al*. (1992) examined the 2D structure and aggregation behaviour of Aβ fragments (1-28, 1-39, 1-42 and 29-42) in HFIP or TFE. They reported that Aβ fragments (1-39 and 1-42) may form α-helix at pH ranges (1-4) and (7-10) and unfold with rising temperature[80]. Aβ fragments (1-39 and 1-42) form β sheet conformation at pH range (4-7) and this conformation has no effect of temperature[80]. They also reported that Aβ (29-42) may form an intermolecular β-sheet structure at any temperature or pH in aqueous solution[80]. Hence, the Aβ hydrophobic segment (29-42) may be responsible to generate the β-pleated sheet structure during amyloidosis[80].

Table 1.4 Morphological studies of Aβ-peptides[18]

Peptide	pH & other conditions	NMR		FTIR	XRD	CD	Other techniques	Morphology
$A\beta_{1-28}$	pH 4-7 TFE (60%)	√						α-helical structure deceased when temperature increased
$A\beta_{1-28}$	pH 2-11 (water)	√						No α-helical structure
$A\beta_{1-28}$	Membrane mimic (SDS)	√						α-helical structure bend at 12 amino acid residue of Aβ
$A\beta_{1-28}$	DMSO	√						C-terminal α-helix and flexible N terminal turn
$A\beta_{1-28}$	pH 1-4 (H_2O)					√		Random coil
$A\beta_{1-28}$	pH > 8			√				Random structure, No fibrils
$A\beta_{1-28}$	pH 3-7				√			Numerious amyloid like fibrils
$A\beta_{1-28}$	Aqueous						EM	Fibrillar, Cross-β
$A\beta_{9-28}$	pH <3			√				Predominantly random with minor β-sheet
$A\beta_{12-28}$	pH 2.6 (SDS)	√						α-helix (16-24)
$A\beta_{15-28}$	pH 10			√				Random structure, No fibrils
$A\beta_{17-28}$	pH 10			√				Random structure, No fibrils
$A\beta_{10-35}$	pH 7.4	ss √						β- sheet (parallel)
$A\beta_{10-35}$	pH7.4, pH3.4						STEM	β- sheet (parallel)
$A\beta_{10-43}$	H_2O,					√		80% β-sheet,
	HFIP					√		28% α-helical structure
$A\beta_{16-22}$	pH 7.0	ss√				√	EM	β- sheet (anti-parallel)
$A\beta_{25-35}$	pH5.5, pH7.4					√		β- sheet
$A\beta_{29-42}$	pH7	ss√		√				β- sheet
$A\beta_{34-42}$	pH7	ss√						β- sheet (anti-parallel)
$A\beta_{1-40}$	pH5.1(SDS)	√						α-helix (15-36)
$A\beta_{1-40}$	pH2.8 TFE (40%)	√						α-helix
$A\beta_{1-40}$	pH7.4	ss√						β- sheet (parallel)
$A\beta_{1-42}$	H_2O					√		β- sheet
$A\beta_{1-42}$	pH7.4	ss√					EM, STEM	β- sheet (parallel)
$A\beta_{1-42}$	pH7.2(SDS)	√						α-helix

SS (Solid state), SDS (Sodium dodecyl sulphate), STEM (Scanning transmission electron microscopy)

Benzinger *et al.* (2000) used magic-angle spinning SS-NMR to analyse the structure of Aβ (10−35)[81]. They reported that Aβ (10-35) may adopt parallel β-sheet structure at pH 7.4[81]. The structural transition (α-helix to β-sheet) is observed between residues 19(Phe) and 20(Phe). However, the β turn is not observed at putative turn region between residues 25(Gly) and 29(Gly)[81] SS-NMR data suggest that the full length amyloid peptide, Aβ (1-42) may also form parallel beta-sheet structure[82].

FTIR spectroscopy studies of Aβ (1-40) suggest that a β-turn structure may be formed in the domain of Aβ (26-29)[83]. XRD analysis of Aβ (11−25) suggests that a hairpin turn structure is located in between residue 17(Leu) and 20(Phe)[84]. Cryo-EM studies suggest that Aβ (11−25) consists of β-sheet that directs β-strands in register[85]. SS-NMR, FTIR and computational simulation data suggest that Aβ (16−22) may form an antiparallel β-sheet structure[86].

NMR analysis of $A\beta_{1-40}$ fibrillar structure suggests that the first ten residues are unstructured[87]. The residues between 11(Glu) and 40(Val) may develop an alternate β-turn-β fold, which is connected by a salt bridge between residues 23(Asp) and 28(Lys)[87] as shown in Figure 1.4.2. Amyloid peptide linkages between 19(Phe)-32(Ile), 19(Phe)-34(Leu), 19(Phe)-36(Val), 15(Gln)-36(Val), and 13(His)-40(Val) are stabilised by H-bonding in $A\beta_{1-40}$. Two or three β-turn-β units are also reported in the cross-section of amyloid fibrils depending upon the morphology of the fibril[87]. Inter molecular connections are located inside the amyloid beta monomer between 35(Met) and 42(Ala) and 19 (Phe) and 38 (Gly)[88, 89] as shown in Figure 1.4.2.

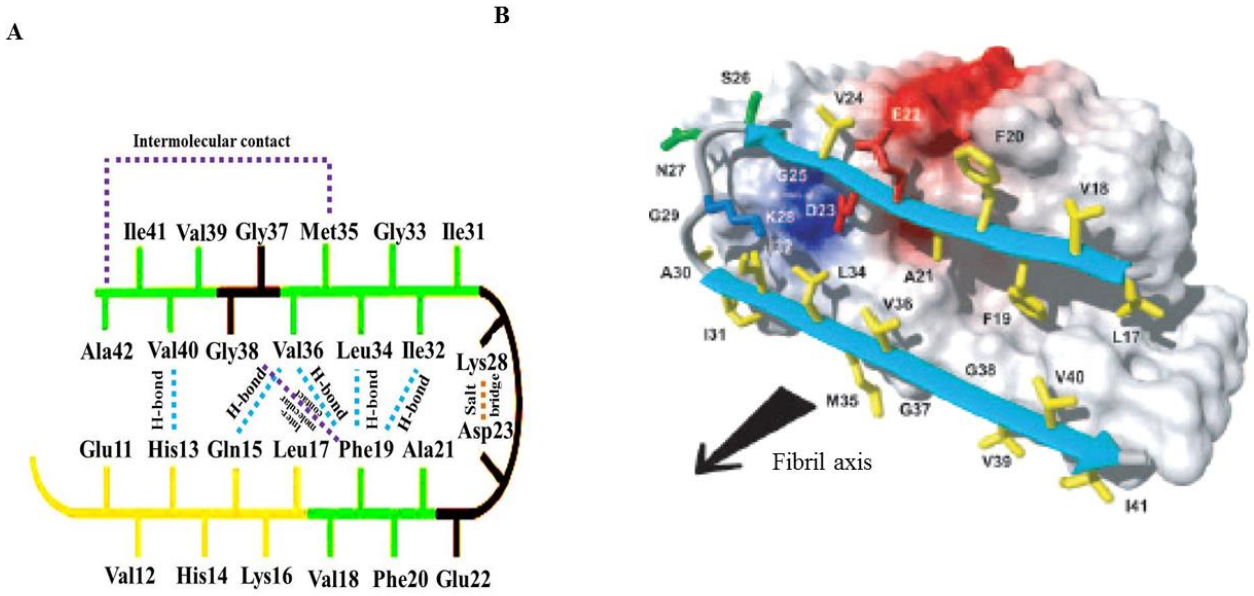

Figure 1.4.2 Schematic diagram of Amyloid beta fibrils. The residues from 11to 40 in $A\beta_{1-40}$ and 18 to 42 in $A\beta_{1-42}$ adopt a β-turn-β fold. (A) H-bonding exists at four different peptide linkages: 19(Phe)-32(Ile), 19(Phe)-34(Leu), 19(Phe)-36(Val), 15(Gln)-36(Val) and 13(His)-40(Val). Salt bridge occurs between 23(Asp) and 28(Lys). Molecular interactions are found inside the monomeric unit of $A\beta_{1-42}$ fibrils between 19(Phe) and 38(Gly), and 35(Met) and 42 (Ala)[87]. (B) Hydrophobic (yellow), polar (green), negatively charged (red) and positively charged (blue) residues of Aβ[90].

1.5 Inhibition of Aβ peptides in therapeutic role for AD

The therapeutic strategies for AD are principally designed to destabilise the AD causing proteins, Aβ and Tau[91]. Many results from molecular, genetic, animal transgenic modelling, and biochemical experiments confirm the notion that the peptide Aβ is the main cause of amyloid plaques, which contributes a crucial role in the pathophysiology of AD[86]. Therefore, the primary aim is to develop the anti-Aβ therapy by reducing the production of Aβ.

The Aβ production may be controlled by inhibiting the amyloidogenic proteases (β- and γ-secretase)[86]. The protein complex of γ-secretase is not only important for cleavage of APP but also essential for cell signalling process which is important for proliferation and differentiation of various cell types[92.] The inhibitors of γ-secretase produce physiological side effects such as, damage the lymphocyte and abnormalities in intestinal goblet cells[93]. The β-secretase protein comprises a big catalytic motif and their inhibitors are also of large size which are not capable to enter the blood-brain barrier (BBB)[94-96]. Hence, due to these drawbacks, the protease

inhibitors are not conceptually applicable to reduce the production of Aβ. Many studies suggest that different chemical compounds have the ability to block Aβ aggregation or disrupt amyloid fibrils[97-100]. It is reported that inositol intermixed with amyloid fibrils hinder the amyloid fibrils accumulation[101]. It is also reported that melatonin has ability to stop the amyloid fibrillogenesis on the neuron[102, 103].

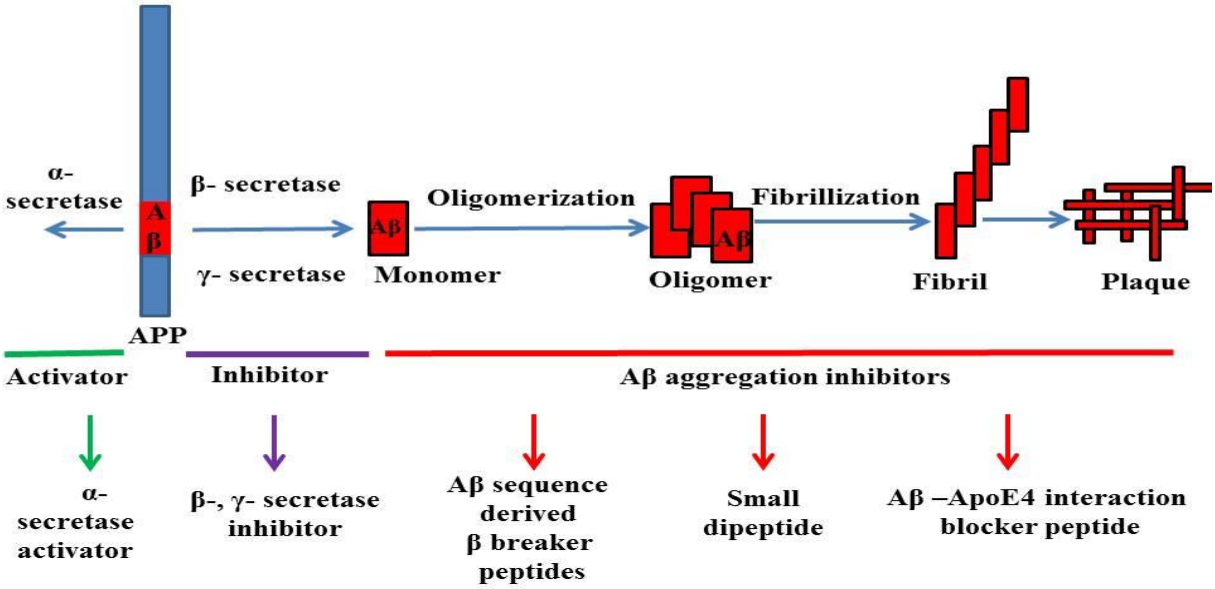

Figure 1.5 Schematic diagram of the possible mechanisms and pathways of Aβ inhibition. The generation of Aβ may be reduced or inhibited either by the action of α secretase activator or by the action of β-,γ-secretase inhibitor. The aggregation of Aβ may be inhibited by small peptides, β breaker peptides or Aβ-Apo E4 blocker peptide[104].

Beta breaker peptides may have the ability to destabilise the oligomer motifs and thus prevent aggregation of Aβ[105]. Beta breaker peptides are short peptides, which are partly homologous to the sequences of the protein and have ability to inhibit the development of fibril assemblies[106-108]. Two main molecular events occur during the action of β-sheet breaker peptide: first, binding between beta breaker peptides and proteins and second, conformational destabilization of β-sheets[109]. Beta breaker peptides such as LPFFD, KLVFF and LVFF have a similar sequence of β-conformation regions of Aβ, which are involved in Aβ peptide-peptide interactions, commonly known as self- recognition motif[105]. The beta breaker peptides, iAβ inhibit amyloid β-protein fibrillogenesis and prevent neuronal death[109]. Tjernberg *et al* (1996) synthesised a small Aβ fragment KLVFF ($A\beta_{16-20}$) and observed that KLVFF bound to Aβ, inhibits the formation of amyloid fibrils[110, 111]. KLVFF was further examined *in vitro* and found

that lysine act as a disrupting elements and helped to protect the cells from amyloid beta toxicity[112].

Table 1.5 Summary of amyloid beta blockers and Beta breaker peptides[104]

Classes of Beta breaker peptides or inhibitors	Beta breaker peptides or inhibitors name	Peptide sequence	Properties
β sheet breaker peptides from Aβ sequence	iAβ Ac-iAβ5-amid LPYFDa	LPFFD, KLVFF Ac-LPFFD-amid LPYFDamid	β sheet breaker Derivatives of iAβ5
Small dipeptides	NH_2-D-Trp-Aib-OH	Ac-Trp-Aib	β sheet breaker
Aβ-Apo E4 blocker peptide	Aβ12-28P	Ac-VHHQKLPFFAEDVGSNK-Amide	β sheet breaker

Soto *et al* (1996) synthesised 11 amino acids (RDLPFFPVPID) peptide, iAβ. This peptide has ability to bind Aβ and prevents Aβ fibril formation[113]. Further, they also synthesised iAβ5 (LPFFD), which is based on the hydrophobic domain of Aβ 17-20 (LVFF) because of their involvement in β-sheet formation[104]. In the beta breaker peptide, iAβ5 (LPFFD) proline (P) is added instead of valine (V) of Aβ sequence (LVFF) to limit the formation of β-sheet[104]. Proline residue has ability to interconvert between *cis* and *trans* conformations and this feature of proline might be important to destabilize intermolecular β-sheet[104]. In this iAβ5 (LPFFD), a charged residue aspartate (D) is added after phenylalaline (F) because aspartate may enhance hydrophobicity and permeability of BBB[104].

1.6 Nuclear magnetic resonance (NMR) spectroscopy

NMR is an influential and multipurpose technique that can be used for investigating structural and dynamic information of organic molecules and biomolecules[114]. One of the major advantages of this technique is its non-invasive ability which permits molecules or compounds to be distinguished in their natural environment[115].

1.6.1 Principle of NMR

The fundamental principle of NMR is based on the fact that all atomic nuclei comprise the magnetic properties which may be important to yield and collect chemical information. The atom is made up of three main fundamental particles; electrons, protons and neutrons[116-120]. These subatomic particles have four basic properties; mass, charge, magnetism and spin. Electric charge and mass influence the physical and chemical properties of elements[116-120]. However, the nuclear magnetism and spin have virtually no effect on the physical and chemical behaviours of the substance. Hence, these two properties are used as wonder tools to determine the internal structure of a substance without disturbing the chemical composition. Spin exists in the form of angular momentum which is important to yield NMR signals[116-120]. Individual unpaired electrons, protons and neutrons possess a spin of ½, which may be +ve or -ve[116-120]. Some atomic nuclei (such as, ^{12}C, ^{16}O etc.) have paired spin which cancel each other[116-120]. Thus these nuclei bear zero spin and lack angular momentum and so they are unable to generate NMR signals. On the other hand, many atoms (^{1}H, ^{13}C, ^{15}N, ^{19}F, ^{31}P etc.) have non zero spin and these atoms are NMR active nuclei to produce NMR signals[116-120]. Nuclear spin is determined by the following rules: if atomic mass and neutrons is an even number then the nucleus has zero spin; if the mass is even and neutrons are in odd number then the nucleus possesses integer spin (1, 2, 3…) and if the mass is odd and the neutron is an even or odd number, then the nucleus has half integer spin (1/2, 3/2/5/2 …)[116-120].

The non-zero spin nuclei having angular momentum are able to interact with the applied magnetic field and their magnitude is determined by:

Equation: $$P = \hbar\sqrt{I(I+1)}$$

Equation : Equation for the magnitude of spin quantum number; where P is angular momentum; I is the nuclear spin quantum number; and ħ is the Planck constant divided by 2π.The value of I is dependent on the mass and charge of nucleus[116].

In simple terms, the proton (spin -1/2) may be considered as a small bar magnet therefore it may have its own local magnetic field. A bar magnet has characteristic of its own magnitude and orientation (i.e. north and south pole) and the same characteristics are applied for the proton[116-120] When there is no external magnetic field applied, the spin may be orientated randomly, which is degenerative. After applying an external magnetic field (B_0), it disrupts the degeneracy and randomly moving spins precess about the magnetic field[116-120]. The precession

of the nucleus is slightly tilted away from the axis of the magnetic field, but the rotation axis is always in the same direction of B_0, which is defined as being in the Z-direction[116-120] as shown in Figure1.6.1, with an angular velocity, which is determined by:

Equation: $\omega_0 = \gamma B_0$

Equation: Equation for the calculation of rate of precession. Where ω_0 is Larmor frequency, B_0 is external magnetic field and γ is magnetogyric ratio. The magnetogyric ratio relates the spin (I) and magnetic moment (μ) as $\gamma = 2\pi\mu/hI$. Each nucleus possess a specific γ value, such as, the proton magnetogyric ratio = 2.674×10^4 gauss^{-1}sec[116-120]

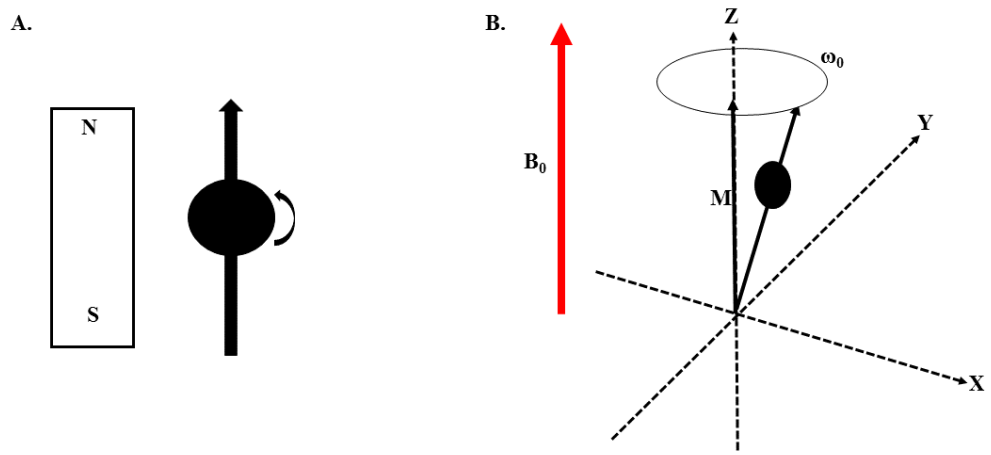

Figure1.6.1 Schematic diagram of (A) bar magnet and a charged nucleus oriented to the direction of bar magnet, which represent the analogy of bar magnet. (B) Precession of a proton parallel to the external magnetic field (B_0) in Z-axis with precession frequency, ω_0, called Larmor frequency and a net magnetization (M).

The Z-axis angular momentum P_z is defined as:

Equation: $P_z = hm$

Equation: Equation for the Z-axis of the angular momentum; where P_z is angular momentum at the Z-axis; *h* is the Planck constant ; m is the magnetic quantum number[116]

The ½ spin nuclei have two possible orientation either along or opposite to external magnetic field as Z-axis and –Z-axis with an angle to the magnetic field[116-120] as shown in Figure 1.6.2.

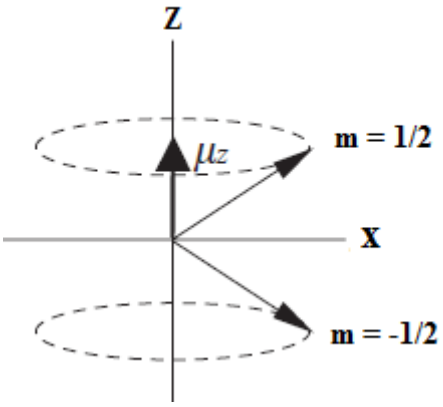

Figure 1.6.2 Schematic diagram of angular momentum of spin ½ has two orientations; Z axis and -Z axis[116].

The non-zero spin quantum number nuclei will rotate about B_0 because of torque produced by the interaction of the angular momentum with magnetic field. The μ is either parallel or antiparallel to the angular momentum[116]: The value of P is same for all nuclei with the same magnetic quantum number (m), whereas the angular moment μ is different for different nuclei

Equation: $$\mu = \gamma P = \gamma \hbar \sqrt{I\,(I+1)}$$

Equation: Equation for the magnetic moment, where μ is magnetic moment; γ is the nuclear gyromagnetic ratio; P is angular momentum; and I is spin quantum number[116].

In other words, all protons are exactly aligned to B_0 and this process is called net magnetisation (M). A short pulse radio frequency energy is involved in NMR process that allows protons to absorb energy at a specific frequency. The absorbed frequency (i.e. Larmor frequency) is directly proportional to B_0[116-120]. The Larmor frequency at 90° pulse cause M to rotate into XY-plane and at this stage net magnetisation is referred as M_1 which is perpendicular to B_0[116-120] as shown in Figure 1.6.3. When the Rf pulse stops, the M1 protons re-align into M plane (Z-axis). During this transition, an induced magnetic field generated in the form of Rf, which is received by receiver coils and after computational programming this NMR signal projects as a spectrum[116-120].

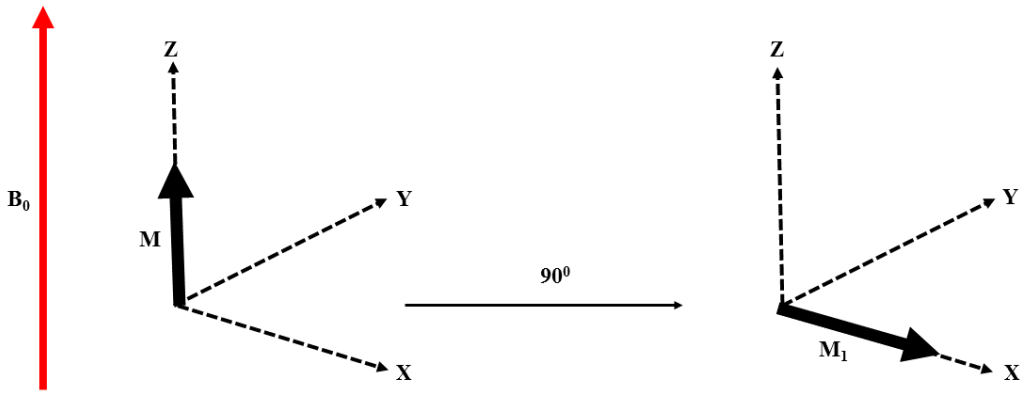

Figure 1.6.3 Schematic diagram of the effect of a 90° pulse on net magnetisation. The protons align themselves along with the external magnetic field (B_0), called net magnetisation (M) at the Z-axis. After an Rf frequency pluse90°, the M is rotated into XY-plane, perpendicular to B_0, referred as M_1.

1.6.2 Energy states and population in NMR

Generally atomic nuclei having non-zero spin quantum numbers orient along precise directions pertaining to the magnetic field. They spin constantly around the direction of magnetic field attributable to the nuclear moment μ influenced by atomic nuclei. These orientation states are commonly known as Zeeman states or spin states. The energy is related to each orientational state, which is mostly characterized by the frequency of the precession[116]. The energy of a Zeeman state with m, can be described as the following equation:

Equation:

$$E = -\mu_z B_0 = -m\hbar\gamma B_0 = m\hbar\omega_0$$

Equation: Equation for the energy of the Zeeman state. Where, E is energy; μ_z is nuclear moment of Z component; B_0 is magnetic field; m is magnetic quantum number; ħ is Plank's constant; γ is gyromagnetic ratio; and ω_0 is Larmor frequency[116].

The NMR signals arise from the two Zeeman states transition. The energy state population is generally directed by the Boltzmann distribution. The population ratio in the energy states is defined by the Boltzmann equation[116]:

Equation:

$$N_\beta/N_\alpha = e^{-\Delta E/kT} = e^{-\hbar\gamma Bo/kT} = 1/\ e^{\hbar\gamma Bo/kT}$$

Equation: The Boltzmann distribution for the population of energy states; where N_α and N_β are the population of lower and higher energy states, respectively; T is the absolute temperature and k is the Boltzmann constant[116].

1.6.3 How does NMR work

NMR machine needs always a superconducting magnet to produce a strong magnetic field. Basically, NMR magnets are coiled with huge amounts of wire and current runs through this wire producing a high magnetic field[121]. The NMR wires are commonly situated at low temperature to develop zero resistance and thus the wire becomes a superconductor. When the electric current is applied to the superconductor it produces a strong magnetic field. To maintain the superconductivity of an NMR, the coils are submerged in liquid helium (having very low temperature about 4K) inside the NMR machine container. It is also shielded by a layer of liquid nitrogen (77K) to reduce the evaporation of liquid helium[121]. The samples are not kept in the liquid helium at very low temperature during an NMR measurement[121]. Hence a vertical tube, called the bore tube of magnet, is constructed in the centre of the NMR and samples are placed in the bore at required temperature[121]. The magnetic field of the bore tube is always the same as the NMR machine magnetic field[121].

The magnetic field should be always in a homogeneous condition to obtain good NMR spectra[121]. However, superconducting magnet cannot generate such a homogeneous magnetic field. Hence, a set of shim coils are used to obtain a homogenous magnetic field, which surround the samples. The shim coils generate a tiny magnetic field with a specific direction. The homogeneity of the magnetic field can be adjusted by passing the current through these shim coils[121].

The probe is an important component of NMR, which is a cylindrical tube and generally placed into the magnetic bore tube area of the NMR machine[121]. The probe possesses small coils, which are used to excite and detect the magnetization of samples to obtain NMR signals. Samples are generally placed very close to probe to gain maximum sensitivity and optimization

of the probe coil magnetization. The probe has many components and they are attached to amplifiers and computational devices through cables. The important components of probe are the tune circuit and the match circuit[121].

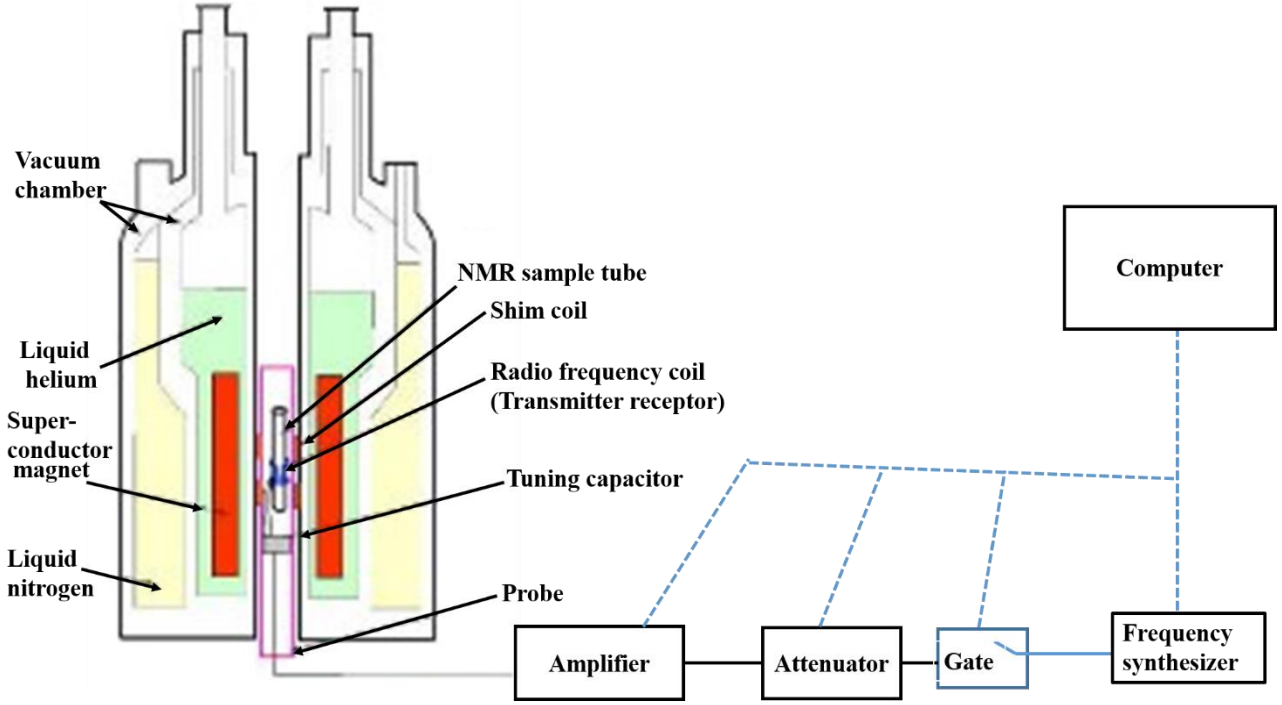

Figure 1.6.4 Schematic diagram of NMR spectrometer. The frequency synthesizer is the source of radio frequency. The gate and attenuator are used to produce pulses and this is connected to amplifier and probe. All these units are controlled by computational program.

The tune circuit is basically a part of the probe coil and has a capacitor. The tune-coil inductance and tune-capacitor capacitance are fixed in a way until the tune circuit is resonant at the Larmor frequency of measuring nuclei[121]. The match circuit is also a part of probe coil and it is used to adjust maximum power transfer between the probe coil and the transmitter or receiver unit. The radio-frequency (Rf) transmitter is a vital component of NMR spectrometer that produces the pulse[121]. The frequency synthesizer is used as an Rf source to generate a constant frequency. Since the Rf is applied for very little time, the frequency synthesizer (frequency source) is channelized or gated to an Rf pulse. The length and timing of Rf pulse from gated frequency source may be controlled by computer programs. Generally, the Rf source exhibits a very low level signal (few milliwatt). Hence, an amplifier is used to boost the Rf signals from low to high levels (100 watt or more) before applying to the probe along with external magnetic field[121]. The attenuator is also used to control the Rf signals. The Rf power is controlled by a tuning capacitor. The NMR signals are converted by analogue to digital

converter (ADC) to a binary number and stored as computational memory. The ADC compiles the NMR signals at constant intervals to produce free induction decay (FID) as data points[121].

In summary, the sample containing atomic nuclei possess spinning charged particles and produces a magnetic field. When the sample is placed in the NMR, the protons align themselves either along or against the direction of external magnetic field1[116-120] as shown in figure 1.6.5. The protons which are aligned in the direction of the external magnetic field possess low energy state (α-spin) and those are aligned opposite direction to the external magnetic field possess high energy state (β-spin) [116-120].

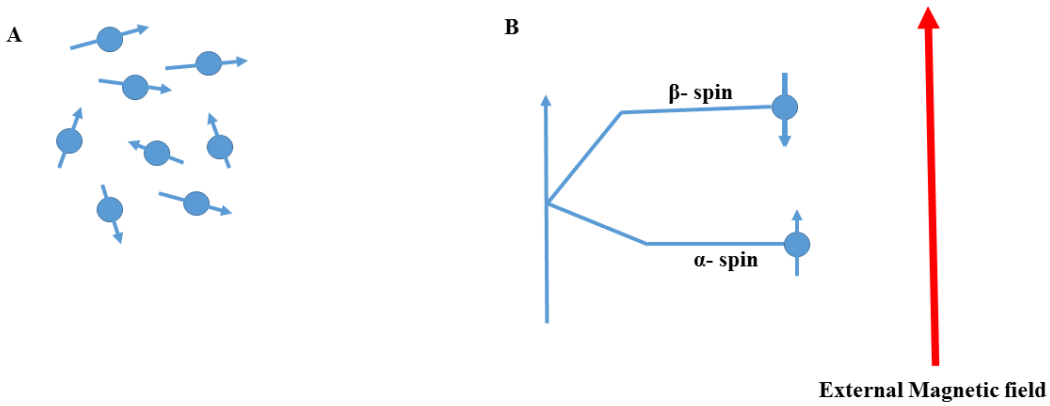

Figure 1.6.5 Schematic diagram of the energy level of nuclei. Atomic nuclei possess spinning charged particles and produce magnetic field. They move randomly but when an external magnetic field is applied they aligned themselves along or against external magnetic field.

The energy difference (ΔE) between β- and α-spin depends upon the external magnetic field. The Rf pulse is applied to flip the direction of nuclear spin and produce net magnetic moment which is perpendicular to the external magnetic field, commonly known as transverse magnetization[116-120]. The precession frequency of the transverse magnetic moment is almost same as the precession frequency of each spin of the nuclei of the sample. Then the atomic nuclei undergo relaxation (nuclei return back to their original state)[116-120]. During this process, the nuclei generate induced magnetic signals. These signals are further collected by the probe receiver coils and processed as Rf signals[116-120]. These Rf signals are processed in the form of

FID. Using Fourier transformation, the FID is further transformed into a frequency domain NMR spectrum[116-120].

1.7 References

1. J.N. Buxbaum, *FEBS Lett*, 2009, **583**, 2663–2673.
2. N. Mimassi, P. Youinou and Y.L. Pennec, *Ann Med Interne. (Paris)*, 2002, **153**, 383-388.
3. D.J. Martin and M. Ramirez-Alvarado, *Amyloid*, 2010, **17**, 129-136.
4. M. Hoshino, H. Katou, Y. Hagihara, K. Hasegawa, H. Naiki and Y. Goto, *Nature Structural Biology*, 2002, **9**, 332-336.
5. J.L. Jiménez, G. Tennent, M. Pepys and H.R. Saibil, *J Mol Biol*, 2001, **311**, 241-247.
6. J.W. Kelly, *Nat. Struct. Biol.*, 2002, **9**, 323-325.
7. I. Cherny, L. Rockah, O. Levy-Nissenbaum, U. Gophna, E.Z. Ron and E. Gazit, *Journal of Molecular Biology*, 2005, **352**, 245-252.
8. C.W. Cairo, A. Strzelec, R.M. Murphy, and L.L. Kiessling, *Biochemistry*, 2002, **41**, 8620-8629.
9. R. Nelson, M.R. Sawaya, M. Balbirnie, A. Madsen, C. Riekel, R. Grothe and D. Eisenberg, *Nature*, 2005, **435**, 773-778.
10. O.S. Makin and L.C. Serpell, *Methods Mol. Bio*., 2005, **299**, 67-80.
11. R. Tycko, *Current Opinion in Structural Biology*, 2004, **14**, 96-103.
12. K.L. Morris and L.C. Serpell, *Amyloid Proteins Methods in Molecular Biology*, 2012, **849**, 121-135.
13. D. Frenzel, J.M. Gluck, O. Brener, F. Oesterhelt, L. Nagel-Steger and D. Willbold, *PLOS One*, 2014, **9**, 1-7.
14. J. Stohr, J.C. Watts, Z.L. Mensinger, A. Oehler, S.K. Grillo, S.J. DeArmonda, S.B. Prusiner and K. Giles, *PNAS*, 2012, **109**, 11025-11030.
15. M. Stefani and S. Rigacci, *Int J Mol Sc.*, 2013, **14**, 12411-12457.
16. J. Greenwarld and R. Riek, *Structure*, 2010, **18**, 1244-1260.
17. K. Irie, K. Murakami, Y. Masuda, A. Morimoto, H. Ohigashi, R. Ohashi, K. Takegoshi, M. Nagao, T. Shimizu and T. Shirasawa, *J Biosci Bioeng*., 2005, **99**, 437-447.
18. L.C. Serpell, *Biochimica et Biophysica Acta*, 2000, **1502**, 16-30.
19. J. Pozueta, R. Lefort and M. Shelanski, *Neuroscience*, 2013, **251**, 51–65. 20.

20. Y. Hashimoto, M. Nawa, M. Tokizawa, A. Iwamatsu and M. Matsuoka, *Cell Death and Disease*, 2013, **4**, e555.
21. L. Crews and E. Masliah, *Human Molecular Genetics*, 2010, **19**, R12–R20.
22. P.T. Francis, A.M. Palmer, M. Snape and G.K. Wilcock, *J Neurol Neurosurg Psychiatry*, 1999, **66**, 137–147.
23. A. Maruszak and S. Thuret, *Frontiers in Cellular Neuroscience*, 2014, **8**, 1-11.
24. X. Wang, M.L. Michaelis and E.K. Michaelis, *Current Genomics*, 2010, **11**, 618-633.
25. D. Selkoe, *Physiol R.*, 2001, **81**, 741-766.
26. A. Mohamed and E.P. deChaves, *International Journal of Alzheimer's Disease*, 2011, **2011**, 1-17.
27. T.A. Bayer and O. Wirths, *Frontiers in Aging Neuroscience*, 2010, **2**, 1-10.
28. D.J. Selkoe and D. Schenk, *Annual Review of Pharmacology and Toxicology*, 2003, **43**, 545-584.
29. H. Hppius and G. Neundorfer, *Dialogues in Clinical Neuroscience*, 2003, **5**, 101-108.
30. K. Maurer, S. Volk and H. Gerbaldo, *The Lancet*, 1997, **349**, 1546-1549.
31. D.P. Perl, *Mt Sinai J Med*, 2010, **77**, 32-42.
32. R.A. Crowther and M. Goedert, *Journal of Structural Biology*, 2000, **130,** 271–279.
33. L.S. Higgins, J.M. Rodems, R. Catalano, D. Quon, and B. Cordell, *Proc Natl Acad Sc.*, 1995, **92**, 4402-4406.
34. R.A. Armstrong, *J Optom*, 2009, **2**, 103-111.
35. G.B. Frisoni, N.C. Fox, C.R. Jack Jr, P. Scheltens and P.M. Thompson, *Nature Reviews Neurology*, 2010, **6**, 67-77.
36. J.M. Schott, J.D. Warren, F. Barkhof, M.N. Rossor and N.C. Fox, *BMJ*, 2011, **343**, 1-5
37. http://www.radiologyinfo.org/en/photocat/gallery3.cfm?pid=1&image=brain-regions-alzheimer-mri.jpg&pg=alzheimers. In (25-10-2014).
38. J. Clinton, G.W. Roberts , S.M. Gentleman and M.C. Royston, *Neuropathol Appl Neurobiol.*, 1993, **19**, 277-281.
39. A. Hafkemeijer, J. van der Grond and S.A.R.B. Rombout, *Biochimica et Biophysica Acta*, 2012, **1822**, 431–44.
40. M.A. Meraz-Rios, D. Franco-Bocanegra, D.T. Rios and V. Campos-Pena, *Oxidative Medicine and Cellular Longevity*, 2014, **2014**, 1-14.
41. T. Lemmin, M. Dimitrov and P.C. Fraering and M.D. Peraro, *J. Biol Chem*, 2014, 289, 6763-6774.

42. E.S. Oh, A.V. Savonenko, J.F. King, S.M. Fangmark Tucker, G.L. Rudow, G. Xu, D.R. Borchelt and J.C. Troncoso, *Neurobiol Aging*, 2009, **30**, 1238-1244.
43. T.L. Young-Pearse, J. Bai, R. Chang, J.B. Zheng, J.J. Lo Turco and D.J. Selkoe, *J. Neurosci.*, 2007, **27**, 14459-14469.
44. H. Meziane, J.C. Dodart, C. Mathis, S. Little, J. Clemens, S.M. Paul and A. Urgere, *Proc Natl Acad Sci USA.*, 1998, **95**, 12683-12688.
45. J.M. Roch, E. Masliah, A.C. Roch-Levecq , M.P. Sundsmo, D.A. Otero , I. Veinbergs and T. Saitoh, *Proc Natl Acad Sci USA.*, 1994, **91**, 7450-7454.
46. J. Lee, C. Retamal, L. Cuitino, A. Caruano-Yzermans, J.E. Shin, P. van Kerkhof, M.P. Marzolo and G. Bu, *J Biol Chem*, 2008, **283**, 11501-11508.
47. R.J. O'Brien and P.C. Wong, *Annu Rev Neurosci*, 2011, **34**, 185-204.
48. T.A. Bayer, R. Cappai, C.L. Masters, K. Beyreuther and G. Multhaup, *Mol Psychiatry*, 1999, **4**, 524-528.
49. Y.G. Kaminsky, M.W. Marlatt, M.A. Smith and E.A. Kosenko, *Experimental Neurology*, 2010, **221**, 26-37.
50. C. Haass, C. Kaether, G. Thinakaran and S. Sisodia, *Cold Spring Harb Perspect Med*, 2012, **2**, a006270.
51. S.E. Hoey, F. Buonocore, C.J. Cox, V.J. Hammond, M.S. Perkinton and R.J. Williams, *Plos One*, 2013, **8**, e78155.
52. V.W. Chow, M.P. Mattson, P.C. Wong and M. Gleichmann, *Neuromolecular Med.*, 2010, **12**, 1-12.
53. S. Chasseigneaux and B. Allinquant, *Journal of Neurochemistry*, 2012, **120**, 99-108.
54. M. Asai, C. Hattori, B. Szabo, N. Sasagawa, K. Maruyama, S. Tanuma and S. Ishiura, *Biochem Biophys Res Commun*, 2003, **301**, 231-235.
55. E. Jorissen, J. Prox, C. Bernreuther, S. Weber, R. Schwanbeck, L. Serneels, A. Snellinx, K. Craessaerts, A. Thathiah, I. Tesseur, U. Bartsch, G. Weskamp, C.P. Blobel, M. Glatzel, B. De Strooper and P. Saftiq, *J Neurosci*, 2010, **30**, 4833-4844.
56. N.M. Hooper and A.J. Turner, *Curr Med Chem.*, 2002, **9**, 1107-1119.
57. J. Mills and P.B. Reiner, *Neuroscience*, 1999, **94**, 1333-1338.
58. A.Y. Hung, C. Haass, R.M. Nitsch, W.Q. Qiu, M. Citron, R.J. Wurtman, J.H. Growdon and D.J. Selkoe, *J Biol Chem*, 1993, **268**, 22959-22962.
59. D.M. Skovronsky, D.B. Moore, M.E. Milla, R.W. Doms and V.M. Lee, *J Biol Chem.*, 2000, **275**, 2568-2575.
60. G. Donmez, D. Wang, D.E. Cohen and L. Guarente, *Cell*, 2010, **142**, 320-332.

61. R. Postina, A. Schroeder, I. Dewachter, J. Bohl, U. Schmitt, E. Kojro, C. Prinzen, K. Endres, C. Hiemke, M. Blessing, P. Flamez, A. Dequenne, E. Godaux, F.V. Leuven and F. Fahrenholz, *J Clin Invest*, 2004, **113**, 1456–1464.
62. B.A. Bergmans and B. De Strooper, *Lancet Neurol*, 2010, **9**, 215-226.
63. B. De Strooper, W. Annaert, P. Cupers, P. Safting, K. Craessaerts, J.S. Mumm, E.H. Schroeter, V. Schrijvers, M.S. Wolfe, W.J. Ray, A. Goate and R. Kopan, *Nature*, 1999, **398**, 518-522.
64. M.S. Wolfe, W. Xia, B.L. Ostaszewski, T.S. Diehl, W.T. Kimberly and D.J. Selkoe, *Nature*, 1999, **398**, 513-517.
65. N. Takasugi, T. Tomita, I. Hayashi, M. Tsuruoka, M. Niimura, Y. Takahashi, G. Thinakaran and T. Iwatsubo, *Nature*, 2003, **422**, 438-441.
66. M. Vestergaard, T. Hamada and M. Takagi, *Biotechnology and Bioengineering*, 2008, **99**, 753-763.
67. L.D. Estrada and C. Soto, *Current Topic in Medicinal chemistry*, 2007, **7**, 115-126.
68. I. Hussain, D.J. Powell, D.R. Howlett, G.A. Chapman, L. Gilmour, P.R. Murdock, D.G. Tew, T.D. Meek, C. Chapman, K. Schneider, F.S. Ratcliffe, C. Dingwall and G. Christie, *Mol Cell Neurosci*, 2000, **16**, 609-619.
69. F.M. Laird, H. Cai, A.V. Savonenko, M.H. Farah, K. He, T. Melnikova, H. Wen, H.C. Chiang, G. Xu, V.E. Koliatsos, D.R. Borchelt, D.L. Price, H.K. Lee and P.C. Wong, *J Neurosci*, 2005, **25**, 11693-11709.
70. M.O. Chaney, S.D. Webster, Y.-M. Kuo and A.E. Roher, *Protein Engineering*, 1998, **11**, 761-767.
71. L. Qiut, C. Buie, A. Reay, M.W. Vaughn and K.H. Cheng, *J Phys Chem B.*, 2011 **115**(32), 9795-9812.
72. C. Soto, E.M. Castano, B. Frangione and N.C. Inestrosa, *The Journal of Biological Chemistry*, 1995, **270**, 363-3067.
73. J. Rajadas, C.W. Liu, P. Novick, N.W. Kelley, M. Inayathullah, M.C. LeMieux, V.S. Pande, *PLoS One*, 2011;**6**, e21776.
74. M.G. Zagorski and C.J. Barrow, *Biochemistry*, 1992, **31**, 5621-5631.
75. J.P. Lee, E.R. Stimson, J.R. Ghilardi, P.W. Mantyh, Y.-A. Lu, A.M. Felix,W. Llanos, A. Behbin, M. Cuings, M.V. Crielunge, W. Timms and J.E. Maggio, *Biochemistry*, 1995, **34**, 5191 -5200.
76. S. Zhang, N. Casey and J.P. Lee, *Fold Des*, 1998; **3**(5), 413-422.

77. J. Talafous, K.J. Marcinowski, G. Klopman and M.G. Zagorski, *Biochemistry* 1994, **33**, 7788-7796.
78. P.E. Fraser, J.T. Nguyen, W.K. Surewicz and D.A. Kirschner, *Biophys J.* 1991, **60**, 1190-1201.
79. J. Danielsson, J. Jarvet, P. Damberg and A. Graslund, *FEBS Journal*, 2005, **272**, 3938-3949.
80. C.J. Barrow, A. Yasuda, P.T.M. Kenny and M.G. Zagorski, *J Mol Biol*, 1992, **225**, 1075-1093.
81. T.L.S. Benzinger, D.M. Gregory, T.S. Burkoth, H. Miller-Auer, D.G. Lynn, R.E. Botto and S.C. Meredith, *Biochemistry*, 2000, **39**, 3491-3499.
82. O.N. Antzutkin, R.D. Leapman, J.J. Balbach and R. Tycko, *Biochemistry*, 2002, **41**, 15436-15450.
83. L.O. Tjernberg, D.J.E. Callaway, A. Tjernbergi, S. Hahne, C. Lilliehook, L. Terenius, J. Thyberg and C. Nordstedt, *The Journal of Biological Chemistry*, 1999, **274**, 12619-12625.
84. L.C. Serpell, C.C.F. Blake, and P.E. Fraser, *Biochemistry,* 2000, **39**, 13269-13275.
85. L.C. Serpell and J.M. Smith, *J Mol Biol*, 2000, **299**, 225-231.
86. I.W. Hamley, *Chem Rev,* 2012, **112**(10), 5147-5192.
87. M. Ahmed, J. Davis, D. Aucoin, T. Sato, S. Ahuja, S. Aimoto, J.I. Elliott, W.E.V. Nostrand and S.O. Smith, *Nature struc and Mol Biol*, 2010, **17**, 561-567.
88. T. Luhrs, C. Ritter, M. Adrian, D. Riek-Loher, B. Bohrmann, H. Dobeli, D. Schubert and R. Riek, *Proc Natl Acad Sci USA*, 2005, **102**, 17342-17347.
89. Y. Masuda, S. Uemura, A. Nakanishi, R. Ohashi, K. Takegoshi, T. Shimizu, T. Shirasawa and K. Irie, *Bioorg Med Chem Lett*, 2008, **18**, 3206-3210.
90. T. Luhrs, C. Ritter, M. Adrian, D. Riek-Loher, B. Bohrmann, H. Dobeli, D. Schubert and R. Riek, *PNAS*, 2005, **102**(48), 17342-17347.
91. M.S. Wolfe, *Scientifica (Cairo)*, 2014, **2014**, 757549.
92. J.L. Ables, J.J. Breunig, A.J. Eisch and P. Rakic, *Nat Rev Neurosci*, 2011; **12**(5), 269-283.
93. R. Olsauskas-Kuprys, A. Zlobin and C. Osipo, *OncoTargets and Therapy*, 2013, **6**, 943-955.
94. M. Citron, *Nature Reviews Neuroscience*, 2004, **5**,677-685.
95. A. Opar, *Nature Reviews Drug Discovery*, 2008, **7**, 717-718.
96. M. Citron, *Nature Reviews Drug Discovery*, 2010, **9**, 387-398.

97. G. Merlini, E. Ascari, N. Amboldi, V. Bellotti, E. Arbustini, V. Perfetti, M. Ferrari, I. Zorzoli, M.G. Marinone, P. Garini, M. Diegoli, D. Trizio and D. Ballibari, *Proc Natl Acad Sci USA*, 1995, **92**, 2959-2963.
98. R. Kisilevsky, L.J. Lemieux, P.E. Fraser, X. Kong, P.G. Hultin and W.A. Szarek, *Nat Med*, 1995, **1**, 143-148.
99. S.J. Wood, L. MacKenzie, B. Maleeff, M.R. Hurle and R. Wetzel, *J Biol Chem.*, 1996, **271**, 4086-4092.
100. W.P. Esler, E.R. Stimson, J.R. Ghilardi, A.M. Felix, Y.A. Lu, H.V. Vinters, P.W. Mantyh and J.E. Maggio, *Nat Biotechnol*., 1997, **15**, 258-263.
101. J. McLaurin, R. Golomb, A. Jurewicz, J.P. Antel and P.E. Fraser, *J Biol Chem.*, 2000, **275**, 18495-18502.
102. M. Pappolla, P. Bozner, C. Soto, H. Shao, N.K. Robakis, M. Zagorski, B. Frangione and J. Ghiso, *J Biol Chem*., 1998, **273**, 7185-7188.
103. A.L. Schwarzman, M. Tsiper, L. Gregori, D. Goldgaber, J. Frakowiak, B. Mazur-Kolecka, A. Taraskina, S. Pchelina and M.P. Vitek, *Amyloid*, 2005, **12**, 199-209.
104. N. Sun, S.A. Funke and D. Willbold, *Mini-Reviews in Medicinal Chemistry*, 2012, **12**, 388-398.
105. U. Murvai, K. Soos, B. Penke and M.S.Z. Kellermayer, *J Mol Recognit*, 2011, **24**, 453-460.
106. C. Soto, E.M. Sigurdsson, L. Morelli, R. Kumar, E. Castano and B. Frangione, *Nat Med*, 1998, **4**, 822-826.
107. B. Permanne, C.I. Adessi, G.P. Saborio, S. Fraga, M-J. Frossard, J.V. Dorpe, I. Dewachter, W.A. Banks, F.V. Leuven and C. Soto, *FASEB J*, 2002, **16**, 860-862.
108. C. Soto, M.S. Kindly, M. Baumann and B. Frangione, *Biochemical and Biophysical Research Communications*, 1996, **226**, 672-680.
109. P. Fraser, J. Nguyen, H. Inouye, W. Surewicz, D. Selkoe, M. Podlisny and D.A. Kirschner, *Biochemistry*, 1992, **31**, 10716-10723.
110. L.O. Tjernberg, J. Naslund, F. Lindqvist, J. Johansson, A.R. Karlstromi, J. Thyberg, L. Terenius and C. Nordstedt, *The Journal of Biological Chemistry*, 1996, **271**, 8545-8548.
111. L.O. Tjernberg, C. Lilliehook, D.J.E. Callaway, J. Naslund, S. Hahne, J. Thybergi, L. Terenius and C. Nordstedt, *The Journal of Biological Chemistry*, 1997, **272**, 12601-12605.
112. M.M. Pallitto, J. Ghanta, P. Heinzelman, L.L. Kiessling and R.M. Murphy, *Biochemistry*, 1999, **38**, 3570-3578.

113. C. Soto, M.S. Kindy, M. Baumann and B. Frangione, *Biochemical and Biophysical Research Communications*, 1996, **226**, 672-680.
114. J.C. Chatham and S.J. Blackband, *ILAR J*, 2001, **42**, 189-208.
115. R. Badar-Goffer and H. Bachelard, *Essays in Biochemistry*, Portland Press, London, 1992.
116. Q. Teng, *Structural Biology Practical NMR Application*, Springer, 2005.
117. I.P. Gerothanassis, A. Troganis, V. Exarchou, and K. Barbarossou, *Chemistry Education: Research and Practice in Europe*, 2002, **3**(2), 229-252.
118. J.N.S. Evans, *Biomolecular NMR Spectroscopy*, Oxford University Press, New York, 1995.
119. P.J. Hore, *Nuclear Magnetic Resonance*, Oxford Science Publication, New York, 1995.
120. M.H. Levitt, *Spin Dynamics Basics of nuclear magnetic resonance*, 2 ed, John Wiley and Sons Ltd., Sussex, UK, 2002.
121. J. Killer, *Understanding NMR Spectroscopy*, John Wiley and Sons Ltd., 2 ed, Sussex, UK, 2002.

Chapter 2
Aggregation properties of amyloid beta (25-35)

2.1 Introduction

The segments of the Aβ that participate in aggregation are mostly composed of 40 to 42 amino acids. The other segments, such as $A\beta_{25-35}$ (GSNKGAIIGLM) are also found in AD brains apart from the full length of beta amyloid[1]. $A\beta_{25-35}$ retains several properties of the full-length Aβ, such as an amphiphilic nature and aggregation properties[1]. However, the small size of $A\beta_{25-35}$ makes it a more convenient model system for examining the structural modifications of Aβ that occur in AD.

Pike *et al* (1995) reported that $A\beta_{25-35}$ possesses the same level of toxic properties as the full length amyloid peptide $A\beta_{1-42}$, introducing amyloid toxicity on cultured hippocampal neurons[2]. Misiti *et al* (2005) reported that small fragment, $A\beta_{25-35}$ has ability to induce toxicity on PC12 cell line (a clonal line of rat pheochromocytoma)[3]. They also found that $A\beta_{25-35}$ induced toxicity is not related to any biochemical characteristics of apoptosis (programmed cell death in multicellular organisms) using 3-[(4,5-dimethylthiazol-2-yl)-5,3-carboxymethoxyphenyl]-2-(4-sulfophenyl)-2H tetrazolium salt (MTS) cell proliferation assay[3]. Clementi *et al* (2005) reported that $A\beta_{25-35}$ in monomeric (non-aggregated) conformations may cause neuronal toxicity. They also suggested that $A\beta_{25-35}$ in monomeric structure may enter into the cell of isolated rat brain cells and mitochondria[4]. However, the exact molecular mechanism of amyloid beta aggregation and toxicity still remains unclear.

2.1.1 Amyloid beta structure in solution

The study of the structural characteristics of peptide, Aβ in soluble form constitutes a fundamental approach to develop molecules against amyloidosis. The detailed structures of $A\beta_{25-35}$ in water are not yet fully understood[5]. However, it is important to determine the $A\beta_{25-35}$ monomeric or α-helix structures, which may be crucial to understand the early properties of amyloid aggregates and the subsequent shape and structure of amyloid fibrils[5]. It is reported that amyloid fibrils may exhibit different morphologies from different monomeric structures and their intermediate species were investigated by AFM, EM, CD and X-ray diffraction methods[6, 7]. By using EM and SS NMR, Petkova *et al* (2005) suggested that different sample preparation methods and conditions (temperature, pH and organic solvents) of amyloid beta produce diverse primary amyloid seeds (monomeric form) which develop into various morphologies of amyloid fibrils[7]. Due to inherent problems related to handing $A\beta_{25-35}$

in water, D'Ursi *et al* (2004) used water/fluoro-alcohol mixtures to determine the 3D structure of $A\beta_{25\text{-}35}$[8].

The conformations of full length amyloid peptide have been investigated by various biphysical methods such as NMR, EM, CD and FTIR and the spectra suggested that the fibrils of Aβ contain a high amount of β-sheet content[9, 10]. Therefore the 2D structure of amyloid beta has been explored in various solvents through FTIR and CD spectroscopy. Wei and Shea (2006) revealed that $A\beta_{25\text{-}35}$ specially exhibit α-helical structure in apolar organic solvent (HFIP)[11]. However, in water, $A\beta_{25\text{-}35}$ adopts distorted coil structures with a reduced size β-hairpin conformation using liquid NMR and simulations methods[11]. The β-hairpin conformation is formed between amino acids G29 and A30 and stabilized by H-bonds between peptide residues K28-I31, N27-I32 and S26-G33[11] as shown in figure 2.1.1.

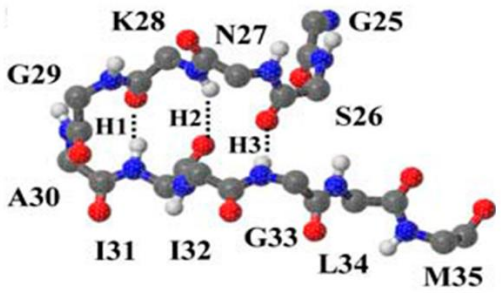

Figure 2.1.1 Schematic diagram of β-hairpin conformation of $A\beta_{25\text{-}35}$. β-turn is formed between residues G29 and A30 with two short β-strands at residues N27-K28 and I31-I32[11].

Kohno *et al* (1996) examined $A\beta_{25\text{-}35}$ in lithium dodecyl sulfate micelles using 2D ^{1}H NMR spectroscopy. They reported that the first four residues of the N-terminus are hydrophilic in nature and the remaining seven residues of C-terminus are hydrophobic[12]. The C-terminal residues of $A\beta_{25\text{-}35}$ are anchored into the membrane as α-helical conformation and the N-terminal residues are submerged into the solvent which act as a flexible structure[12]. Shanmugam and Polavarapu (2004) suggested that $A\beta_{25\text{-}35}$ may adopt β-sheet confirmation in solution (methanol), gel (prepared from methanol/acidic acetate buffer), and film (formed from methanol through evaporation) using IR absorption, ECD and VCD spectroscopy[13]. $A\beta_{25\text{-}35}$ residues from I31 to M35 of C- terminal form a β-turn conformation and the residues from 25G to A30 of N-terminal are involved in the formation of β-sheet[13]. Amyloid peptides may acquire α-helix conformation in fluorinated alcohols (HFIP) and adopt β-conformations (either β-turn or β-sheet) in water or buffer, which can be altered by peptide purification/preparation process,

peptide concentration, incubation time and pH[8-14]. CD spectroscopy data suggest that $A\beta_{25-35}$ at low concentration (0.1mM) can adopt coil, β-turn and β-sheet conformations in phosphate buffer saline (PBS)[8].

2.1.2 Amyloid beta aggregation properties

The Aβ in apolar solvent (mixture of HFIP/water) and micelles models suggest that the monomeric α-conformations may be the possible early structure of the amyloid peptides[11, 15]. Based on recent studies, the β-turn structure of amyloid peptide may be important to initiate aggregation[11, 16]. NMR, VCD and ECD data suggest that the C-terminus hydrophobic region of two $A\beta_{25-35}$ may interact and form dimers[11, 13]. These dimers may be arranged parallel or antiparallel which are stabilized by H-bonds or hairpin structure at N-terminal regions and may further aggregate into fibrils[11, 13-18]. Khurana *et al* (2001) suggest that the amyloid aggregates may form intermediate conformations before fibril formation using NMR, CD, FTIR and X-ray scattering[19, 20]. *In vitro* studies suggest that monomeric form of Aβ aggregates follow nucleated polymerization mechanism[21]. The oligomeric nucleus of Aβ subsequently adds monomers at the end of nuclei very rapidly until the fibril formation[21]. The computer simulations data of Aβ suggest that the oligomerization of peptide occurs into two steps. In the first step, the amyloid monomers in solution form "molten" oligomers. In the next step, the oligomers reorganise and form a β- sheet rich fibrillar structure[22].

2.1.2.1 Beta breaker peptide

The development of new inhibitory molecules against amyloid fibril formation may be a fundamental approach to understand the disease mechanism and amyloid aggregation in AD. The misfolding and aggregation of Aβ peptide at an early stage is stopped by small fragments of peptide, known as β-sheet breaker that is competent to block the growth of Aβ[23]. It is reported that synthetic β-sheet breaker peptide, iAβ5 (LPFFD), has the ability to prevent the amyloid fibrils formation *in vitro*[23-25]. The amino acids sequence (LPFFD) of iAβ5 is homologous to hydrophobic region of $A\beta_{1-42 \text{ or } 1-40}$ (LVFFA) that is crucial for the specific interactions between β-sheet breaker and Aβ peptides. Specifically, the amino acid, proline of β-sheet breaker is vital for the disruption of intermolecular β-sheets formation during $A\beta_{1-42}$ or $A\beta_{1-40}$ aggregation[26-28].

Tjernberg *et al* (1996) found that full length amyloid peptides incorporating a small amyloid peptide fragment, KLVFF ($A\beta_{16-20}$) may bind $A\beta_{1-42}$ or $A\beta_{1-40}$ and inhibit beta sheet formation and amyloid fibril aggregation[29]. The amyloid sequence, KLVFF, has been identified as important region of Aβ during proteolytic cleavage of APP[29]. α-secretase cleaves APP between residues 16 (Lys) and 17 (Leu) of $A\beta_{1-42}$ or $A\beta_{1-40}$ and form p3 ($A\beta_{17-40}$ or $A\beta_{17-42}$), which is released by the action of γ-secretase during non-amyloidogenic process[30-32]. This pathway may interrupt the sequence KLVFF of Aβ. The non-amyloidogenic pathway suggests that p3 ($A\beta_{17-40}$ or $A\beta_{17-42}$) fragment does not contain toxic amyloidogenic properties either *in vitro* or *in vivo*[33]. It is reported that the C-terminus of the peptide sequence rather than KLVFF may be involved in polymerization and formation of fibrillar structure of $A\beta_{1-40}$ or $A\beta_{1-42}$ and p3[34, 35]. Many studies also suggest that amyloid peptide amino acid residues within or close to KLVFF ($A\beta_{16-20}$) are capable of forming beta-pleated sheet structures of beta amyloid peptide[36].

2.1.3 2D NMR spectroscopy

One dimensional NMR spectrum is called '1D' because it possesses one dimension frequency (ν), however in reality 1D spectrum also contains additional dimension of intensity[37] as shown in figure 2.1.3.1. 1D NMR peaks reveal the chemical site of particular atom i.e. chemical shift and intensity (integral). It also shows the multiplicity (splitting) of nuclei but is unable to tell about the connection between them[37].

Two dimensional (2D) NMR spectrum comprises two frequency dimensions. The intensity represents the third dimension and hence generally displays as contour/stacked plots[38] as shown in figure 2.1.3.2. The 2D spectrum is important to observe the coupling between individual nuclei[38]

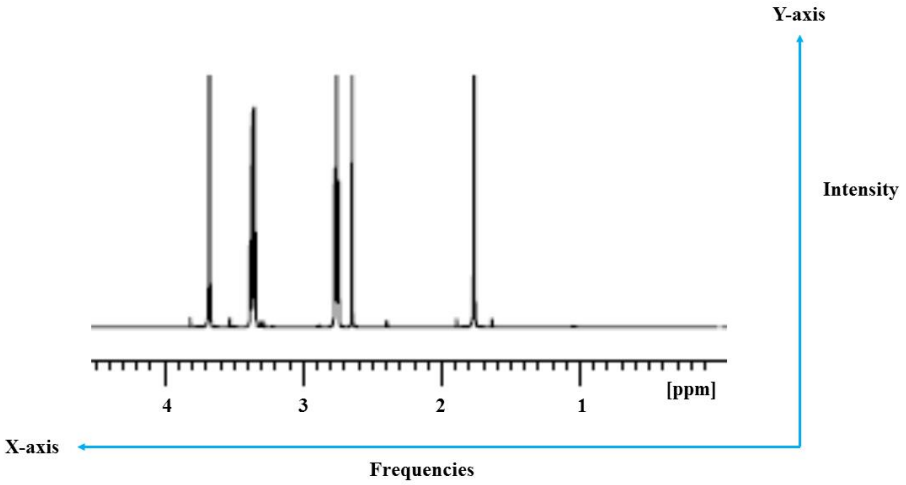

Figure 2.1.3.1One dimension (1D) NMR spectra. The X-axis represents the frequencies (chemical shifts in ppm) and Y-axis represents the intensity of nuclei[38].

.

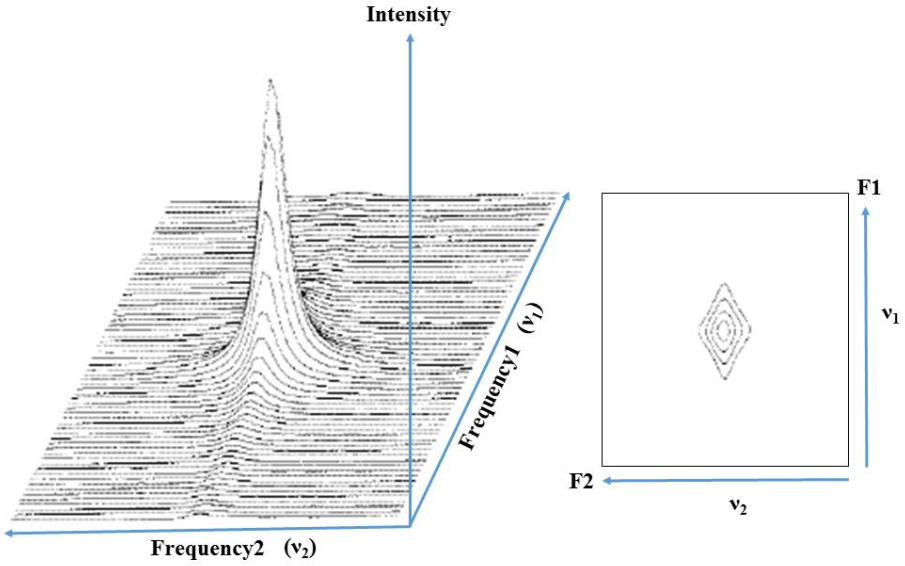

Figure 2.1.3.2Two dimension (2D) NMR spectra. According to the Bruker spectrometer, the X-axis represents the direct dimension, frequency2 (F2) and the Y-axis signifies the indirect dimension, frequency1 (F1). However, in Varian spectrometer, F2 is the indirect dimension and F1 is the direct dimension. The Z-axis represents the intensity[38].

2.1.3.1 Basic principle of 2D NMR

The fundamental principle of all 2D spectroscopies is based on 1D NMR. In 1D NMR, the gaining of signals begins directly after the excitation of a radiofrequency (rf) pulse. In 2D NMR, the spectrum is generated after a continuous series of 1D NMR processes, where a single delay is interrupted in length of time[37]. In other words, the measurement of FID of 2D NMR spectrum does not start immediatly after the pulse. Basically, the pulse sequence of 2D NMR is divided into preparation, evolution, mixing and detection periods as shown in figure 2.1.3.3. The evolution time (t_1) represents the time period between preparation and mixing whereas the detection time (t_2) signifies the acquisition of signals[37-39]. In the preparation period, the magnetisation is generally arranged along the transverse axis. The magnetisation develops with chemical shifts during evolution time (t_1). In the mixing period, the coherences are shifted from one spin (F1) to another spin (F2). The signals are finally collected as an FID during the detection time (t_2)[37-39]. If the two spins are dissimilar then the coherence transfer generates cross peaks otherwise it produces diagonal peaks[38, 39] as shown in figure 2.1.3.4.

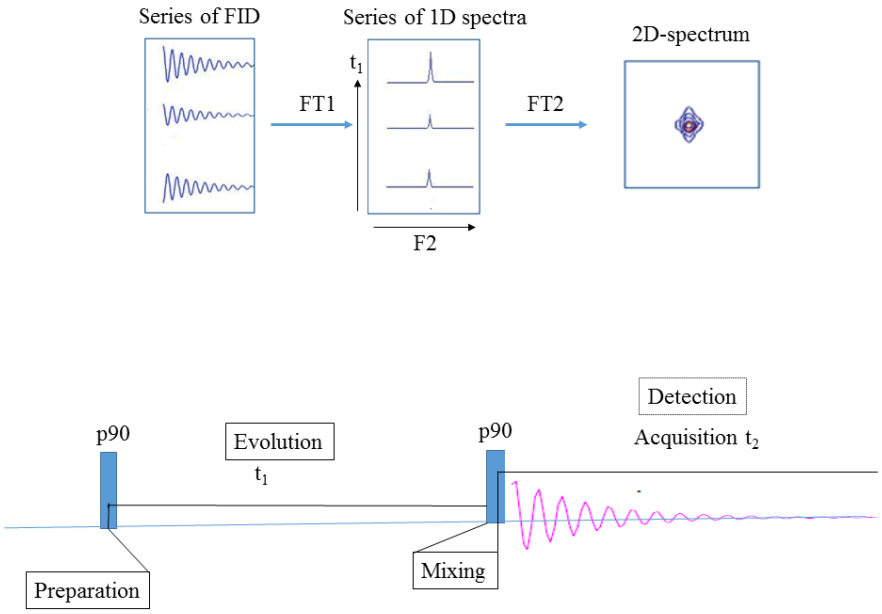

Figure 2.1.3.3 Schematic diagram of 2D NMR pulse program. Series of FID are Fourier transformed (FT) into a series of 1D spectra. These 1D spectra Fourier transformed relating to t_1 generate 2D spectrum (top figure) at a preparation period (p90 or pulse 90°). During evolution time (t_1), the magnetizations evolve as chemical shifts. Later in the mixing period, coherences are transferred from one spin system to another through bond or space or chemical exchange. Finally signals are collected in the detection period (t_2) and an FID generates 2D spectra (bottom figure)[39].

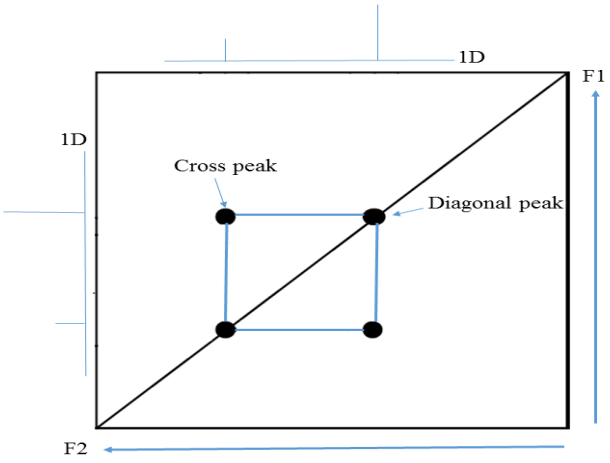

Figure 2.1.3.4 Schematic diagram of diagonal and cross peaks of 2D NMR spectrum. Cross peaks arise between spins with different frequencies and diagonal peaks generate due to similar spins frequencies. Diagonal peaks somehow signify the 1D spectrum[39].

2.1.3.2 COSY and TOCSY

COrrelation SpectroscopY (COSY) is a common 2D-NMR method that permits finding coupling between the nuclei[37-39]. In other words, COSY is a useful technique to correlate nuclei through their scalar couplings, which is commonly known as spin-spin coupling and facilitated by electrons through bonds. COSY spectrum provides information about three bond coupling (proton of one carbon to the adjacent carbon then to that carbon's proton). Both vertical and horizontal dimensions deliver chemical shifts[37-39]. Diagonal peaks of COSY spectrum represent the normal 1D spectrum whereas cross peaks are generated due to spin-spin coupling and appear as a pair in coordinated places of the diagonal peaks[34-35] as shown in figure 2.1.3.5.

TOtal Correlation SpectroscopY (TOCSY) is another important 2D-NMR method to determine the correlation between nuclei of scalar coupled spin systems. More precisely, it correlates all protons of a same spin system[37-39] (Figure 2.1.3.5).

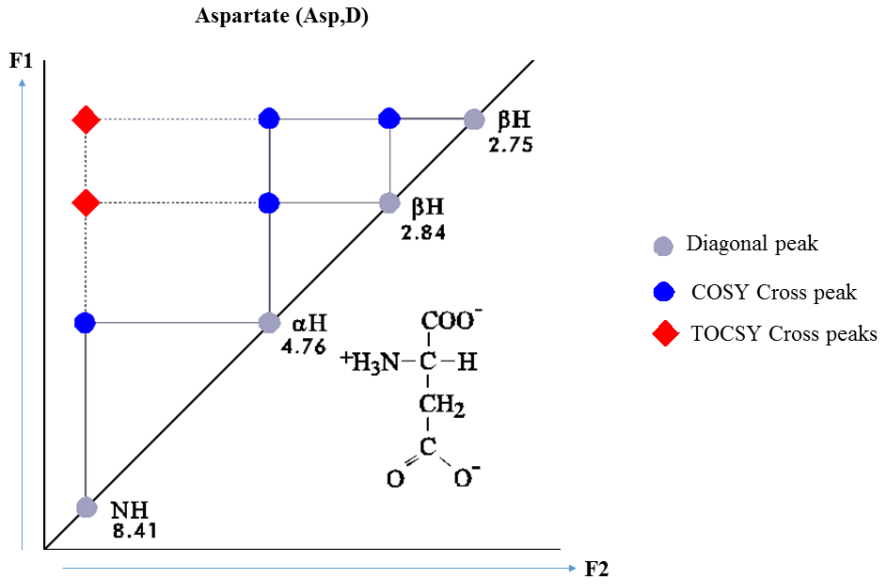

Figure 2.1.3.5 COSY and TOCSY spectrum of a typical aspartate amino acid[40]. In COSY, proton cross peaks are spin-spin coupled whereas in TOCSY the cross peaks of all protons correlate in a same spin system[40].

2.1.4 Aims

The main objective of this study was to investigate the aggregation properties of amyloid peptide, $A\beta_{25-35}$ with beta breaker peptide (KLVFF) by liquid NMR.

2.2 Materials

Chemicals were purchased from Sigma-Aldrich, Alfa Aesar, and Novabiochem at the highest grade of purity available, and were used as received. Peptide grade DMF was purchased from Fisher Scientific. Electrospray ionisation (ESI) mass spectra were performed on a Varian 500-MS ion trap spectrometer, equipped with a Varian Prostar 212LC binary gradient pumping system and a Varian ProStar 410 autosampler. A standard Varian ESI source was used operating in positive ion mode. Data was acquired and processed using a varian workstation software. Solid phase extractions were performed on Supelco Discovery DSC-18 cartridges (1 g). RP-HPLC analyses were performed on a system consisting of a Perkin Elmer series 200 LC pump, and a Perkin Elmer 785A UV/vis detector. The separations were performed on a Gemini C18, 5 µ, 150 x 4.6 mm, 110 Å (Phenomenex, UK), equipped with a SecurityGuard C18 (ODS) 4 x 3.0 mm ID guard column (Phenomenex, UK) at a flow rate of 1 mL/min. The mobile phase consisted of 0.1% TFA in water (solvent A) and 0.1% TFA in acetonitrile (solvent B). Gradient: 0.0–10.0 min 0-95% solvent B, 10.0–15.0 min 95% solvent B, 15.0–15.1 min at 95-5% solvent

B, 15.1–18.0 min 5% solvent B. $A\beta_{25-35}$ was purchased from Stratech Scientific Ltd., Newmarket Suffolk, UK.

2.3 Methods

2.3.1 Synthesis of peptide KLVFF

The beta breaker peptide, KLVFF was prepared and gifted by Dr. Francesca Giuntini.

The synthesis of the pentapeptide was accomplished manually in a 6 mL fritted SPE tube (Supelco, UK), equipped with a cap and plastic valve (Chromabond, UK) according to the Fmoc/t-Bu strategy. Loading of the resin was achieved by treating 2-chlorotrityl chloride polystyrene resin (300 mg of 1.22 mmol/g loading resin, 0.37 mmol) with a solution of *N*-α-Fmoc-phenylalanine (170 mg, 0.44 mmol) and DIPEA (305 μL, 1.75 mmol) in dry DCM (5 mL) for 120 min. Unreacted sites on the resin were capped by treatment with a solution of DCM/MeOH/DIPEA (3:1:0.5 v/v/v, 5 mL, 2 x 15 min). The first residue loading was measured spectrophotometrically, and was estimated to be 0.34 mmol/g. Coupling reactions were performed by treating the resin (400 mg) with a solution of *N*-α-Fmoc-amino acid (2 equiv relative to the resin loading), PyBOP (1.9 equiv) and diisopropylethylamine (4 equiv) in DMF (5 mL) for 45 min. The efficiency of the coupling reactions was assessed by Kaiser test[41]. *N*-α-Fmoc deprotection was performed by treatment with piperidine/DMF (1:4 v/v, 10 mL/g resin, 4 x 3 min).

The cleavage was performed by treating 150 mg of the *N*-α-Fmoc-deprotected peptidyl-resin with TFA/water/TIS (95/2.5/2.5 v/v/v, 1 h). The cleavage solution was concentrated to a small volume and the crude peptide was precipitated by addition of diethyl ether, recovered by centrifugation, and triturated with diethyl ether (10mL). The residue was dissolved in 0.5 mL of 0.01% aqueous TFA and purified by filtration on Supelco Discovery DSC-18 cartridges (1 g), eluting with 0.1% TFA in acetonitrile/water (5/95). The solvent was evaporated, the residue was taken in MeOH, and the TFA salt of the peptide was recovered from the solution by precipitation with diethyl ether and centrifugation. The white solid was dried *in vacuo* (22 mg, 67 %). RP-HPLC (detector: λ = 220nm): t_R = 6.47 min; ESI-MS (m/z): 653.4 $[M+H]^+$ ($C_{50}H_{78}N_9O_{13}S$ requires 652.4)

2.3.2 Preparation of Aβ/KLVFF mixtures

Aggregation experiments were performed by re-suspending $A\beta_{25-35}$ in 10mM sodium phosphate buffer, 10mM $MgCl_2$, 0.1mM EDTA, 10% (v/v) D_2O pH 7.2 (degassed with argon) to a concentration of 400μM. Equimolar beta breaker peptide (KLVFF) was included in samples where appropriate.

2.3.3 NMR data acquisition and processing

All data were acquired on a 500 MHz Bruker Avance II NMR spectrometer. ^1H measurements were performed with 512 scans at 30 minute intervals at 278K. 2D COSY and TOCSY spectra were acquired at 278K. For each spectrum, 64 transients were collected using 16 dummy scans with spectral widths of 12 ppm in both dimensions, using 128 complex points for F2 and 64 complex points for F1. All chemical shifts were measured from the two-dimensional TOCSY spectra. The solvent signal was suppressed using 90° pulse sequence with gradients. Spectra were processed using standard Bruker software (TOPSPIN, version 1.3) and analyzed with CCPN software (CcpNmr Analysis, version 2.0.2).

2.4 Results

2.4.1 Aggregation properties of Aβ25-35 in the presence and absence of KLVFF in solution

The $A\beta_{25-35}$ has the ability to aggregate during aqueous contact[15]. Liquid NMR spectroscopy was used to assign the residues of $A\beta_{25-35}$. To avoid immediate aggregation of $A\beta_{25-35}$, the sample was dissolved in cold (4°C) sodium-phosphate buffer pH7.2 and prepared inside an ice-container. The sample of $A\beta_{25-35}$ (400µM) was measured by ^{1}H NMR immediately after preparation using 512 scans and 278K. The samples were prepared according to the protocol described in section 2.3 and measured at 30 minutes interval with constant temperature (278K) by ^{1}H NMR.

The proton NMR signals of $A\beta_{25-35}$ including methyl groups appeared on the spectrum when the sample was measured immediately after preparation as shown in figure 2.4.1.1D. The NMR signal of the methyl groups were lost after incubation for 24 hours at 278K (Figure 2.4.1.1C). This phenomenon suggests that $A\beta_{25-35}$ may aggregate in the solution during the time course. After addition of equimolar KLVFF to $A\beta_{25-35,}$ the NMR spectra remain unchanged in both conditions (Figure 2.4.1.1A&B). These NMR spectra confirmed that KLVFF may have ability to stop the aggregation of $A\beta_{25-35}$ in solution.

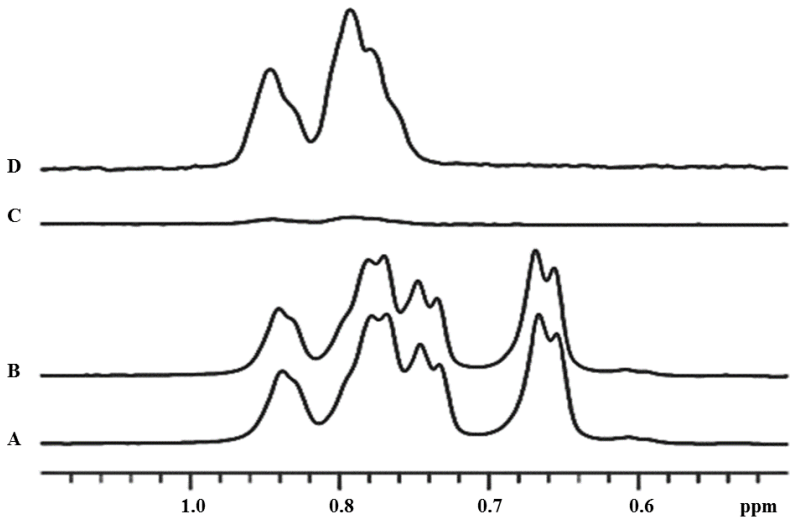

Figure 2.4.1.1 Methyl region of the liquid state ^{1}H NMR spectra for Aβ25-35 (A) immediately after preparation and (B) after incubation at 278K for 24 hours. $A\beta_{25-35}$ and equimolar $A\beta_{16-20}$ (C) immediate after sample preparation and (D) after incubation at 278K for 24 hours.

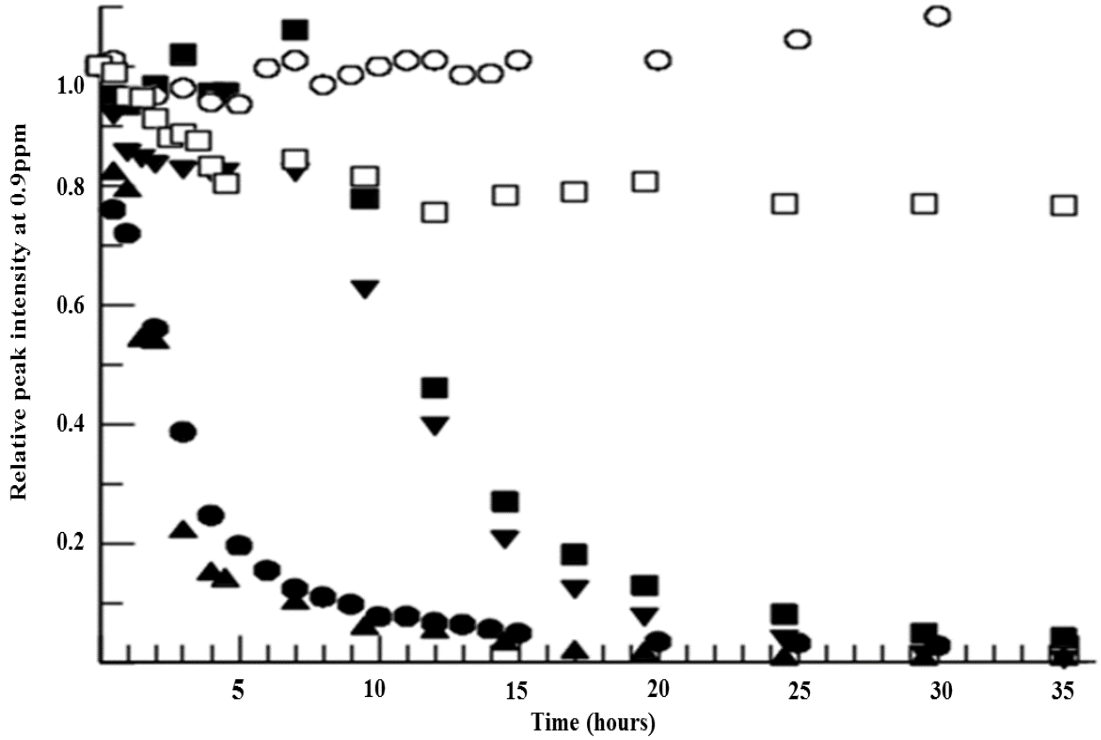

Figure 2.4.1.2 Time course of $A\beta_{25-35}$ aggregation in presence and absence of equimolar KLVFF in sodium phosphate buffer at pH7.2 and temp 278K**.** Filled squares, circles and triangles represent the $A\beta_{25-35}$ without KLVFF. The aggregation rate of $A\beta_{25-35}$ is impossible to duplicate. $A\beta_{25-35}$ aggregation may occur immediately (filled circles and upright triangles) or after a substantial lag phase (filled squares and inverted triangles). However in the presence of KLVFF, the solubility of $A\beta_{25-35}$ (empty squares and circles) is maintained throughout.

Relative peak intensity was calculated at 0.9ppm (peptide methyl groups) and the graph is plotted against time. The relative peak intensities of $A\beta_{25-35}$ show asymmetrical aggregation rates. The plots of $A\beta_{25-35}$ also show an irregular lag phase before the onset of aggregation (Figure 2.4.1.2). The graph suggests that $A\beta_{25-35}$ may acquire complete fibrillation after 24 hours. However, the graphs of relative peak intensity of $A\beta_{25-35}$ plus KLVFF remain unchanged over the time course (Figure2.4.1.2). The data suggest that KLVFF may obstruct the $A\beta_{25-35}$ aggregation.

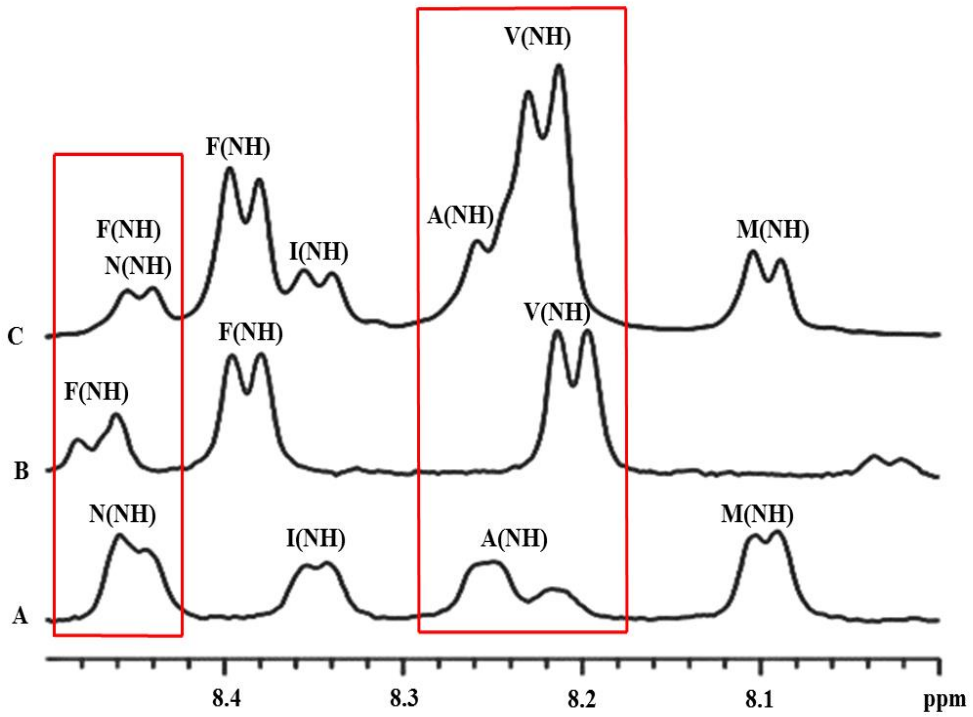

Figure 2.4.1.3 ^{1}H NMR spectra of peptide amide regions of (A) $A\beta_{25\text{-}35}$ (B) KLVFF (C) equimolar mixture of $A\beta_{25\text{-}35}$ and KLVFF. The amide peaks of valine and phenylalanine of KLVFF undergo a shift when the $A\beta_{25\text{-}35}$ are mixed.

The spectrum of co-dissolved samples of $A\beta_{25\text{-}35}$ plus KLVFF suggest that valine(18) and phenylalanine(20) amide peaks of KLVFF undergo a shift with alanine and asparagine of $A\beta_{25\text{-}35}$ as shown in figure 2.4.1.3C. The spectra clearly suggest that the interactions between two peptide species may be responsible for the inhibition of amyloid peptide aggregation.

2.4.2 NMR spectroscopy of KLVFF in solution

The beta breaker peptide, KLVFF, is homologous to $A\beta_{16\text{-}20}$ of amyloid peptide[42]. It has been suggested that the KLVFF motif may be accountable for the aggregation of $A\beta_{1\text{-}42/1\text{-}40}$ using CD, NMR and atom molecular dynamics simulations [43, 44]. Due to low solubility in water, KLVFF (400μM) was dissolved in 10mM sodium phosphate buffer containing 0.1mM EDTA and 10% (v/v) D_2O plus 15μl TMS. Sodium phosphate buffer with pH 7.2 was used because at this pH KLVFF did not aggregate over a long period of time. The protocol of KLVFF sample preparation and NMR measurement are described in section 2.3.2 and 2.3.3.

The ^1H NMR spectrum of KLVFF in sodium phosphate buffer solution is shown in figure 2.4.2.2. Proton signals of NH, CH, CH_2 and CH_3 groups of KLVFF were assigned by analysing cross-peaks of 2D COSY and TOCSY (Figure 2.3.2.3) spectra using CCPN software (CcpNmr analysis software version 2.0.2). The spectra (1D or 2D) were externally referenced to tetramethylsilane (TMS) at zero ppm. The corresponding chemical shifts of KLVFF are listed in table 2.4.1.

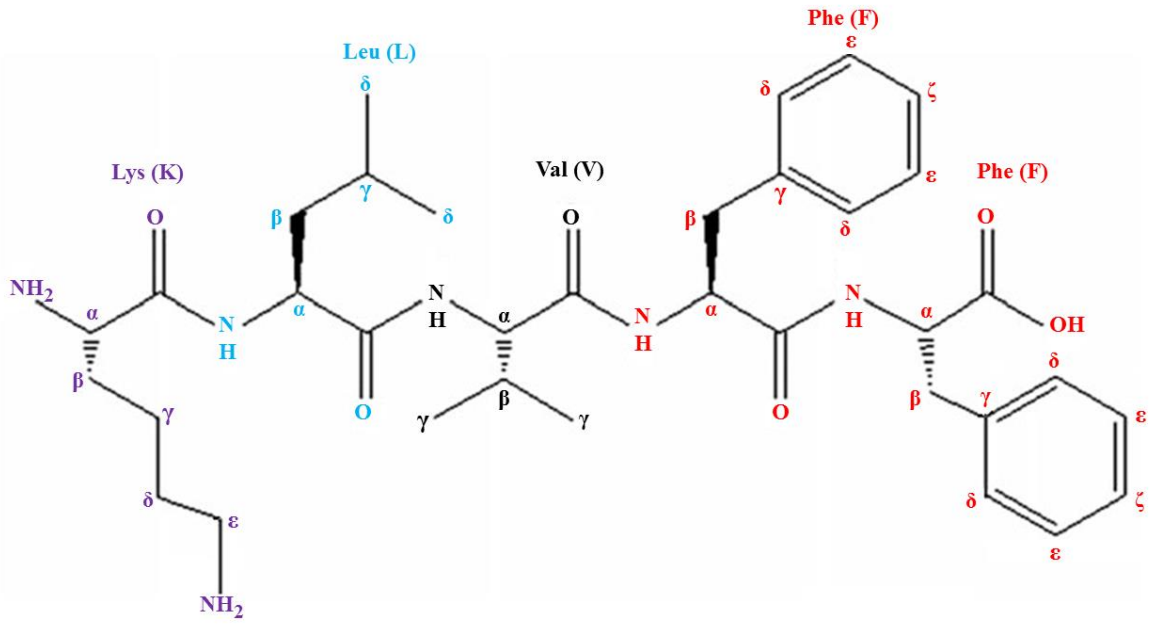

Figure 2.4.2.1 Chemical structure of beta breaker peptide KLVFF.

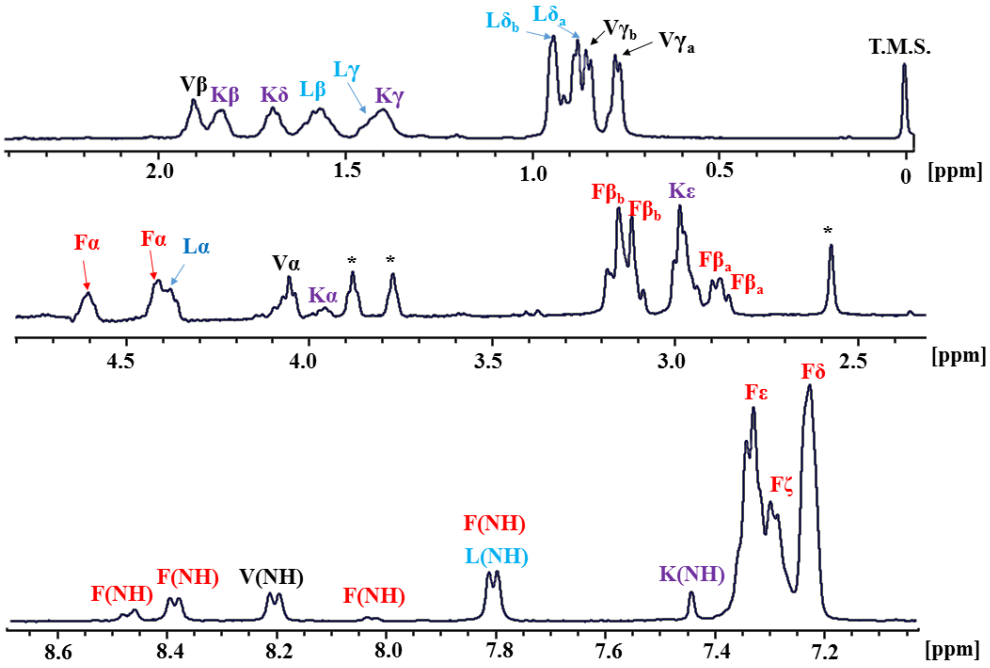

Figure 2.4.2.2 ^{1}H NMR spectrum of KLVFF in sodium phosphate buffer at pH 7.2 and T=278K. Peaks are assigned by analysing cross-peaks of 2D COSY and TOCSY spectra. Peaks labelled as "*" are unassigned peaks. (F-phenylalanine, K-lysine, L-leucine, V-valine).

The proton peaks of KLVFF appeared between 2.5 and 2.6ppm (one peak) as well as 3.7 and 3.9ppm (two peaks) were unassigned (Figure 2.4.2.2). These peak signals may be due to the impurity in aqueous solution or from beta breaker peptide. Further, to check the error in the sample preparation, four different samples were prepared from four different stocks of beta breaker peptide (two stocks were prepared by Dr. Fransicsa as described in section 2.3.1 and other two were purchased from Peptide Protein Research Ltd , UK). The NMR spectrum of each sample showed the same result. Each time, argon degassed and filtered buffer was used to prepare sample to avoid contaminations.

Table 2.4.1 ^{1}H NMR Chemical shifts of KLVFF

Residue	NH	Hα	Hβ	Hγ	others
Lys (K)-16	7.44ppm	3.96ppm	1.83ppm	1.40ppm	Hδ(1.69ppm) Hε(2.98ppm)
Leu (L)-17	7.80ppm	4.38ppm	1.58ppm	1.42ppm	$H\delta_b$(0.94ppm) $H\delta_a$(0.87ppm)
Val (V)-18	8.21ppm	4.05ppm	1.90ppm	γb(0.85ppm) γa (0.78ppm)	
Phe (F)-19	8.03ppm; 7.81ppm	4.41ppm	βb(3.15ppm) βa(2.90ppm)		Hε(7.33ppm);Hζ(7.28ppm) Hδ(7.22ppm)
Phe (F)-20	8.46ppm 8.39ppm	4.60ppm	βb(3.11ppm) βa(2.87ppm)		Hε(7.34ppm); Hζ(7.30ppm);Hδ(7.22ppm)

The 2D COSY spectrum of KLVFF showed the cross peaks of Lys between Hα(3.96ppm)-Hβ(1.83ppm), Hβ(1.83ppm)-Hγ(1.40ppm), and Hε(2.98ppm)-Hδ(1.69ppm). TOCSY spectrum cross peaks of Lys were found between NH(7.44ppm)- Hα(3.96ppm), Hα(3.96ppm)-Hε(2.98ppm), Hα(3.96ppm)-Hβ(1.83ppm), Hα(3.96ppm)-Hδ(1.69ppm), Hα(3.96ppm)-Hγ(1.40ppm), Hε(2.98ppm)-Hβ(1.83ppm), Hε(2.98ppm)-Hβ(1.83ppm), Hε(2.98ppm)-Hδ(1.69ppm), Hε(2.98ppm)-Hγ(1.40ppm), Hβ(1.83ppm)-Hδ(1.69ppm), Hβ(1.83ppm)-Hγ(1.40ppm), and Hδ(1.69ppm)-Hγ(1.40ppm) as shown in Figure 2.4.1.3.

Leu cross peaks were assigned between NH(7.80ppm)-Hα(4.38ppm), Hα(4.38ppm)-Hβ(1.58ppm), Hβ(1.58ppm)-Hγ(1.42ppm), Hβ(1.58ppm)-$H\delta_a$(0.87ppm), and Hγ(1.42ppm)-$H\delta_b$(0.94ppm) in the COSY spectrum of KLVFF. In 2D TOCSY spectrum, the cross peaks of Leu were assigned between NH(7.80ppm)-Hα(4.38ppm), Hα(4.38ppm)-Hβ(1.58ppm), Hα(4.38ppm)-Hγ(1.42ppm), Hα(4.38ppm)-$H\delta_b$(0.94ppm), Hα(4.38ppm)-$H\delta_a$(0.87ppm), Hβ(1.58ppm)-Hγ(1.42ppm), Hβ(1.58ppm)-$H\delta_b$(0.94ppm), Hβ(1.58ppm)-$H\delta_a$(0.87ppm) as shown in Figure 2.4.1.3.

A.

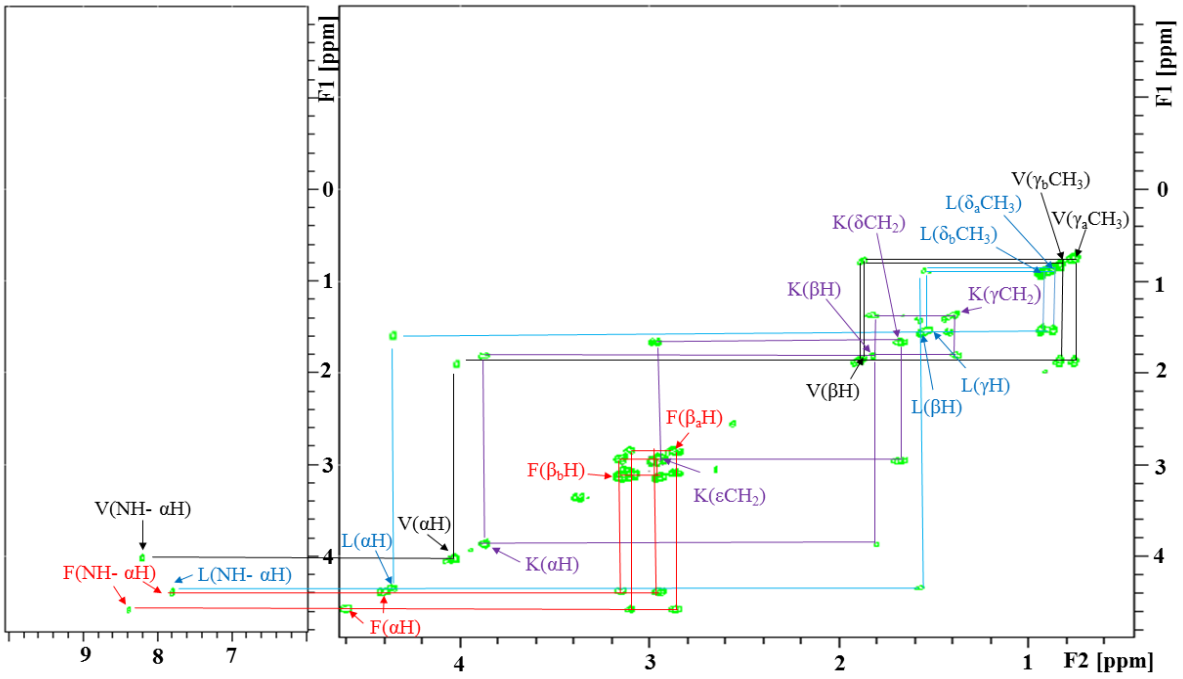

B.

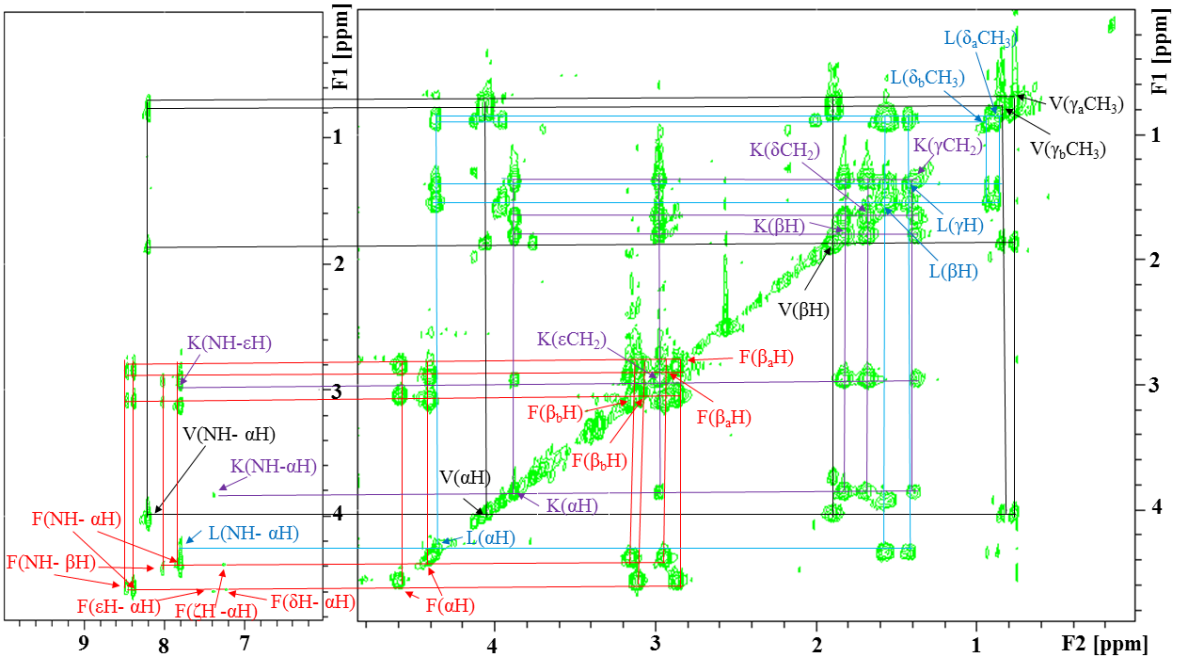

Figure 2.4.2.3 2D NMR spectra of KLVFF. (A) ^{1}H-^{1}H COSY NMR spectrum (B) ^{1}H-^{1}H TOCSY NMR spectrum of KLVFF in sodium-phosphate buffer at pH 7.2 and T=278K. Peaks from 0 to 5ppm (F1 and F2) show the diagonal and cross peaks from CH, CH_2 and CH_3 groups of KLVFF. The peaks between 6 to 10ppm (F2) and 0 to 5ppm (F1) show the cross peaks between NH (peptide amide group) and CH, CH_2 and CH_3 groups of KLVFF.

Val cross peaks of COSY spectrum of KLVFF were assigned between NH(8.21ppm)-Hα(4.05ppm), Hα(4.05ppm)-Hβ(1.90ppm), Hβ(1.90ppm)-$H\gamma_b$(0.85ppm), and Hβ(1.90ppm)-$H\gamma_a$(0.78ppm). TOCSY spectrum cross peaks of Val were assigned between NH(8.21ppm)-Hα(4.05ppm), NH(8.21ppm)-Hβ(1.90ppm), NH(8.21ppm)-$H\gamma_b$(0.85ppm), NH(8.21ppm)-$H\gamma_a$(0.78ppm), Hα(4.05ppm)-Hβ(1.90ppm), Hα(4.05ppm)-$H\gamma_b$(0.85ppm), Hα(4.05ppm)-$H\gamma_a$(0.78ppm), Hβ(1.90ppm)-$H\gamma_b$(0.85ppm), and Hβ(1.90ppm)-$H\gamma_a$(0.78ppm) as shown in Figure 2.3.1.3.

2D COSY spectrum of KLVFF showed two different Phe peaks in the positions between NH(8.39ppm)-Hα(4.60ppm), NH(7.81ppm)-Hα(4.41ppm), Hα(4.60ppm)-$H\beta_b$(3.11), Hα(4.41ppm)-$H\beta_b$(3.15), Hα(4.60ppm)-$H\beta_a$(2.87), Hα(4.41ppm)-$H\beta_a$(2.90ppm), $H\beta_b$(3.15ppm)- $H\beta_a$(2.90ppm) and $H\beta_b$(3.11ppm)- $H\beta_a$(2.87ppm). TOCSY cross peaks of Phe were assigned between NH(8.39ppm)-Hα(4.60ppm), NH(8.39ppm)-$H\beta_b$(3.11ppm), NH(8.39ppm)-$H\beta_a$(2.87ppm), NH(7.81ppm)-Hα(4.41ppm), NH(7.81ppm)-$H\beta_b$(3.15ppm), NH(8.39ppm)-$H\beta_a$(2.90ppm), Hα(4.60ppm)-$H\beta_b$(3.11), Hα(4.60ppm)-$H\beta_a$(2.87), Hα(4.41ppm)-$H\beta_b$(3.15), Hα(4.41ppm)-$H\beta_a$(2.90ppm), $H\beta_b$(3.15ppm)-$H\beta_a$(2.90ppm) and $H\beta_b$(3.11ppm)-$H\beta_a$(2.87ppm) as shown in Figure 2.3.1.3.

2.4.3 NMR spectroscopy of $A\beta_{25-35}$ and $A\beta_{25-35}$ plus KLVFF

2D COSY and TOCSY spectra of $A\beta_{25-35}$ were not effective to assign the residues because $A\beta_{25-35}$ aggregated quickly in the aqueous system. Without COSY and TOCSY spectra of $A\beta_{25-35}$, it is difficult to assign the residues of $A\beta_{25-35}$. To hinder the $A\beta_{25-35}$ aggregation, the co-dissolved sample of $A\beta_{25-35}$ and KLVFF was prepared and measured according to protocol described in section 2.3.2 and 2.3.3. ^{1}H NMR spectra of $A\beta_{25-35}$, KLVFF and $A\beta_{25-35}$ plus KLVFF in sodium phosphate buffer (pH7.2) are shown in Figure 2.4.3.2A, B and C, respectively.

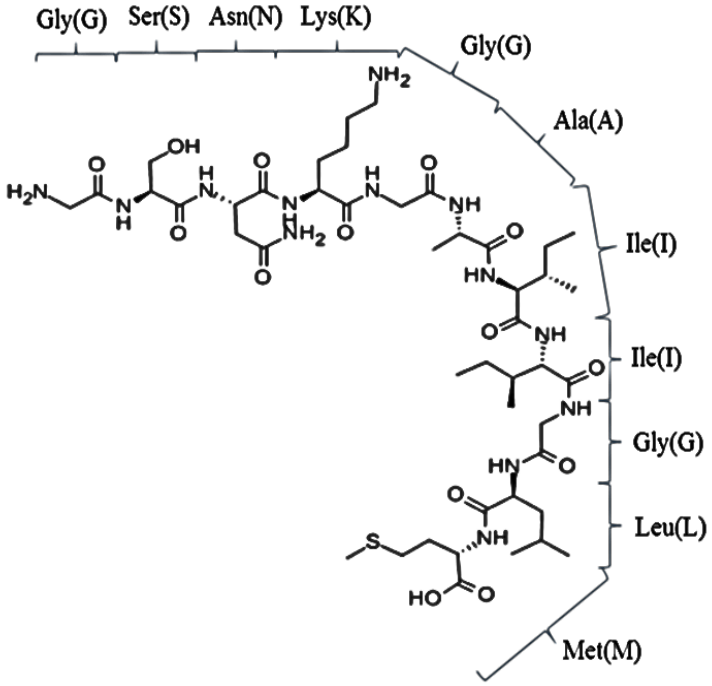

Figure 2.4.3.1 Chemical structure of $A\beta_{25-35}$ containing residues Gly-Ser-Asn-Lys-Gly-Ala-Ile-Ile-Gly-Leu-Met.

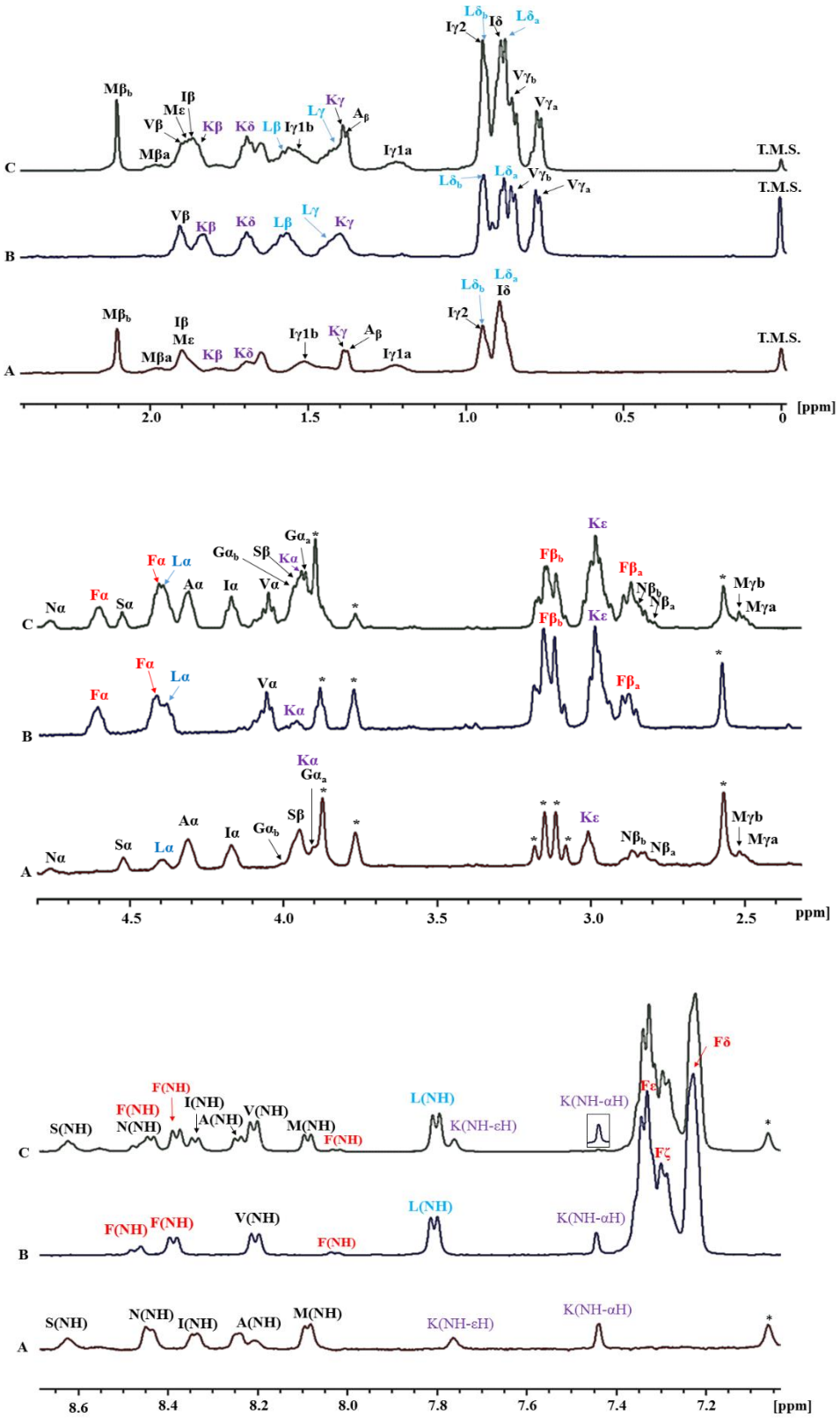

Figure 2.4.3.2 ^{1}H NMR spectrum of A) Aβ$_{25-35}$, B) KLVFF C) Aβ$_{25-35}$ plus KLVFF in sodium phosphate buffer solution at pH7.2 and T=278K. Peaks are assigned by analysing cross-peaks of 2D COSY and TOCSY spectra. Peaks labelled as "*" are unassigned peaks. (F-phenylalanine, K-lysine, L-leucine, V-valine, S-serine, N-asparagine, I-isoleucine, A-alanine, M-methionine, G-glycine).

Table 2.4.2 ^{1}H NMR Chemical shifts of Aβ$_{25-35}$

Residue	NH	Hα	Hβ	Hγ	others
Lys (K)	7.44ppm 7.76ppm	3.96ppm	1.83ppm	1.40ppm	Hδ(1.69ppm), Hε(2.98ppm)
Leu (L)	7.80ppm	4.38ppm	1.58ppm	1.42ppm	$H\delta_b$(0.94ppm), $H\delta_a$(0.87ppm)
Ser (S)	8.62ppm	4.52ppm	3.87ppm		
Asn (N)	8.45ppm	4.75ppm	β_a(2.80ppm) β_b(2.87ppm)		
Ala (A)	8.20ppm	4.30ppm	1.37ppm		
Met(M)	8.09ppm	4.31ppm	β_a(1.97ppm) β_b(2.10ppm)	γ_a(2.51ppm) γ_b(2.52ppm)	Hε(1.87ppm)
Ile(I)	8.33ppm	4.16ppm	1.87ppm	$\gamma 1_a$(1.21ppm) $\gamma 1_b$(1.51ppm) γ2(0.88ppm)	Hδ(0.87ppm)
Gly(G)		α_a(3.88ppm) α_b(4.07ppm)			

The COSY cross peaks of KLVFF plus Aβ$_{25-35}$ (red) and KLVFF (green) occur almost at the same positions of the residues (Figure 2.4.3.3A). The TOCSY spectrum suggests that the residues of KLVFF plus Aβ$_{25-35}$ (red) cross peaks appear at different positions, which are not found in the TOCSY spectrum of KLVFF (green; Figure 2.4.3.3B). These different cross peaks of KLVFF plus Aβ$_{25-35}$ residues of TOCSY spectrum characterise the Aβ$_{25-35}$ residues. The cross peaks between NH, CH, CH_2 and CH_3 groups of Aβ$_{25-35}$ plus KLVFF were assigned by using CCPN software (CcpNmr analysis software version 2.0.2). The spectra were externally referenced to TMS at zero ppm. The corresponding chemical shifts of Aβ$_{25-35}$ are listed in table 2.4.2.

A.

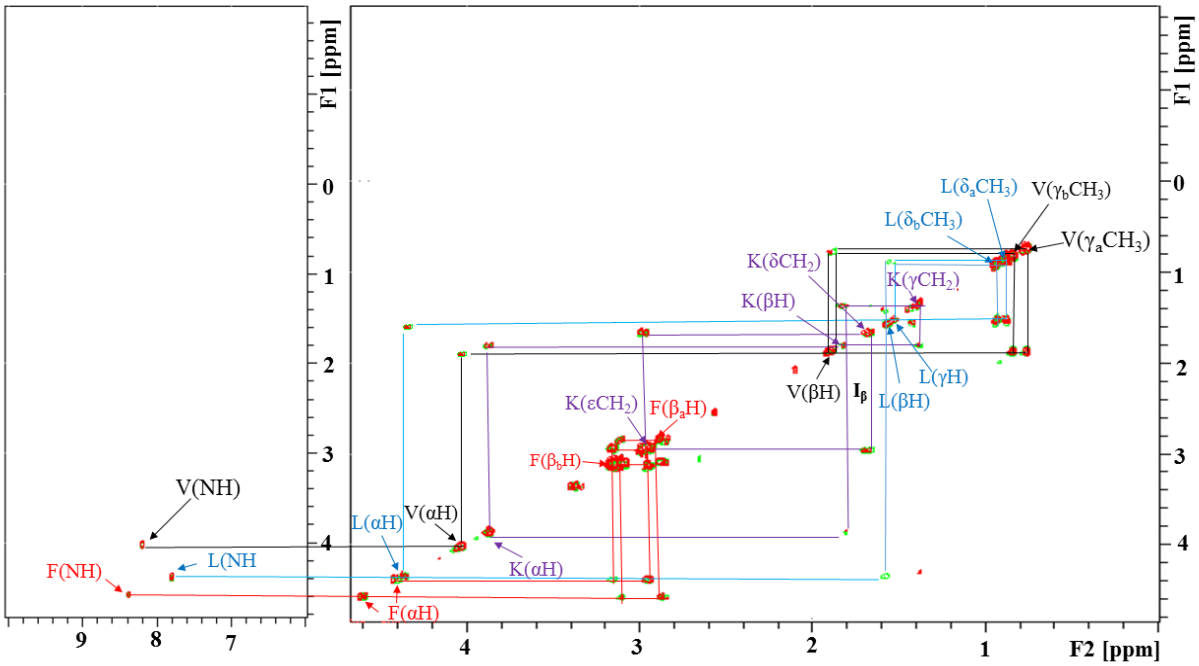

B.

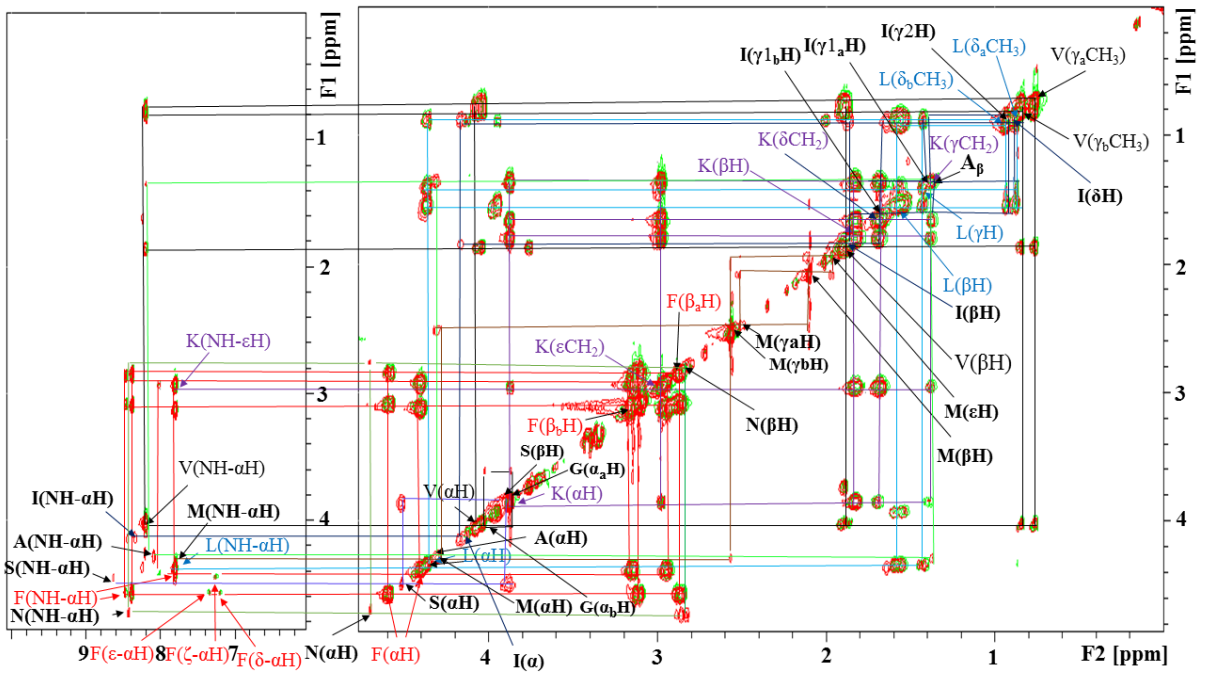

Figure 2.4.3.3 2D NMR spectra of KLVFF plus Aβ25-35. (A) ^{1}H-^{1}H COSY NMR spectrum (B) ^{1}H-^{1}H TOCSY NMR spectrum of KLVFF plus Aβ25-35 in sodium-phosphate buffer at pH 7.2 and T=278K. Peaks from 0 to 5ppm (F1 and F2) show the diagonal and cross peaks from CH, CH_2 and CH_3 groups of KLVFF plus Aβ25-35. The peaks between 6 to 10ppm (F2) and 0 to 5ppm (F1) show the cross peaks between NH (peptide amide group) and CH, CH_2 and CH_3 groups of KLVFF plus Aβ25-35. KLVFF diagonal and cross peaks (green) overlay with diagonal and cross peaks of KLVFF plus Aβ25-35 (red).

The 2D COSY spectrum of KLVFF showed the cross peaks of Lys between Hα(3.96ppm)-Hβ(1.83ppm), Hβ(1.83ppm)-Hγ(1.40ppm), and Hε(2.98ppm)-Hδ(1.69ppm). TOCSY spectrum cross peaks of Lys were found between NH(7.44ppm)- Hα(3.96ppm), NH(7.76ppm)-Hε(2.98ppm), Hα(3.96ppm)-Hε(2.98ppm), Hα(3.96ppm)-Hβ(1.83ppm), Hα(3.96ppm)-Hδ(1.69ppm), Hα(3.96ppm)-Hγ(1.40ppm), Hε(2.98ppm)-Hβ(1.83ppm), Hε(2.98ppm)-Hβ(1.83ppm), Hε(2.98ppm)-Hδ(1.69ppm), Hε(2.98ppm)-Hγ(1.40ppm), Hβ(1.83ppm)-Hδ(1.69ppm), Hβ(1.83ppm)-Hγ(1.40ppm), and Hδ(1.69ppm)-Hγ(1.40ppm) as shown in Figure 2.4.2.3.

Leu cross peaks assigned between NH(7.80ppm)-Hα(4.38ppm), Hα(4.38ppm)-Hβ(1.58ppm), Hβ(1.58ppm)-Hγ(1.42ppm), Hβ(1.58ppm)-$H\delta_a$(0.87ppm), and Hγ(1.42ppm)-$H\delta_b$(0.94ppm) in the COSY spectrum of KLVFF. In 2D TOCSY spectrum, the cross peaks of Leu assigned between NH(7.80ppm)-Hα(4.38ppm), Hα(4.38ppm)-Hβ(1.58ppm), Hα(4.38ppm)-Hγ(1.42ppm), Hα(4.38ppm)-$H\delta_b$(0.94ppm), Hα(4.38ppm)-$H\delta_a$(0.87ppm), Hβ(1.58ppm)-Hγ(1.42ppm), Hβ(1.58ppm)-$H\delta_b$(0.94ppm), Hβ(1.58ppm)- $H\delta_a$(0.87ppm) as shown in Figure 2.4.2.3.

TOCSY spectrum of KLVFF plus $A\beta_{25\text{-}35}$, the cross peaks of Ser positioned between NH(8.62ppm)-Hα(4.52ppm) and Hα(4.52ppm)-Hβ(3.87ppm). Asn cross peaks assigned between NH(8.45ppm)-Hα(4.75ppm), Hα(4.75ppm)-Hβa(2.80ppm) and Hα(4.75ppm)-Hβb(2.87ppm). Ala TOCSY cross peaks assigned between NH(8.20ppm)-Hα(4.30ppm), Hα(4.30ppm)-Hβa(1.37ppm). Gly cross peak assigned between $H\alpha_a$(3.88ppm)-$H\alpha_b$(4.07ppm) in the TOCSY spectrum of KLVFF plus $A\beta_{25\text{-}35}$ as shown in Figure 2.4.2.3B.

In 2D TOCSY spectrum of KLVFF plus $A\beta_{25\text{-}35}$, the cross peaks of Ile assigned between NH(8.33ppm)-Hα(4.16ppm), Hα(4.16ppm)-Hβ(1.87ppm), Hα(4.16ppm)-Hγ2(0.88ppm), Hα(4.16ppm)-Hδ(0.87ppm), Hβ(1.87ppm)-$H\gamma1_a$(1.21ppm), Hβ(1.87ppm)-$H\gamma1_b$(1.51ppm), Hβ(1.87ppm)-Hγ2(0.88ppm) and Hβ(1.58ppm)-Hδ(0.87ppm) as shown in figure 2.3.2.3B. The residue Met cross peaks assigned between NH(8.09ppm)-Hα(4.31ppm), Hα(4.31ppm)-$H\gamma_a$(2.51ppm), Hα(4.31ppm)-$H\gamma_b$(2.52ppm), $H\beta_a$(1.97ppm)-$H\gamma_a$(2.51ppm), $H\beta_b$(2.10ppm)-$H\gamma_b$(2.52ppm) and $H\beta_a$(1.97ppm)-Hε(1.87ppm) as shown in Figure 2.4.2.3B.

2.3.4 3-(4,5 Dimethylthiazol-2-yl)-2,5-diphenyltetrazolium bromide (MTT) cell-toxicity assay

The cell toxicity experiments of $A\beta_{25-35}$, KLVFF and $A\beta_{25-35}$ plus KLVFF on PC12 cell line were carried out by N. Acerra under supervision of Dr. J. Mason of the University of Essex, UK. The results are reproduced here with permission.

Rat phaeochromocytoma (PC12) cells were used to examine the effect of the toxicity of $A\beta_{25-35}$ and KLVFF plus $A\beta_{25-35}$. The MTT VybrantV cell proliferation assay kit (Invitrogen, UK) was used to measure the conversion of the water soluble MTT dye to formazan. The concentrations were determined by monitoring absorbance at 570nm. The change in absorbance can be converted to a percentage MTT reduction which can be used as an indicator of the PC12 cell health in the assay.

PC12 cells were maintained in RPMI 1640±2 mM glutamine medium mixed with 10% horse serum, 5% fetal bovine serum, supplemented with a 20mg/mL Gentamicin. Cells were transferred to a sterile 96-well plate with 30,000 cells per well. $A\beta_{25-35}$, KLVFF, and equimolar ratio of $A\beta_{25-35}$ plus KLVFF at different concentrations (1, 10, 100, 200 and 400μM) were added into PC12 cells of 96-well plate and incubated for 24 hrs at 37°C and 5% CO_2, prior to the addition of the MTT dye. About 10μl of the MTT dye was added to each well and incubated for another 4 hrs at 37°C and 5% CO_2. After that 100 μl of DMSO (stop/solubilization solution) was added to each well and incubated for 10 mins at room temperature. The absorbance was measured at 570nm by Versamax tunable microplate reader. Assay values for incubation with buffer were taken as 100% and inhibition of cell function by incubation with buffer containing peptide alone was taken as 0%. Raw data were then scaled as follows: (raw data point - peptide mean) / (buffer mean - peptide mean) × 100. The scaled mean for each data set was then plotted with the error given by the standard deviation.

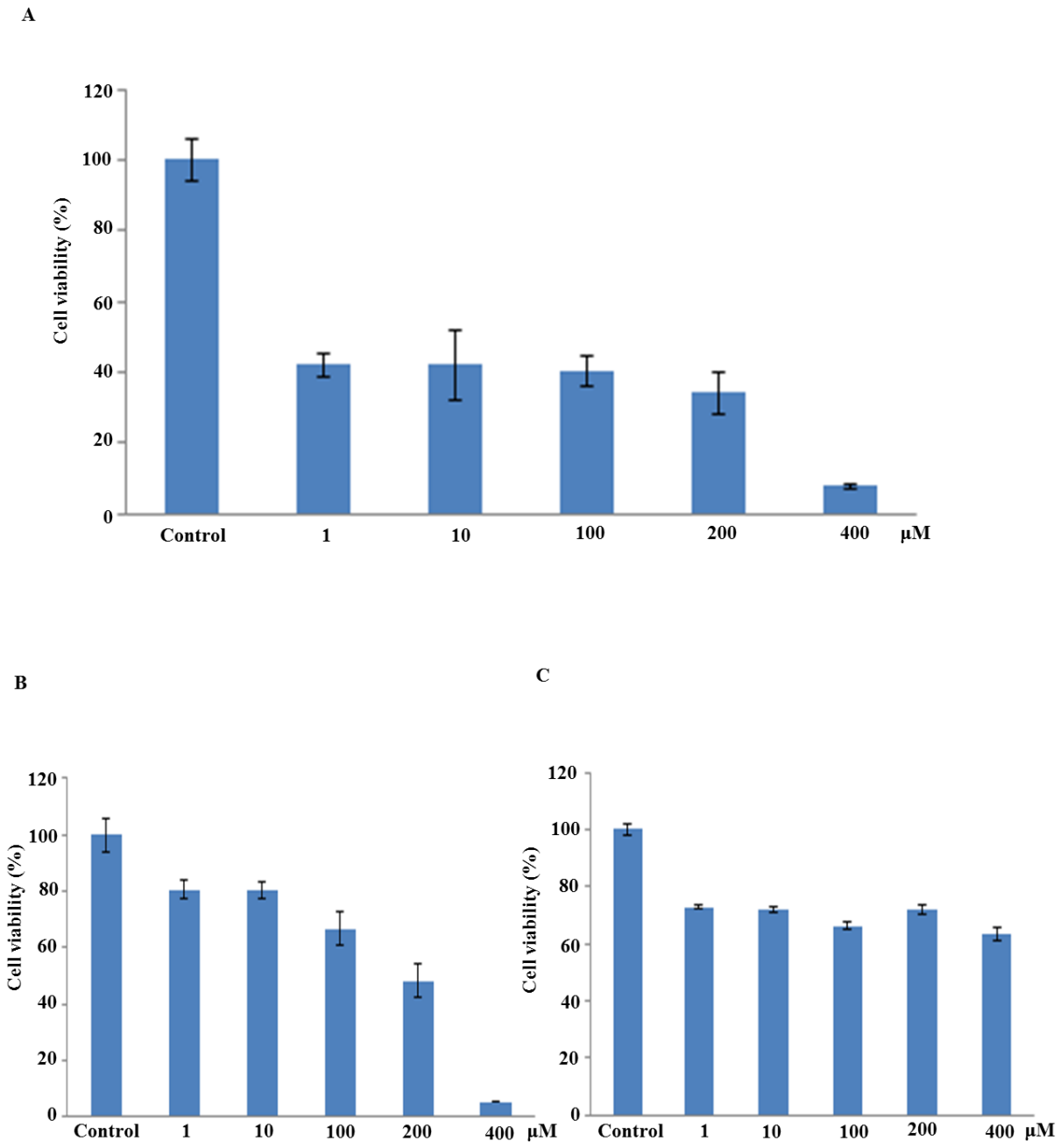

Figure 2.3.4 MTT toxicity assay. PC12 cells were cultured in RPMI 1640±2mM glutamine medium and treated with (A) $A\beta_{25-35}$ (B) KLVFF (C) equimolar $A\beta_{25-35}$ plus KLVFF at different concentrations (1, 10, 100, 200, 400µM). Data are expressed as mean ± S.E.M. (*n*= 8 for each group)

$A\beta_{25-35}$ at concentrations 1, 10 and 100μM decreased the cell viability about 60% whereas at concentration 400μM it decreased the viability about 90-95% (Figure 2.4.4A). The data suggest that $A\beta_{25-35}$ causes toxicity to the cells even at very low concentration (1μM). KLVFF may also cause toxicity to the cell and cell viability decreased about 20% at 1-10μM, 30% at 100μM, 50% at 200μM and 90-95% at 400μM (Figure 2.4.4B). The data suggest that KLVFF is less toxic to cells in comparison to $A\beta_{25-35}$ at concentration range between 1 to 200μM. However, at high concentration (400μM), the toxic effect of $A\beta_{25-35}$ and KLVFF are almost same which cause about 90-95% of cell death. The equimolar ratio of $A\beta_{25-35}$ plus KLVFF maintained the cell viability between 70-80% at concentrations 1, 10, 100, 200 and 400μM (Figure 2.4.4C). The data suggest that KLVFF together with $A\beta_{25-35}$ decreases the toxic effect to the PC12 cell line. ^{1}H NMR and cell viability MTT toxic assay data suggest that the equimolar ratio of KLVFF and $A\beta_{25-35}$ may together reduce the amyloid beta toxicity and aggregation.

2.5 Discussion

The real cause and molecular mechanism of AD is a crucial challenge in medical research because of the rising numbers of its pathology related to the life span. Currently many new molecules are synthesised that interact with the residues of Aβ peptide and act as inhibitors of amyloid fibril aggregation. These inhibitory molecules can provide a fundamental approach to investigate about amyloidosis and development of new therapies against AD. Although plenty of research data are available but it is not clear whether the amyloid fibrils are the real cause of AD pathology or its role in the disruption of neuronal membrane.

The main aim of this study was to investigate the aggregation properties of amyloid beta using $A\beta_{25-35}$ and KLVFF by liquid ^{1}H NMR. $A\beta_{25-35}$ peptide may play an important role in the etiology of AD because of its high toxicity and self-assembling abilities into stable and insoluble aggregated forms[44, 45]. Due to its great propensity to aggregate and insolubility in water, the conformation of this amyloid peptide is still unknown[44, 45]. Beta breaker peptide (KLVFF) is identified as the hydrophobic core of $A\beta_{1-42}$ and essential for amyloid fibrillogenesis[46].

$A\beta_{25-35}$ aggregates were clearly observed in sodium-phosphate buffer (pH 7.2) at room temperature. To avoid the aggregation of peptide, samples were prepared in cold (278K) buffer. The experimental setups were achieved at 278K because at this temperature peptides did not achieve quick aggregation. NMR signals of $A\beta_{25-35}$ were obtained when the sample was measured very quickly after its preparation (Figure 2.4.2.2A). However, NMR signals were lost when it was incubated for 24 hrs at 278K and amyloid fibrils were clearly visible in the NMR tube. In the presence of KLVFF, the spectrum of $A\beta_{25-35}$ remain unchanged during the time course. The plot of relative peak intensity of peptide at 0.9ppm (peptide methyl groups) vs time also confirms that the aggregation rate of $A\beta_{25-35}$ plus KLVFF is almost symmetrical over time. However, the aggregation rate of $A\beta_{25-35}$ alone is extremely unpredictable, as is apparent from repetitions of NMR measurements. It also shows a lag phase before the onset of aggregation (Figure 2.4.3.2). The data suggest that KLVFF may hinder the aggregation of $A\beta_{25-35}$ in solution. Using surface plasmon resonance spectroscopy and electron microscopy, Tjernberg *et al* (1996) proposed that KLVFF may act as beta breaker peptide because it binds and blocks the homologous sequence ($A\beta_{16-20}$) of full length Aβ [29, 47]. In this study, the $A\beta_{25-35}$ plus KLVFF data also support the hypothesis of Tjernberg *et al* that KLVFF may prevent the

amyloid beta aggregation and fibril formation. The 1D and 2D peaks analysis of sample containing $A\beta_{25-35}$ plus KLVFF suggest that the –NH peak of valine (8.21ppm) and phenylalanine (8.46 ppm) of KLVFF change its position after contacting with alanine (8.20ppm) and asparagine (8.45ppm) of $A\beta_{25-35}$, respectively (Figure 2.4.1 and 2.4.3). The data suggest that two different peptide species interaction may cause the inhibition of $A\beta_{25-35}$ aggregation.

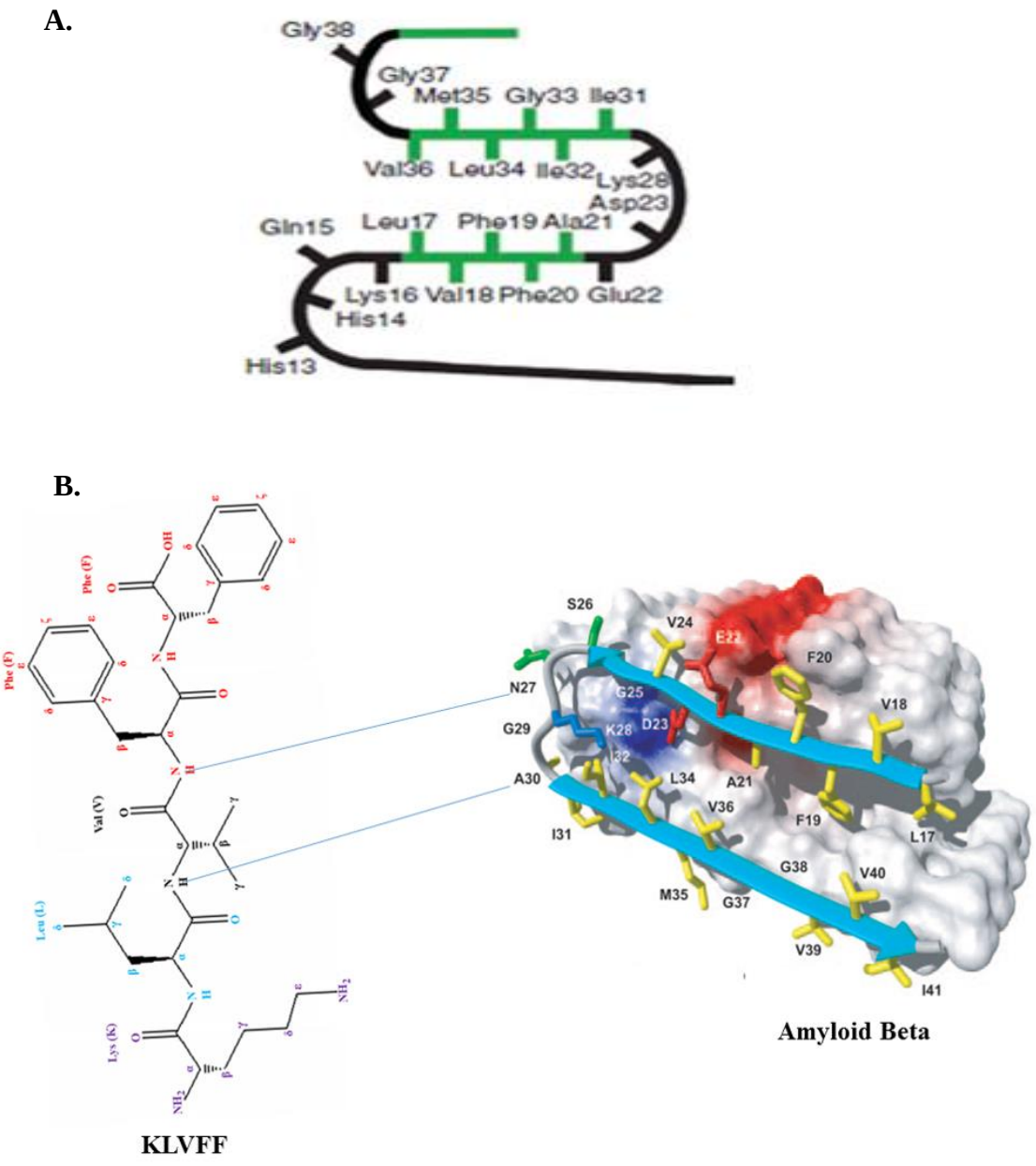

Figure 2.5 Schematic diagram of amyloid beta model[48, 49]. (A) Model shows that KLVFF is partially opposite to $A\beta_{25-35}$ sequence from Ile(32) to Val(35). (B) Model shows that KLVFF is not opposite to $A\beta_{25-35}$ sequence. The interaction may occur between the side chain of Ala(30) of $A\beta_{25-35}$ with Val(18) of KLVFF and Asn(27) of $A\beta_{25-35}$ with Phe(20) of KLVFF. These interactions may cause the inhibition of fibril formation of $A\beta_{25-35}$.

Two models of full length amyloid beta (1-40/42) have been proposed[48, 49]. In amyloid beta model (2.5A), KLVFF sequence is parallel to sequence of $A\beta_{25-35}$ from Ile(32) to Val(35). In another model (2.5B), KLVFF is not placed parallel to the sequence of $A\beta_{25-35}$ in full length of amyloid peptide. Based on first model, KLVFF sequence may break the H-bond of $A\beta_{25-35}$ and thus inhibit the aggregation and fibril formation. The data of this chapter signifies the second model, where Val(18) and Phe(20) of KLVFF may interact with Ala(27) and Asn(30) of $A\beta_{25-35}$ and thus inhibit the amyloid aggregation and fibril formation.

The MTT cell viability assay data suggest that $A\beta_{25-35}$ causes toxicity. The death of PC12 cells is found about 50-60% at 1μM and about 90-95% at 400μM of $A\beta_{25-35}$. The equimolar mixture of $A\beta_{25-35}$ plus KLVFF causes cell death about 20-30% at concentrations ranging 1-400μM (Figure 2.3.4C). The MTT assay data suggest that KLVFF may lower the toxic effect of $A\beta_{25-35}$. Lowe *et al* (2001) also reported that the equimolar KLVFF (25μM) may prevent the aggregation of $A\beta_{1-40}$ using PC12 cell lines and MTT assay[36]. The MTT assay data of $A\beta_{25-35}$ plus KLVFF support the data of KLVFF plus $A\beta_{1-40}$. Hence, it is evidenced that KLVFF has ability to prevent aggregation and toxicity of either $A\beta_{1-40}$ or $A\beta_{25-35}$ *in vivo*.

In conclusion, the small amyloid fragment $A\beta_{25-35}$ can aggregate rapidly in the solution and cause toxicity to the neuronal cells. The peptide KLVFF may not only act as inhibitor peptide to hinder the aggregation properties of homologous sequence of full length amyloid peptide ($A\beta_{1-40/42}$). But also act as inhibitor to prevent aggregation and fibrillation of $A\beta_{25-35}$ in aqueous and *in vivo* models. Thus KLVFF may be useful peptide to investigate the cause of disease and therapeutics of AD.

2.6 References

1. T. Kubo, S. Nishimura, Y. Kumagae and I. Kaneko, *Journal of Neuroscience Research* 2002, **70**, 474-483.
2. C.J. Pike, A.J. Walencewicz-Wasserman, J. Kosmoski, D.H. Cribbs, C.G. Glabe and C.W. Cotman, *J. Neurochem*., 1995, **64**, 253-65.
3. F. Misiti, B. Sampaolese, M. Pezzotti, S. Marini, M. Coletta, L, Ceccarelli, B. Giardina and M.E. Clementi, *Neurochemistry International*, 2005, **46**, 575-583.
4. M.E. Clementi, S. Marini, M. Coletta, F. Orsini, B. Giardina and F. Misiti, *FEBS Letters*, 2005, **579**, 2913-2918
5. M. Cheon, I. Chang, S. Mohanty, L.M. Luheshi, C.M. Dobson, M. Vendruscolo and G. Favrin, *PLOS Computational Biology*, 2007, **3**, e173.
6. M. Bucciantini, E. Giannoni, F. Chiti, F. Baroni, L. Formigli, J. Zurdo, N, Taddei, G. Ramponi, C.M. Dobson and M. Stefani, *Nature*, 2002, **416**, 507-511.
7. A.T. Petkova, R.D. Leapman, Z. Guo, W.M. Yau, M.P. Mattson and R. Tycko, *Science*, 2005, **307**, 262-265.
8. A.M. D'Ursi, M.R. Armenante, R. Guerrini, S. Salvadori, G. Sorrentino and D. Picone, *J. Med. Chem.* 2004, **47**, 4231-4238.
9. L.C. Serpell, *Biochimica et Biophysica Acta*, 2000, **1502**, 16-30.
10. P.P. Mager, *Inc. Med Res Rev*., 1998, **18**, 403-430.
11. G. Wei and J.-E. Shea, *Biophysical Journal*, 2006, **91**, 1638-1647.
12. T. Kohno, K. Kobayashi, T. Maeda, K. Sato and A. Takashima, *Biochemistry*, 1996, **35**, 16094-16104.
13. G. Shanmugam and P.L. Polavarapu, *Biophysical Journal*, 2004, **87**, 622-630.
14. I.D. Limo´n, A, Dı´az, L. Mendieta, G, Chamorro, B. Espinosa, E. Zenteno and J. Guevara, *Neuroscience Research*, 2009, **63**, 129-137.
15. X. Yu, Q. Wang and J. Zheng, *Biophysical Journal*, 2010, **99**, 666-674.
16. C. Wu and J.-E. Shea, *PLOS Computational Biology*, 2013, **9**, e1003211.
17. M. Manna and C. Mukhopadhyay, *PLOS One*, 2013, **8**, e71308.
18. B. Ma and R. Nussinov, *Biophysical Journal*, 2006, **90**, 3365-3374.
19. A.L. Fink, *Folding & Design***,** 1998, **3**, R9-R23.
20. R. Khurana, J.R. Gillespie, A. Talapatra, L.J. Minert, C. Ionescu-Zanetti, I. Millett, and A.L. Fink, *Biochemistry*, 2001, **40**, 3525-3535.
21. J. Lee, E.K. Culyba, E.T. Powers and J.W. Kelly, *Nat Chem Biol*., **7**, 602-609.

22. M. Cheon. I. Chang, S. Mohanty, L.M. Luheshi, C.M. Dobson, M. Vendruscolo, G. Favrin, *PLOS Computational Biology*, 2007, **3**, e173.
23. C. Soto, E.M. Sigurdsson, L. Morelli, A. Kumar, E.M. Castano and B. Frangione, *Nature Medicine*, 1998, **4**, 822-826.
24. B. Permanne, C, Adessi, G.P. Saborio, S. Fraga, M.-J. Frossard, J.V. Dorpe, I. Dewachter, W.A. Banks, F.V. Leuven and C. Soto, *FASEB Journal*, 2002, **16**, 860-862.
25. P. DeBona, M.L. Giuffrida, F. Caraci, A. Copani, B. Pignataro, F. Attanasio, S. Cataldo, G. Pappalardoc and E. Rizzarellia, *J. Pept. Sci.*, 2009, **15**, 220-228.
26. V. Moretto, M. Crisma, G.M. Bonora and C. Toniolo, *Macromolecules*, 1989, **22**, 2939-2944.
27. M. Mutter, A. Nefzi, T. Sato, X. Sun, F. Wahl and T. Wohr, *Pept. Res*., 1995, **8**, 145-153.
28. S.J. Wood, R. Wetzel, J.D. Martin and M.R. Hurle, *Biochemistry*, 1995, **34**, 724-730.
29. L.O. Tjernberg, J. Naslund, F. Lindqvist, J. Johansson, A.R. Karlstromi, J. Thyberg, L. Terenius and C. Nordstedt**,** *The Journal of Biological Chemistry*, 1996, **271**, 8545-8548.
30. J. Naslund, M. Jensen, L.O. Tjernberg, J. Thyberg, L. Terenius and C. Nordstedt, *BBRC*, 1994, **204**, 780-787.
31. F.S. Esche, P.S. Keim, E.C. Beattie, R.W. Blacher, A.R. Culwell, T. Oltersdorf, D. McClure and P.J. Ward, *Science*, 1990, **248**, 1122-1124.
32. C. Haass, A.Y. Hung, M.G. Schlossmacher, D.B. Teplow and D.J. Selkoe, *The Journal of Biological Chemistry*, 1993, **268**, 3021-3024.
33. J. Naslund, A. Schierhorn, U. Hellman, L. Lannfelt, A.D. Roses, L.O. Tjernberg, J. Silberring, S.E. Gandy, B. Winblad, P. Greengard, C. Nordstedt and L. Terenius, *Proc. Natl. Acad. Sci. USA*, 1994, **91**, 8378-8382.
34. D. Burdick, B. Soreghan, M. Kwon, J. Kosmoski, M. Knauer, A. Henschen, J. Yates, C. Clotman and C. Glabe, *The Journal of Biological Chemistry*, 1992, **267**, 546-554.
35. J.T. Jarrett, E.P. Berger and P.T. Lansbury Jr., *Biochemistry*, 1993, **32**, 4693-4697.
36. T.L. Lowe, A. Strzelec, L.L. Kiessling and M. Murphy, *Biochemistry*, 2001, **40**, 7882-7889.
37. M.H. Levitt, *Spin Dynamics Basics of nuclear magnetic resonance*, 2 ed., John Wiley and Sons Ltd., Sussex, UK, 2002.
38. A.E. Derome, *Modern NMR Techniques for Chemistry Research*,

39. S. Xu, *1D and 2D NMR experiment methods*., Emory University, Atlanta, USA, 2011.
40. K. Wüthrich, *NMR of Proteins and Nucleic Acids*, Wiley, New York, USA, 1986.
41. E. Kaiser, R.L. Colescott, C.D. Bossinger and P.I. Cook, *Anal. Biochem.*, 1970, **34**, 595-598.
42. M.H. Viet, S.T. Ngo, N.S. Lam and M.S. Li, *J. Phys. Chem. B*., 2011, **115**, 7433-7446.
43. W.P. Esler, E.R. Stimson, J.R. Ghilardi, Y.-A. Lu,| A.M. Felix, H.V. Vinters, P.W. Mantyh, J.P. Lee and J.E. Maggio, *Biochemistry*, 1996, **35**, 13914-13921.
44. L. Larini and J.-E. Shea, *Biophysical Journal*, 2012, **103**, 576-586.
45. L. Millucci, R. Raggiaschi, D. Franceschini, G. Terstappen and A. Santucci, *J. Biosci.*, 2009, **34**(2), 293-303.
46. C.K. Bett, W.K. Serem, K.R. Fontenot, R.P. Hammer, and J.C. Garno, *ACS Chem. Neurosci*., 2010, **1**, 661-678.
47. L.O. Tjernberg, J. Naslund, F. Lindqvist, J. Johansson, A.R. Karlstromi, J. Thyberg, L. Terenius and C. Nordstedt, *The Journal of Biological Chemistry,* 1996, **271**, 8545-8548.
48. M. Ahmed, J. Davis, D. Aucoin, T. Sato, S. Ahuja, S. Aimoto, J.I. Elliott, W.E.V. Nostrand and S.O. Smith, *Nature struc. and Mol. Biol*., 2010, **17**, 561-567.
49. T. Luhrs, C. Ritter, M. Adrian, D. Riek-Loher, B. Bohrmann, H. Dobeli, D. Schubert and R. Riek, *PNAS*, 2005, **102**(48), 17342-17347.

Chapter 3
Interactions between peptide, amyloid beta and lipid bilayers studied by magic angle solid state NMR

3.1 Introduction

The biological membranes are the outer most envelope of cells and cellular organelles. The plasma membrane is a barrier between inner cytoplasmic organelles and the outer matrix[1]. In eukaryotes, the internal cellular organelles (mitochondria, Golgi apparatus, endoplasmic reticulum, lysosomes, peroxisomes and chloroplasts) possess membranous boundaries, which are almost similar in composition to plasma membrane[1, 2].

Lipids are the major constituents of biological membrane together with proteins and saccharides. Lipids may form various shapes such as bilayers, bicelles, micelles and hexagonal phases. However in all biological membranes, lipids commonly form bilayer structures. The mass ratio of lipids and proteins varies from 1:4 to 4:1 in the biological membranes[1, 2]. In the membrane, lipids and proteins together cover about 70% of the total surface and form an extremely complex structure[1].

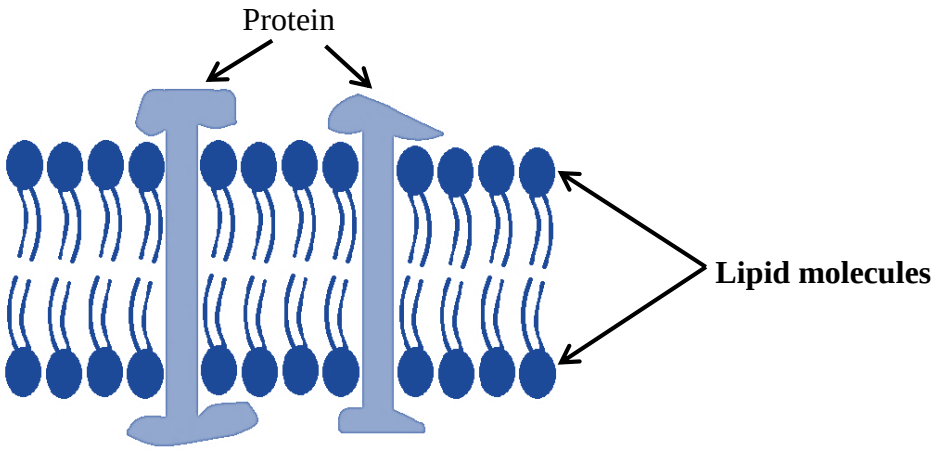

Figure 3.1 Schematic diagram showing two dimensional views of typical biological membranes composed of lipid and protein molecules.

3.1.1Biological membrane model and lipid vesicles

Biological membranes are fluid dynamic lipid bilayer structures, and other molecules, such as proteins and carbohydrates float on them[1, 2]. The first model of membrane was given by Danielli and Davson (1935)[6] and they suggested that lipids might be covered by proteins[6]. This model was again improved by Danielli (1975)[6] and suggested that lipids might be incorporated with proteins, and form patches and pores in the membrane[6]. The most accepted model of biological membrane was given by Jonathan Singer and Garth Nicolson (1972)[4], commonly

known as "fluid mosaic model". According to this model, the membranous proteins are surrounded by lipids mainly phospholipid bilayers[4]. The lipid bilayers provide the fundamental structure of membranes whereas proteins of biological membranes are involved in many biological functions such as cellular trafficking and signalling[4, 5]. The lipids act as a permeability barrier and proteins play an important role in transport systems via many mechanisms such as pumps and ion channels. Thus lipids and proteins together act as a selective or semi permeable barrier in the biological membranes[1].

Lipid vesicles or liposomes are composed of lipid bilayers in a hollow sphere[3]. Vesicles are of various types depending upon their size and lipid compositions[6]. The unilamellar vesicles are composed of single lipid bilayer shell. Small unilamellar vesicles (SUVs) are 30 - 100 nm in diameter. Large unilamellar vesicles (LUVs) and giant unilamellar vesicles (GUVs) are 100 - 200 nm and 1-100 μm in diameter, respectively[6]. Lipid vesicles are very important and realistic mimics of biological membranes to understand the dynamics of lipids and role of other components of cellular membranes such as integral proteins and polysaccharides[6, 7].

The biological membrane models such as lipid vesicles are widely used for understanding the molecular mechanisms underlying the progression of amyloid diseases[8]. This study is mainly emphasised on the possible applications of lipid bilayer models to understand the mechanisms of amyloid beta induced toxicity and degeneration of neuronal membrane, aiming on the modulating effect of lipid bilayer compositions.

3.1.2 Lipids in biological membrane

The lipid constituents of cell membrane are generally phospholipids, cholesterol, sphingolipids, and glycerolipids. In eukaryotic organisms, the main structural lipids of biological membrane are glycerophospholipids[9]. Basically, the glycerophospholipids are the derivatives of diacylglycerol (DAG)[9]. The structure of phospholipids are broadly divided into three regions: (a) the head region, mainly made up of an alcohol and phosphate, which are polar in nature (b) middle region, made up of glycerol, which acts as backbone (c) tail region, consists of two fatty acid chains[9]. The tail regions of glycerophospholipids possess two saturated or *cis*-unsaturated fatty acyl chains[9]. The fatty acid of phospholipids are composed of 14-24 carbon

atoms, containing one or more double bonds but most common are 16 and 18 carbon atoms chain[2, 4].

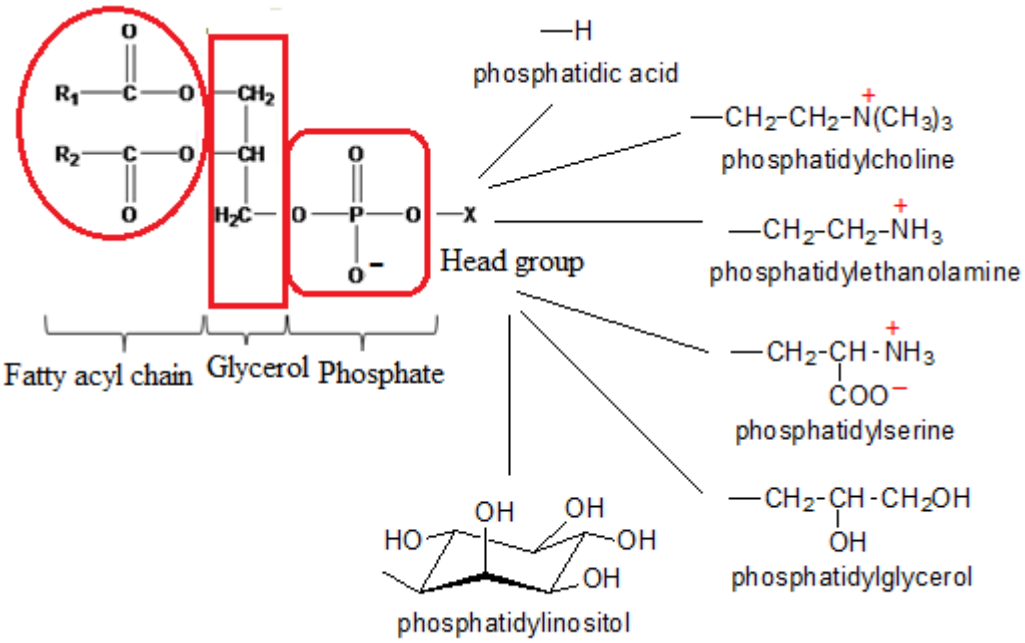

Figure: 3.1.2 Chemical structure of glycerophospholipids, 'X' is different head groups containing phosphatidylcholine (PC), phosphatidylserine (PS), phosphatidylglycerol (PG), phosphatidylethanolamine (PE) and phosphatidylinositol (PI). R_1 and R_2 are acyl chain.

The head group of glycerophospholipids are composed of different alcohol moieties such as choline, serine, glycerol, ethanolamine and inositol[4]. About 50-55% PC, 20-25% PE, 10-15% PS and 1-5% PI of total glycerophospholipids are found in a typical eukaryotic plasma membrane[9, 10]. However, in the brain cells, PE is about 45% of total phospholipids[10].

Sphingolipids are the other important structural lipids of membrane, derived from the sphingosine base. The head group of sphingolipid may consist of different alcohol moieties (PC, PS, PE and PI similar to glycerophospholipids) and form sphingomyelin. Sphingolipid and carbohydrate head group produce ceramide[4]. The tail region possesses single fatty acyl unsaturated chain linked through an amide bond to sphingosine[4]. Cerebrosides are one of the major lipid constituents of the neuronal cells[11].

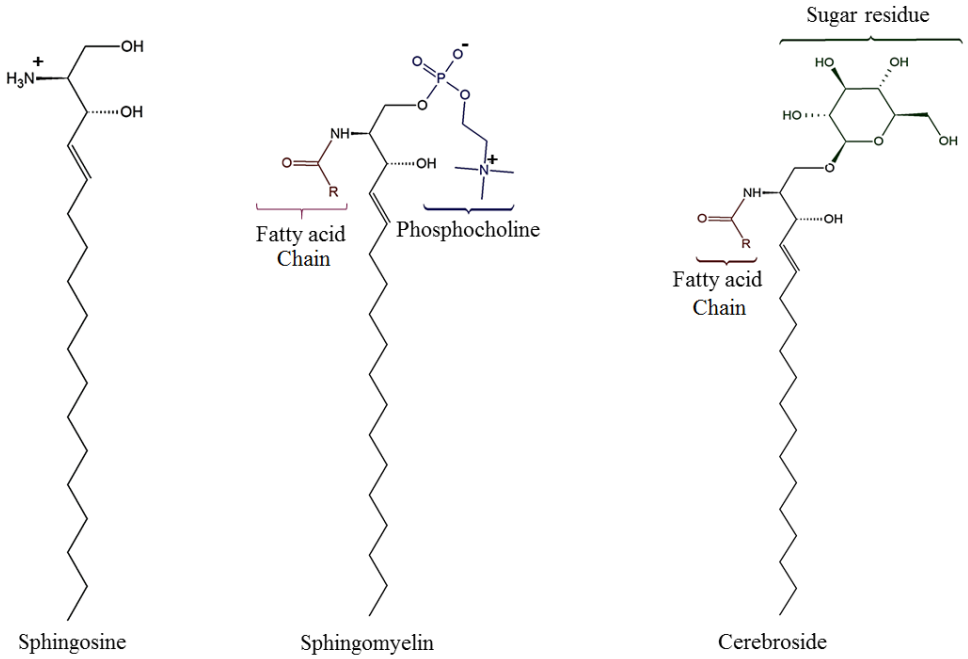

Figure 3.1.3 Chemical structure of sphingosine, sphingomyelin and cerebroside. 'R' represents the fatty acid acyl chain region.

Sterol lipids, mainly cholesterol, are an important lipid constituent of the mammalian membrane[9]. Cholesterol is distinctive among the membranous lipids due to its annulated structure[4] and small hydrophobic region[4]. The hydrophilic region of cholesterol is smaller than other membranous lipids, glycerolipids or sphingolipids[9].

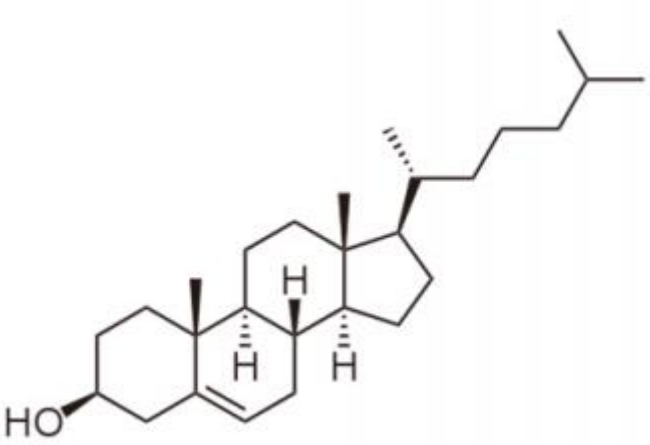

Figure 3.1.4 Chemical structure of cholesterol, most abundant sterol in eukaryotic membrane except fungi (yeast)[9], consists of three cyclohexane rings connected to a cyclopentane ring.

3.1.2.1 Cholesterol and phospholipid bilayer

The hydroxyl region of cholesterol is mainly exposed at the phospholipid bilayer interface[12]. Generally, the water contact with the nonpolar part of cholesterol produces poor impact to the free energy[12]. Once the cholesterols incorporate into phospholipid bilayers, the head groups of phospholipids protect the nonpolar region of cholesterol from water contact. The head groups of phospholipid act similar to umbrellas to cover the cholesterol. Under the head groups of phospholipids, fatty acid acyl chains and cholesterols are compactly packed. The shielding of cholesterol by phospholipids bilayers is known as umbrella model[12]. The hydroxyl groups of cholesterol may interact with water to give partial protection to the nonpolar part of cholesterol. However, hydroxyl group cannot entirely protect nonpolar part of cholesterol without the head groups of phospholipids[12, 13].

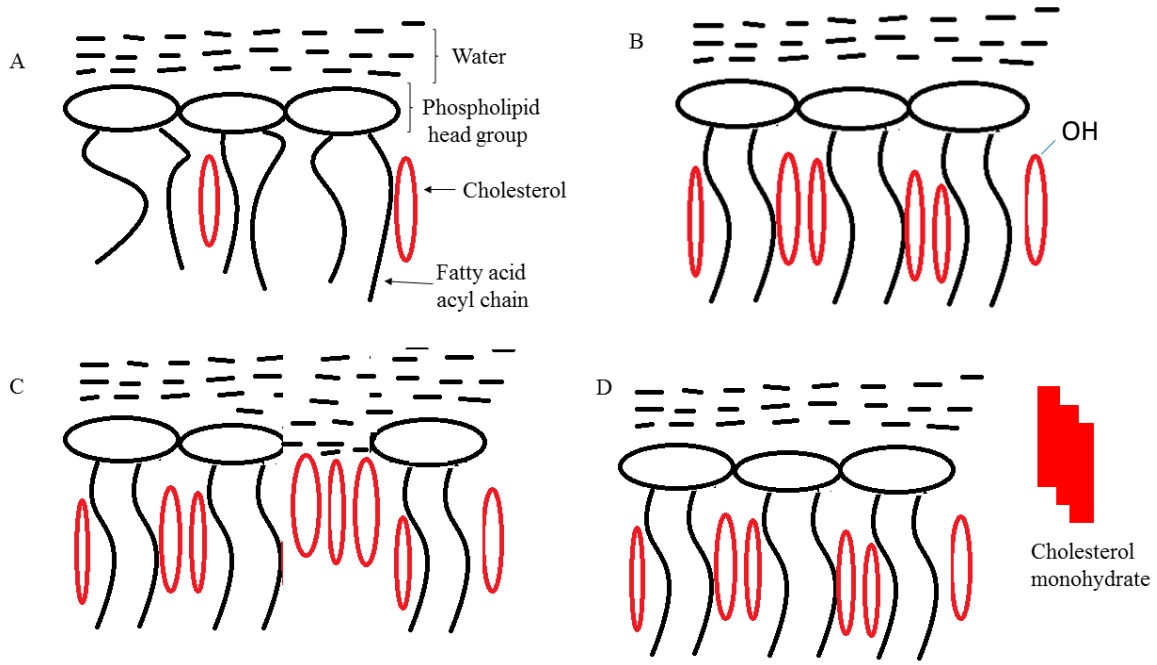

Figure 3.1.5 Schematic diagram of umbrella model[12] (A) head groups of phospholipid shield the cholesterol nonpolar region from water; (B) increased cholesterol concentration provide stiffness of acyl chains and stretch the head groups to cover the cholesterol; (C) some cholesterol molecules contact to water and cholesterol hydroxyl groups protect nonpolar cholesterol part along with phospholipid head groups; (D) additional cholesterol molecules precipitate and may form cholesterol monohydrate crystals to overcome the free energy[12].

The umbrella model also emphasizes the cholesterol condensing effect. The cholesterol condensing effect is the motion of acyl chains in the phospholipid bilayer which is reduced by cholesterol. These effects may reduce the lipid bilayer permeability with increasing cholesterol

concentration. The hydrophobicity of cholesterol may also force cholesterol and fatty acid acyl chains together. The umbrella model suggests that the compression of acyl chains help to expand phospholipid head groups[12, 13].

3.1.2.2 Shape and arrangement of phospholipids

Phospholipids are mostly amphiphilic[4]. The head group (charged and polar) is hydrophilic whereas the tail group (nonpolar fatty acid chain) is hydrophobic in nature[4]. Phospholipids have an ability to self-organise into various shapes and forms, in aqueous contact, depending upon the composition and concentration of the head group[14, 15]. Single acyl chain (lyso-lipid) or two small acyl chains with large head group of phospholipids promote curvature towards water and form micelles[16, 17] (Figure 3.1.6A&B).

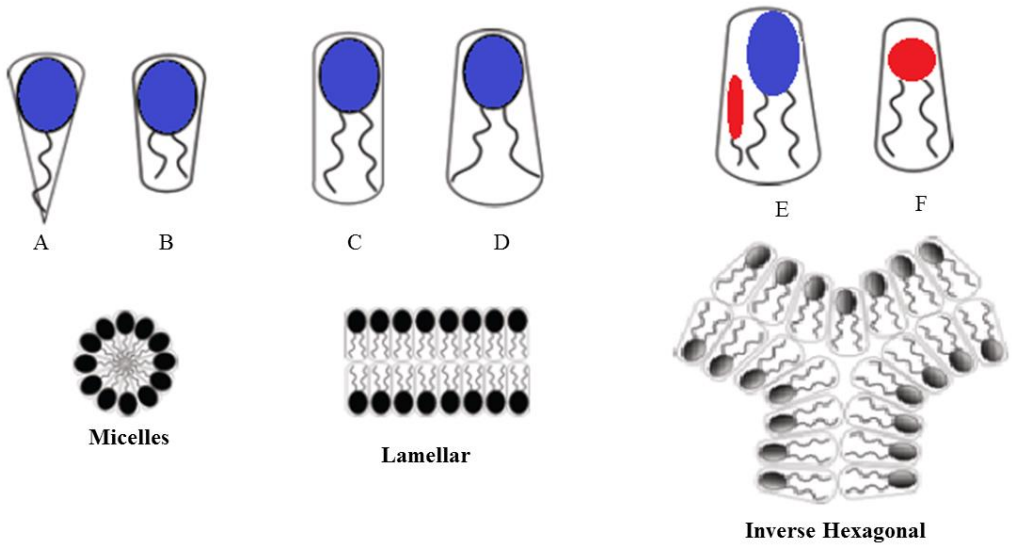

Figure 3.1.6 Schematic diagram of lipid shapes and arrangement. (A) lyso-phospholipid; large head group and single fatty acid acyl chain adopt a tapering cone shape, (B) two short chain saturated fatty acid acyl chain, (C) two long chain saturated fatty acid acyl chain, (D) monounsaturated fatty acid acyl chain, (E) unsaturated two fatty acid chains incorporated with sterol, (F) small head group with unsaturated two fatty acid chains. In aqueous environment, a single acyl chain and two small saturated acyl chains with large head group assemble into micelles, saturated and mono-unsaturated acyl chain with large head group form lamellar and small head group and unsaturated acyl chain with sterol form inverse hexagonal phase.

Cylindrical lipids, saturated or monounsaturated acyl chains with a large head group such as phosphocholine, assemble into a lamellar (bilayer) form in the aqueous environment. Unsaturated acyl chains and small phospholipid head groups with sterol molecules increase the

tendency of the bilayers to curve towards water and are likely to form an inverse hexagonal phase such as phosphoethanolamine[16, 17] (Figure 3.1.6E&F).

3.1.3 Interaction between lipid bilayers and peptide Aβ

An extracellular deposition of Aβ on the neuronal membrane is one of the pathological hallmarks of AD[18]. It is reported that lipids may play an important role for the polymerization and fibrillation of Aβ[19]. Aβ and lipid bilayer interactions have been widely examined to interpret the mechanisms behind the Aβ-induced toxicity causing AD. It is believed that Aβ interacts with lipid bilayers because it is originated from transmembrane protein APP[19]. Many experimental studies suggest that the aggregation and accumulation of Aβ may be influenced by lipids. Bieschke *et al* (2006) reported that oxidative small molecules, secosterols (derivative of cholesterol) and 4-hydroxynonenal (product of lipid peroxidation), found in AD brain, can accelerate the misfolding and accumulation of Aβ on neurons using atomic force microscopy and circular dichroism (CD) spectroscopy[20]. Murray *et al* (2005) reported that $A\beta_{1-42}$ may encourage oxidative damage of lipid bilayers (DMPC vesicles) through fibril formation in presence of copper (0.5-5 μM) under mass spectroscopy[21-23].

Terzi *et al* (1997) suggested that $A\beta_{1-40}$ binds electrostatically to the surface of polar head group of phospholipids without penetrating them using CD spectroscopy, ^{2}H and ^{31}P SS NMR[28]. CD spectroscopy data suggested that a β-structure - α-helix transition occurs at a lipid-to-peptide ratio more than 55[28]. ^{31}P NMR data suggested that lipid phase maintained the bilayer arrangement at any lipid-to-amyloid peptide ratios[28]. ^{2}H NMR data suggested that the lipid head group conformation and order parameter of the hydrocarbon chains of fatty acid are unchanged by $A\beta_{1-40}$ using PC–PG vesicles containing deuterated choline head group and *cis*-double bond of the oleic acyl chain[28].

McLaurin and Charkrabartty (1996) examined Aβ and lipid bilayer interactions using lipid vesicles, prepared from bovine brain lipids under CD spectroscopy and dye release assay[24]. They found that Aβ disrupts the membrane model at pH 6 (typical endosomal pH)[24]. They also reported that at neutral pH (typical extracellular pH), gangliosides encourage Aβ to adopt α/β conformation[24]. Kremer *et al* (2000) suggested that Aβ (monomeric conformation to fibrillar structure) exposes the lipid bilayers at hydrophobic sites and also causes reduction in membranous fluidity[25]. Kakio *et al* (2001) investigated the role of membranous mono-sialotetrahexosyl-ganglioside (GM1) and cholesterol on the binding of Aβ using detergent-

insoluble glycolipid-rich domain (DIG) lipid bilayers and fluorescent dye-labeled $A\beta_{1-40}$[26]. GM1 and cholesterol are very important for neuronal plasticity. Increasing the cholesterol contents in the membrane enables the initiation of GM1-Aβ complex via GM1 cluster that provides an important site for binding of Aβ[26].

Using CD spectroscopy Ji *et al* (2002) suggested that the insertion capability of Aβ may be regulated by the lipid bilayers cholesterol ratio. Lipid-free Aβ comprises 48.9% random-coil, 23.5% β-sheet, and 1.7% α-helix conformations[27]. DMPC vesicles with Aβ significantly increase the β-sheet (31.2%) and α-helix (9.5%) conformation. However, DMPC plus cholesterol (>30 mol%) with Aβ drastically reduce the β-sheet (0 %) conformation and increase α-helix (58.8 %) structure, which help Aβ to enter in the lipid bilayers by its C-terminus[27]. Micelli *et al* (2004) examined the incorporation of $A\beta_{1-40}$ into the lipid bilayers using a single-channel system[29]. They reported that $A\beta_{1-40}$ is unable to interact with PC lipid bilayers, but in the presence of cholesterol or ergosterol it may form channels on the membrane[29]. The membrane channels may imbalance the cellular ion ingredients, which may be one of the reasons accountable for cytotoxicity in AD[29].

Bokvist *et al* (2004) suggested that membrane incorporated $A\beta_{1-40}$ may be inhibited by acidic phospholipids (DMPC/DMPG) using ^{31}P MAS SS NMR and CD spectroscopy[30]. The α-helix form of transmembrane residues ($A\beta_{29-40}$) may stabilize the release of Aβ through an electrostatic attachment between basic residue (Lys28) and negatively charged phospholipid[30]. On the other hand, $A\beta_{1-40}$ may be released as soluble (monomeric) form on the negatively charged phospholipid bilayers that act as aggregation-templates to enhance the amyloid peptide aggregation and attachment to the membrane[30] as shown in Figure 3.1.7.

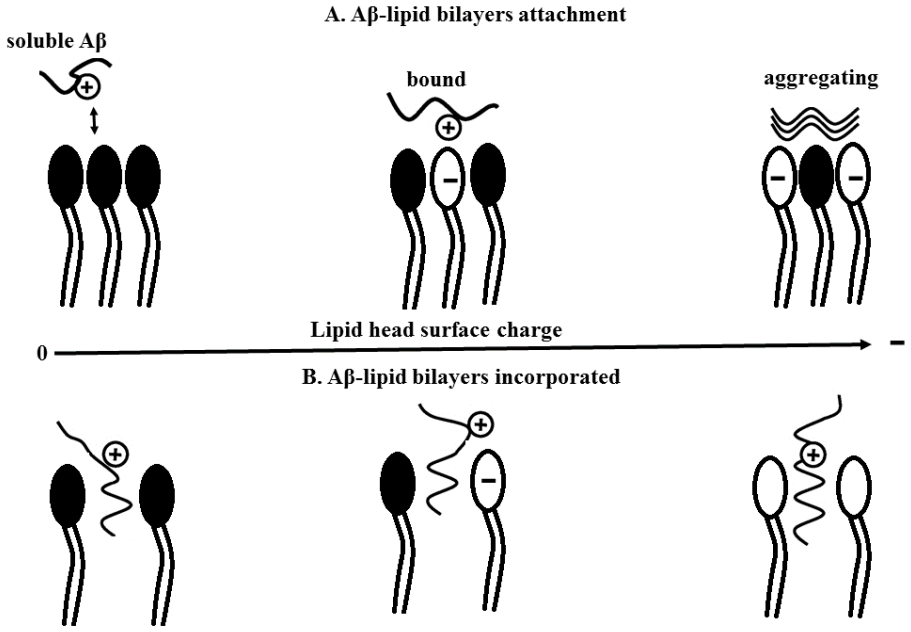

Figure 3.1.7 Schematic diagram for the interactions between Aβ and lipid bilayers[30]. (A) Electrostatic attachment between lipid bilayers and Aβ to the membrane surfaces and soluble $A\beta_{1-40}$ accelerates into β-sheet aggregates. (B) Membrane incorporated charged residues of $A\beta_{1-40}$ increase the insertion of Aβ segment as a monomeric form in the lipid bilayers[30].

Martinez-Senac *et al* (1999) reported that $A\beta_{25-35}$ may interact with negatively charged phospholipid head groups and form β-fibrils on the lipid-water interphase by Fourier transform infrared spectroscopy (FT-IR) and differential scanning calorimetry (DSC)[34]. Dante *et al* (2002) examined the location of $A\beta_{25-35}$ in the lipid bilayers using neutron diffraction and selective deuterated amino acids and found two distinct sites of amyloid peptide in the lipid environment: One in the extracellular aqueous region of the membranous surface and other in the hydrophobic region of the lipid bilayers[32]. Dante *et al* (2006) reported that cholesterol (20% of molar weight) may completely alter the monomeric form of $A\beta_{25-35}$ and hinder the penetration of lipid bilayers by $A\beta_{25-35}$[33]. Dies *et al* (2014) examined the interaction between $A\beta_{1-42}$/$A\beta_{25-35}$ and anionic phospholipid vesicles using x-ray diffraction[31]. They reported that $A\beta_{1-42}$ inserted in the hydrocarbon core of the phospholipid bilayers. However, $A\beta_{25-35}$ attach to the hydrophillic lipid head groups where they align parallel to the membrane and insert into the hydrophobic phospholipid bilayers[31]. How the peptide amyloid beta interacts with lipid bilayers and what is the role of lipids during amyloid fibril formation is still a matter of debate among the scientific community.

3.1.4 Magic angle spinning solid state NMR

The spectra of liquid NMR show sharp peaks and this is due to fast random tumbling in the liquid molecules. On the other hand, the spectra of solid-state NMR shows broad peak and this happens due to the effects of anisotropic or orientation-dependent interactions between molecules of solids.

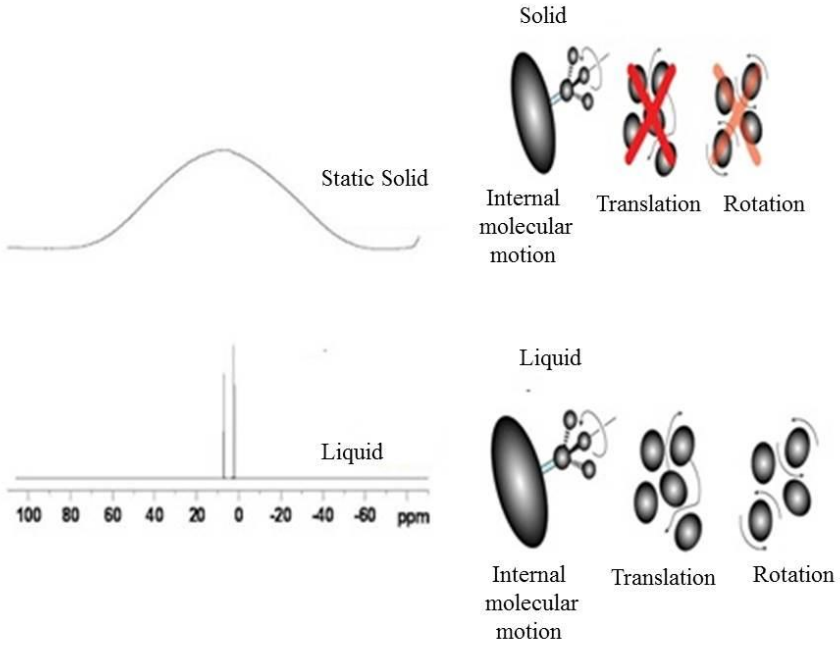

Figure 3.1.4.1 Schematic diagram of liquid and solid molecules and ^{1}H NMR spectroscopy. Liquid molecules possess both rotational and translational motion. In isotropic condition the motions are in all directions. Solid molecules do not possess rotational and translational motion. Liquid NMR spectrum generates sharp peaks due to fast tumbling between liquid molecules where solid state NMR produces broad peaks due to anisotropic condition of solid molecules[35, 36].

More precisely, in liquid NMR, anisotropic interactions of liquids molecules are averaged by the random molecular motion. But in solid-state NMR, the interactions between molecules are strong and compact hence the chemical shift anisotropy are large and dipolar coupling are high. Therefore, the NMR spectral line widths of solid nuclei are relatively broad compare to the liquid NMR spectra. This problem was first resolved by E.R. Andrew and I.J. Lowe. They supressed the anisotropic dipolar interactions of solid nuclei by applying an artificial motion (spinning) and placed the solid sample at angle 54.74° (average orientation of x, y and z plane)

to the external magnetic field and this is commonly known as magic-angle spinning (MAS)[35, 36].

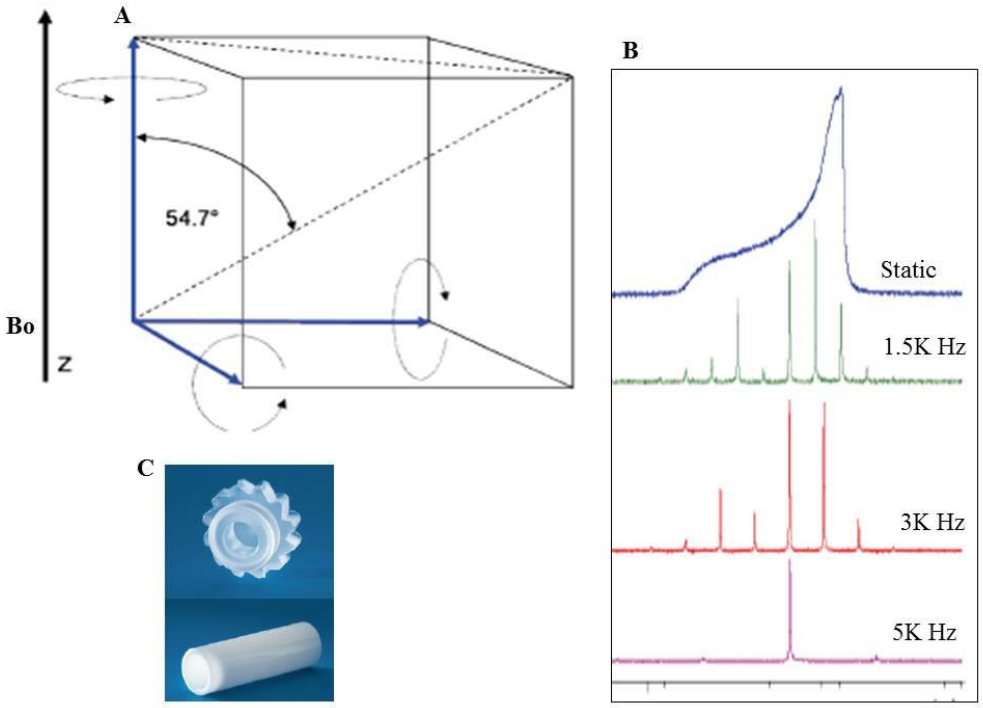

Figure 3.1.4.2 Magic angle spinning along with external magnetic field B_0 (A) MAS angle 54.7 degree (B) MAS spinning frequency of 5K Hz, 3K Hz, 1.5K and MAS static (C) MAS rotor with cap

MAS is a well-designed procedure to analyse various solid compounds, biomolecules, polymers and crystals. Samples are packed in a rotor, which is made up of zirconia or silicon nitride and capped. The loaded sample rotor is placed at the magic angle (54.74^o) to external magnetic field and mechanically spun at high frequency ranging from 500 Hz to 67 KHz depending upon the experiment. At the magic angle and high speed rotation, the anisotropic part of the solid sample generates NMR sidebands and with rapid spinning, these sidebands are gradually shifted away, and the spectrum resides into thin lines at the isotropic shifts and finally a high resolution spectrum is achieved in the solid state[35, 36].

3.1.5 Interpretation of transmembrane molecular cross-relaxation rates

MAS 2D NOESY are used to determine the intermolecular cross relaxation rate inside the lipid membrane. The initial pulse sequence of NOESY generates transverse magnetization, allowing it to progress under the effect of the chemical shift of isotropic molecules in time, t_1[37].

Therefore, the individual spin is identified through a specific resonance frequency. The next pulse sequence causes a flip of the transverse magnetization towards the z-axis, at a mixing time, t_m. Hence, this flipping of magnetization produces cross peaks where the interrelating spins are within 5A° during the mixing time[37]. The cross peaks are exclusively produced due to the dipolar cross-relaxation of two very close proton spins. This phenomenon may be defined as cross-relaxation rate[37]. The cross relaxation rate is mainly determined by the distance between the two proton spins and the association time of the molecular mobility[37]. The cross-relaxation rate is important for determining the interaction possibility between the intermembrane molecules and lipid membrane because of the mobility and molecular disorder in the lipid bilayers[37]. Hence, in lipid bilayers the cross-relaxation rate is proportional to the contact frequency between the two nuclei. The high frequency contact gives a large cross-relaxation rates and low frequency contact produces small cross-relaxation rates[37].

3.1.6 Aims

The main aim of this project was to investigate the interaction mechanisms between amyloid beta and lipid bilayer based on an amyloid beta toxic protofibril hypothesis. Protofibrils of amyloid beta are an intermediate species between amyloid fibrils and oligomers/monomers, which may cause toxicity of a neuronal membrane and could be a strong clinical and pathological feature to investigate the amyloid diseases. The other objective of this study was to investigate that how amyloid beta species can insert into the lipid bilayer. For this, a lipid bilayer mimic, lipid vesicles were prepared using brain lipids, DMPC phospholipids and cholesterol and measured by magic angle solid state ^{1}H NMR.

Objectives:-

1) To examine the role of brain lipids with the interaction of amyloid beta using total brain lipid vesicles under ^{1}H NMR.
2) To examine the interaction between amyloid beta and phospholipids in the lipid membrane using DMPC vesicles and measured by ^{1}H NMR.
3) To examine the role of cholesterol with the interaction of amyloid beta in the lipid bilayers using deuterated DMPC plus cholesterol lipid vesicles under ^{1}H NMR.
4) To examine the location of amyloid beta in the lipid bilayers using NOESY ^{1}H NMR.

5) To investigate the attachment dynamics of amyloid beta with a lipid bilayer, a potential beta breaker peptide (KLVFF) was used to understand the amyloid disease mechanism as well as the development of new drugs against amyloid diseases.

3.2. Materials

Total brain lipid (TBL) extracts and 1, 2- dimyristoylphosphatidylcholine (DMPC) solvated in chloroform, were purchased from Avanti Polar Lipids (Alabaster, AL, USA). $A\beta_{25-35}$ was purchased from Cambridge Biosciences (Cambridge, UK). Tris (hydroxymethyl) aminomethane (TRIS), ethylene diamine tetra acetic acid (EDTA), magnesium chloride ($MgCl_2$), hexafluoroisopropanol (HFIP) and cholesterol (laboratory grade) were purchased from Sigma-Aldrich (UK).

3.3 Methods

3.3.1 Preparation of lipid cakes

The total brain lipid extract from porcine brain was used consisting of phosphatidylethanolamine (16.7% w/w), phopatidylserine (10.6% w/w), phospatidylcholine (9.6% w/w), phosphatidic acid (2.8% w/w), phosphatidylinositol (1.6%), and other (58.7% w/w), of which the majority is cholesterol (~30-40% w/w total brain lipid)[38].

Chloroform was evaporated from chloroform dissolved TBL or DMPC (5ml) under vacuum using a rotary evaporator, and after evaporation of chloroform, the lipid cake was obtained. The lipid cake was suspended in 1 ml of doubly distilled water and frozen at -80 °C for an hour and then lyophilized overnight under high vacuum using freeze dyer to remove any trace of chloroform.

TBL (10 mg) was suspended in 50 µl buffer (10mM sodium phosphate, 10mM MgCl2, 0.1mM EDTA; pH 7.4) and centrifuged at 18,000g for 1 minute. The supernatant was removed and then TBL containing sodium phosphate buffer was transferred into 4 mm MAS rotors.

Samples of DMPC/$A\beta_{25-35}$, DMPC/cholesterol, DMPC/cholesterol/$A\beta_{25-35}$, DMPC/KLVFF, DMPC/cholesterol/KLVFF, DMPC/$A\beta_{25-35}$/KLVFF, and DMPC/cholesterol/$A\beta_{25-35}$/KLVFF were prepared at molar ratio of 9:1, 8:2, 8:2:1, 9:1, 8:2:1, 9:1:1, 8:2:1:1, respectively. The amyloid peptide or KLVFF was co-dissolved with phospholipid/cholesterol.

The lipid/cholesterol and $A\beta_{25-35}$/KLVFF were co-dissolved in chloroform/HFIP (1:1 v/v). The lipid/peptide mixture cake was prepared as TBL sample. The lipid/peptide mixture (7 μg) was hydrated with 30 μl of TRIS buffer (pH 7.8) to make lipid vesicles. Then it was centrifuged at 1200 rpm for 1 minute and lipid- mixture pellet was obtained. After that, this lipid-mixture pellet was transferred into a 4mm MAS rotor.

3.3.2 Aliquoting the amyloid peptide

The white lyophilized powder of $A\beta_{25-35}$ (5 mg) was dissolved into the organic solvent, HFIP (1 ml) and aliquoted (100 μl of HFIP + $A\beta_{25-35}$) into ten glass tubes (0.5 mg/tube). HFIP gives the monomeric form of Aβ. After evaporation of HFIP, the amyloid beta was stored at -20°C for further use.

3.3.3 Buffer preparation

TRIS buffer was prepared at concentration of 10 mM TRIS, 10 mM $MgCl_2$ and 0.5 mM EDTA at pH 7.8. The buffer was then filtered with 0.45 μm syringe filters and stored at 4°C.

3.3.4 ^{1}H MAS NMR measurement

The ^{1}H NMR experiments were performed using a spinning rate of 10 KHz MAS speed at 303K. All ^{1}H NMR spectra were internally referenced to the lipid chain CH_3 groups with a chemical shift of 0.9 ppm. The 1D ^{1}H NMR experiments were carried out with a typical $\pi/2$ pulse length of 5.68μsec and a relaxation delay of 2 seconds and the spectra were recorded using either 128, 256 or 512 scans.

3.3.5 2D NOESY measurement

2D NOESY experiments were conducted at 303K using a spinning rate of 10 KHz MAS speed. The spectra were recorded using 96 or 256 scans and 256 or 512 increments. A typical $\pi/2$ pulse length of 5.68 at 6.00 DB was used. The NOESY spectra were also referenced to the methyl group, which produces a diagonal peak with a chemical shift of 0.9 ppm.

3.3.6 Interpretation of NOESY cross-relaxation rates

Cross-relaxation rate of amyloid peptides and lipids bilayers was determined by NOESY spectrum. NOESY experiments produce diagonal and cross peaks resonances[39]. The diagonal peaks of a spectrum were assigned to the DMPC lipid functional groups. Whereas the cross peaks were assigned to the corresponding DMPC functional group and amino acids of $A\beta_{25\text{-}35}$ or beta breaker peptide (KLVFF).

The cross relaxation rate evaluates the position and orientation of specific particles in the lipid bilayers[37]. Cross relaxation rates were determined according to a spin-pair interaction model[37, 39, 40] of lipids and amyloid peptides. It is calculated by the following equation:

$$\sigma_{ij} = A_{ij}(tm) / A_{jj}(tm)tm$$

[σ_{ij} = cross relaxation rate; $A_{ij}(tm)$ = cross peak volume at mixing time (tm);
$A_{jj}(tm)$ = diagonal peak volume at mixing time zero][40]

The diagonal peaks volume among lipid molecules and cross peaks volume between lipid molecules and Aβ residues/beta breaker peptide were measured using CCPN software (CcpNmr Analysis, version 2.0.2). The cross relaxation rate equation was applied to calculate the rate of cross relaxation of peptide residues in lipid molecules. The cross relaxation rates were plotted against carbon number of lipid molecules for calculated residues of amyloid peptide to determine the orientation and localization of amyloid residues in the lipid bilayers.

3.4 Results

3.4.1 ^{1}H MAS SS-NMR spectra of total brain lipid (TBL) bilayers

Extracted total brain lipids from porcine brain (purchased from Avanti Polar, USA) were used to prepare lipid bilayer models to understand the interaction mechanism between peptide, amyloid beta and lipid bilayers. TBL vesicles were prepared according to protocol as described in section 3.3.1. The TBL vesicles were measured at magic angle spinning (MAS) speed of 10 KHz and 303K using a ^{1}H MAS solid state 4mm NMR probe.

TBL peaks were assigned according to the published value of 1, 2-dioleoyl-*sn*-glycero-3-phosphocholine (DOPC)[41] and cholesterol as shown in figure 3.4 and matched to the total brain lipid molecules. The reasons for using ^{1}H NMR chemical shifts of DOPC functional groups to assign the TBL functional groups are: (i) TBL containing unsaturated fatty acid chains are similar to DOPC lipids. (ii) DOPC lipid bilayer resembles to the properties of the membrane lipid bilayer such as thickness, fluidity, structural order and polarity[42, 43]. (iii) PC is the most abundant phospholipid of mammalian membrane accounting approximately 50% of the total phospholipids[9].

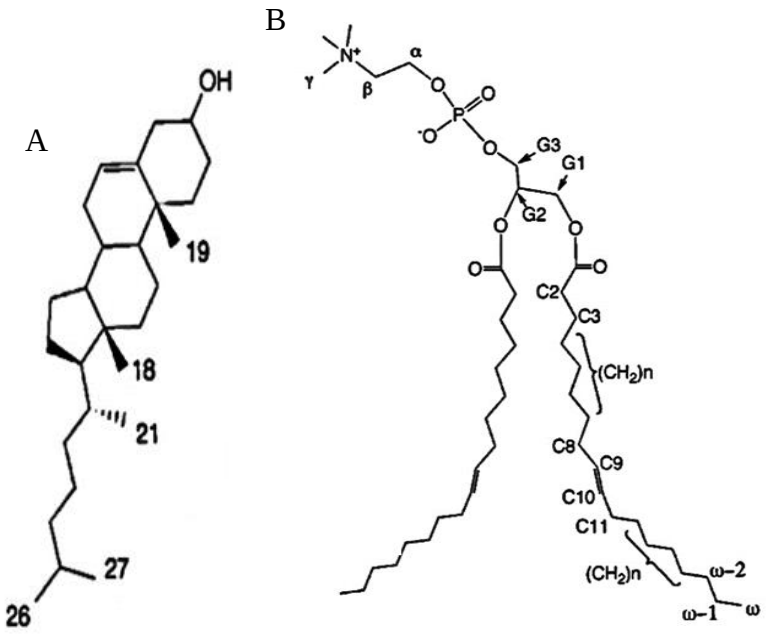

Figure 3.4 Chemical structures of (A) cholesterol and (B) DOPC

Table 3.4.1 DOPC functional groups and their chemical shift values[5]

DOPC ^{1}H NMR Chemical Shifts	DOPC functional groups
0.90ppm	ω
1.31ppm	CH_2(n)
1.55ppm	C3
2.06ppm	C8 and C11
2.42ppm	C2
3.26ppm	γ
3.71ppm	β
4.04ppm	G3
4.32ppm	α
4.60ppm	G_1
5.36ppm	C9, C10 and G2

Four different stocks of TBL were used in this experiment. TBL samples A and B were prepared from two different TBL stocks and ^{1}H- MAS SS-NMR spectrum of these samples did not show any peaks between 7 and 10ppm (Figure 3.4.1A&B). After running out of these stocks, two different TBL stocks were purchased from the same company (Avanti Polar, USA) and samples C and D were prepared. ^{1}H- MAS SS-NMR spectra of TBL samples C and D showed one peak between 7 and 8ppm in the sample C (Figure 3.3.1C) and two peaks between 9 and 10ppm in the sample D (Figure 3.4.1D).

The spectra of TBL samples C and D suggested that there were some amide, aromatic or aldehyde contaminants in the lipids, which were not found in the pure TBL samples of previous stock samples A and B. Further TBL vesicles were prepared and measured four times from the new TBL stocks to check the error in the sample preparation and the NMR spectrum of each experiment showed the same result. Each time, fresh and filtered buffer was used to prepare TBL vesicles to avoid contaminations. Hence it was decided to not use TBL to prepare lipid bilayer models for further experiments.

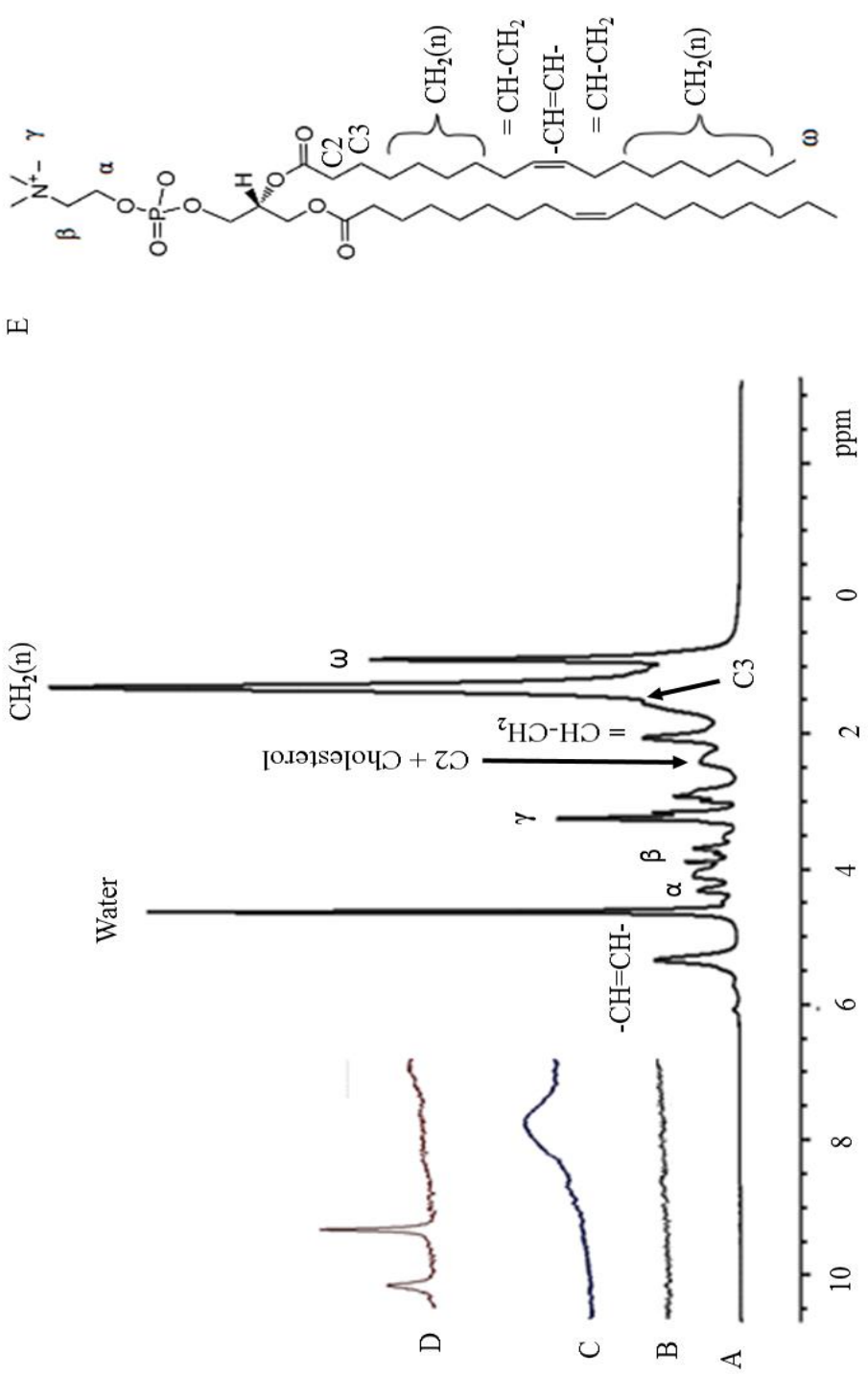

Figure 3.4.1 ^{1}H MAS NMR spectra of TBL. TBL peaks were assigned according to published values of the peaks of DOPC; (A) and (B) spectra of TBL samples did not show peaks between 6 and 10ppm; (C) and (D) spectra of TBL samples indicated peaks between 6 and 10ppm; (E) chemical structure of DOPC.

3.4.2 Investigation of amyloid beta interactions with DMPC lipid bilayers using ^{1}H MAS SS-NMR

DMPC lipid vesicles were used as lipid bilayer models to examine the interaction mechanism between membrane and amyloid beta. $A\beta_{25-35}$, a small toxic fragment of amyloid beta was used in this experiment. DMPC was chosen to prepare lipid vesicles because of its chain length and phase transition temperature. DMPC is a glycerol-phospholipid with two saturated fatty acids chains, containing 14 carbon atoms each, which has resemblance to various mammalian membranes[44]. The gel–liquid crystalline phase transition temperature (Tm) of DMPC is 297K[12]. Amyloid beta conformations and fibrillar elongations are also influenced by temperature ranges from 278K to 318K[45, 46].

Co-dissolved samples of DMPC with $A\beta_{25-35}$/ KLVFF or $A\beta_{25-35}$ plus KLVFF were prepared according to protocol described in section 3.3.1 and experimental setup is described in section 3.3.4. Samples were measured at MAS speed 10kHz and 303K. ^{1}H NMR spectrum of DMPC peaks were assigned according to published values for DMPC[8] (Figure 3.4.2E) and matched to the DMPC lipid molecules, which are listed in table 3.4.2. The ^{1}H NMR spectrum of $A\beta_{25-35}$ plus DMPC sample did not show amide peaks of amyloid peptide, and DMPC lipid peaks were also unchanged in presence of $A\beta_{25-35}$ (Figure 3.4.2B).The spectrum of $A\beta_{25-35}$ plus DMPC suggests that the $A\beta_{25-35}$ adopts fibrillar conformation very soon after aqueous contact and therefore amyloid fibrillar structure does not produce peaks at amide regions (5.5-8.5ppm). The spectrum of DMPC and $A\beta_{25-35}$ also suggests that the molecules of fibrillar $A\beta_{25-35}$ are too large to be obtained by NMR spectrum.

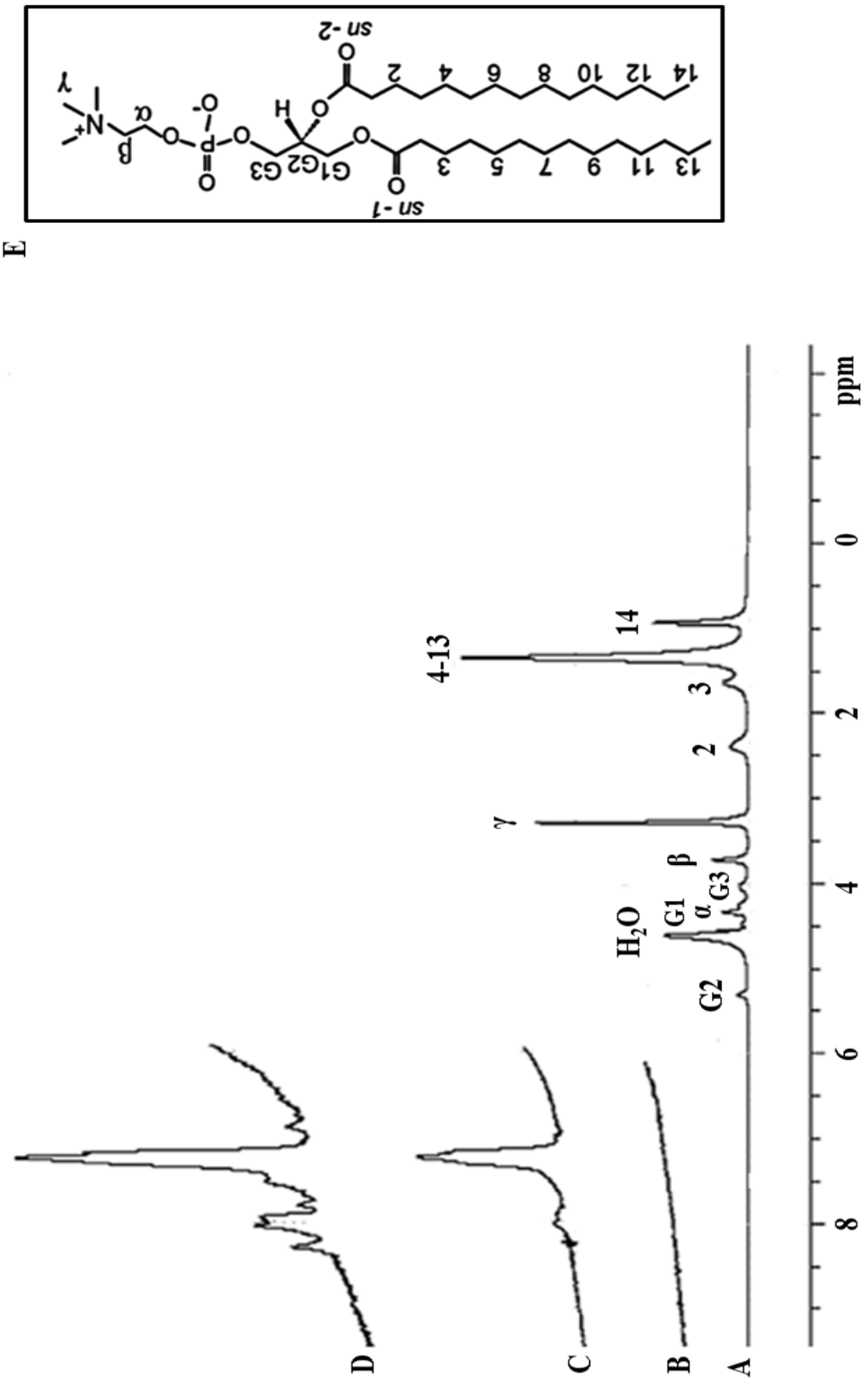

Figure 3.4.2. ^{1}H MAS NMR spectra of DMPC with Aβ$_{25-35}$. (A) Assigned peaks of DMPC: (B) DMPC plus Aβ$_{25-35}$: (C) DMPC plus KLVFF: (D) DMPC with KLVFF plus Aβ$_{25-35}$; (E) chemical structure of DMPC

Table 3.4.2 DMPC functional groups and their chemical shift values

DMPC ^{1}H NMR Chemical Shifts	DMPC functional groups
0.90ppm	14 (CH_3)
1.33ppm	4-13 (CH_2)
1.62ppm	3 (CH_2)
2.37ppm	2 (CH_2)
3.26ppm	γ
3.71ppm	β
4.02ppm	G3
4.31ppm	α
4.47ppm	G1
5.33ppm	G2

KLVFF, which is a small fragment ($A\beta_{16-20}$) of full length amyloid beta, $A\beta_{1-42}$ as shown in Figure 3.4.2.1, was co-dissolved with DMPC lipids at equimolar concentration of $A\beta_{25-35}$ (1:1). The co-dissolved sample containing DMPC lipid and KLVFF was measured at MAS speed 10KHz and 303K. The spectrum showed a peak at 7.25 ppm along with the DMPC peaks (Figure 3.4.2C). The peak at 7.25 ppm represents the -OH functional group of Phe(F) of KLVFF. DMPC plus KLVFF spectrum suggests that the residues of KLVFF does not adopt fibrillar structure in aqueous contact. The spectrum also suggest that the residues of KLVFF and DMPC lipid molecules are mobile in the same experimental system.

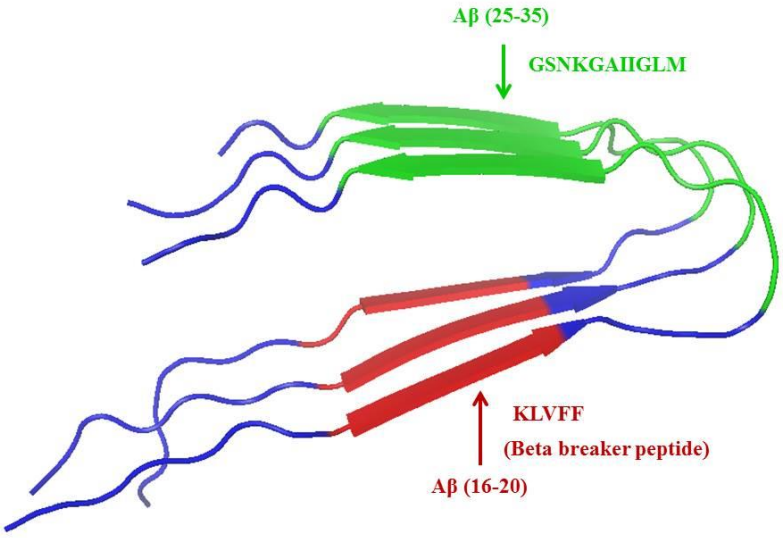

Figure 3.4.2.1 Solid state NMR structure of $A\beta_{1-40}$ fibrils (blue colour); small toxic fragment $A\beta_{25-35;}$ green colour); Beta breaker peptide (KLVFF) $A\beta_{16-20}$ (red colour).

The ^{1}H MAS SSNMR spectrum of co-dissolved mixture of DMPC lipid vesicles and $A\beta_{25-35}$ plus KLVFF sample showed peaks at the amide regions between 7.5 and 8.5ppm (Figure 3.4.2D) along with the peaks of KLVFF and DMPC. The spectrum suggests that the KLVFF might have the ability to prevent the fibrillation of $A\beta_{25-35}$ during lipid bilayer contact. The peaks of $A\beta_{25-35}$ at amide regions suggest that the residues of $A\beta_{25-35}$ are also mobile in presence of KLVFF together with DMPC lipid molecules.

3.4.3 Investigation of amyloid beta interactions with cholesterol using ^{1}H MAS SS NMR

To examine the role of membranous cholesterol with amyloid beta interactions, phospholipid bilayers with cholesterol models were prepared. It is reported that cell membranes generally contain 20-50% cholesterol molecules depending upon the cell types[9]. In this study, 20% cholesterol was co-dissolved with 80% deuterated DMPC (DMPC-d_{54}) to prepare lipid vesicles. DMPC-d_{54} was used to prepare lipid vesicle because the signals of deuterated DMPC tail groups are not obtained under ^{1}H MAS SS-NMR and thus cholesterol signals are only obtained along with DMPC head groups. Hence, DMPC-d54 lipid vesicle with cholesterol (membrane mimic) was prepared to investigate the interaction between cholesterol and amyloid

peptide. Sample preparation and experimental setup are described in section 3.3.1 and 3.3.4, respectively.

The spectrum peaks were assigned according to published chemical shift values of DMPC and cholesterol functional groups[41, 47] (Figure 3.4.3A). The peaks of lipid molecules remain unchanged in the presence of $A\beta_{25-35}$ of a sample containing DMPC-d_{54}, cholesterol and $A\beta_{25-35}$ (Figure 3.4.3B). The spectrum suggests that $A\beta_{25-35}$ acquires fibrillar structure as soon as it contacts with lipids. Thus the non-mobile molecules of amyloid fibres are unable to produce NMR signals. The DMPC-d_{54} plus cholesterol and KLVFF sample produced a peak at 7.25 ppm together with lipid peaks between 0.90 to 5.33 ppm (Figure 3.4.3C). The spectrum suggests that the 7.25 ppm peak arises due to the –OH of phenylalanine of KLVFF.

The sample of DMPC-d_{54} with cholesterol plus KLVFF and $A\beta_{25-35}$ showed the peaks between 7.5 and 8.5 ppm along with the peaks of lipids and KLVFF (Figure 3.4.3D). The spectrum suggests that the peaks between 7.5 and 8.5 ppm are the amide peaks of peptide, $A\beta_{25-35}$. The spectrum also suggests that KLVFF inhibits the fibrillation of $A\beta_{25-35}$ under the lipid environment. The spectra demonstrate that the lipid peaks (DMPC head groups and cholesterol) remain unchanged from 0.90 to 5.33 ppm by KLVFF and $A\beta_{25-35}$.

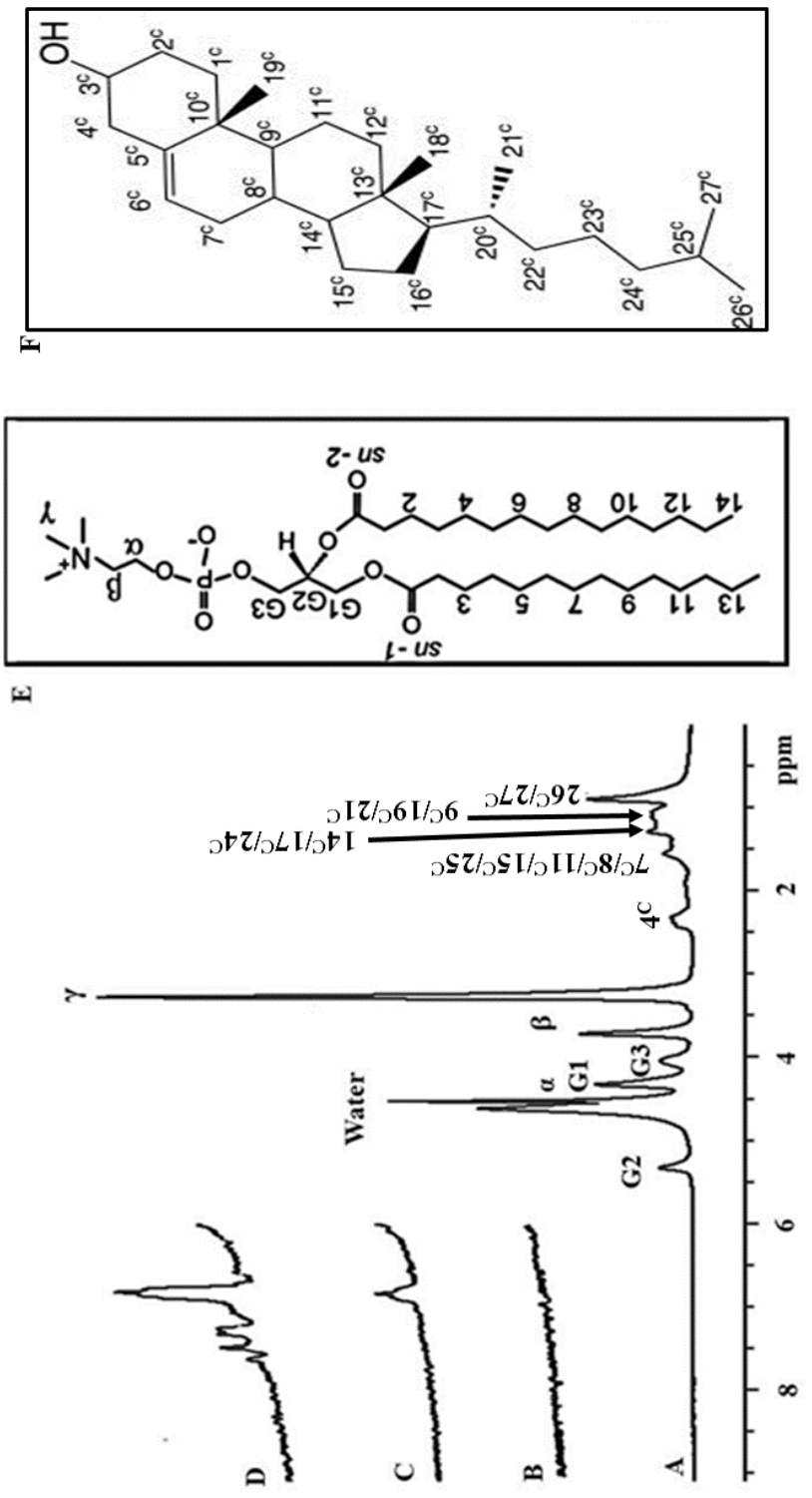

Figure 3.4.3 ^{1}H MAS NMR spectra of DMPC-d_{54} and cholesterol with amyloid peptide. (A) Assigned peaks of DMPC-d_{54}+Cholesterol; (B) DMPC-d_{54} + cholesterol and $A\beta_{25\text{-}35}$ (C) DMPC-d_{54} + Cholesterol and KLVFF; (D) DMPC-d_{54}+Cholesterol and KLVFF plus $A\beta_{25\text{-}35}$; (E) Chemical structure of DMPC; (F) Chemical structure of Cholesterol.

Table 3.4.3 DMPC-d_{54} and cholesterol functional groups and their chemical shifts

DMPC-d54 and cholesterol ^{1}H NMR Chemical Shifts	DMPC-d54 and cholesterol functional groups
0.91ppm	$26^{c}/27^{c}$
1.07ppm	$9^{c}/19^{c}/21^{c}$
1.29ppm	$14^{c}/17^{c}/24^{c}$
1.56ppm	$7^{c}/8^{c}/11^{c}/15^{c}/25^{c}$
2.38ppm	4^{c}
3.26ppm	γ
3.71ppm	β
4.02ppm	G3
4.31ppm	α
4.47ppm	G1
5.33ppm	G2

3.4.4 Amyloid beta interactions with phospholipid and cholesterol under ^{1}H MAS SS NMR

To investigate the combined role of phospholipid and cholesterol with amyloid beta interactions in the membrane, DMPC phospholipid (80%) and cholesterol (20%) were used to prepare lipid vesicles. Co-dissolved samples of DMPC with cholesterol and $A\beta_{25\text{-}35}$/KLVFF or $A\beta_{25\text{-}35}$ plus beta breaker peptide were prepared according to protocol described in section 3.3.1 and experimental setup is described in section 3.3.4. Samples were measured at MAS speed 10 KHz and 303K.

The spectrum peaks were assigned according to published chemical shift values of DMPC and cholesterol functional groups[41, 47] (Figure 3.4.4A).The ^{1}H NMR spectrum of a sample DMPC with cholesterol and $A\beta_{25\text{-}35}$ did not show peptide amide peaks between 6.5 and 8.5ppm (Figure 3.4.4B).The spectrum suggests that $A\beta_{25\text{-}35}$ are non-mobile fibrillar structures in the lipid environment. The non-mobile amyloid fibrils molecules do not produce peaks whereas mobile DMPC and cholesterol molecules yield peaks between 0 and 5.5 ppm in the same experimental conditions.

The sample containing DMPC plus cholesterol and KLVFF showed a peak at 7.25ppm together with lipid peaks (Figure 3.4.4C). The 7.25ppm peak arises due to the –OH group of phenylalanine of KLVFF. The peak at 7.25ppm suggests that the molecules of KLVFF do not acquire fibrillar structure with lipids contact.

The sample of DMPC with cholesterol and KLVFF plus $A\beta_{25\text{-}35}$ produced peaks at peptide amide regions between 7.5 and 8.5ppm (Figure 3.4.4D). The spectrum suggests that beta breaker peptide inhibits the growth of fibrillar structure of $A\beta_{25\text{-}35}$ during lipid contact. The peaks of cholesterol and DMPC are unaffected by $A\beta_{25\text{-}35}$ and KLVFF in the same environment.

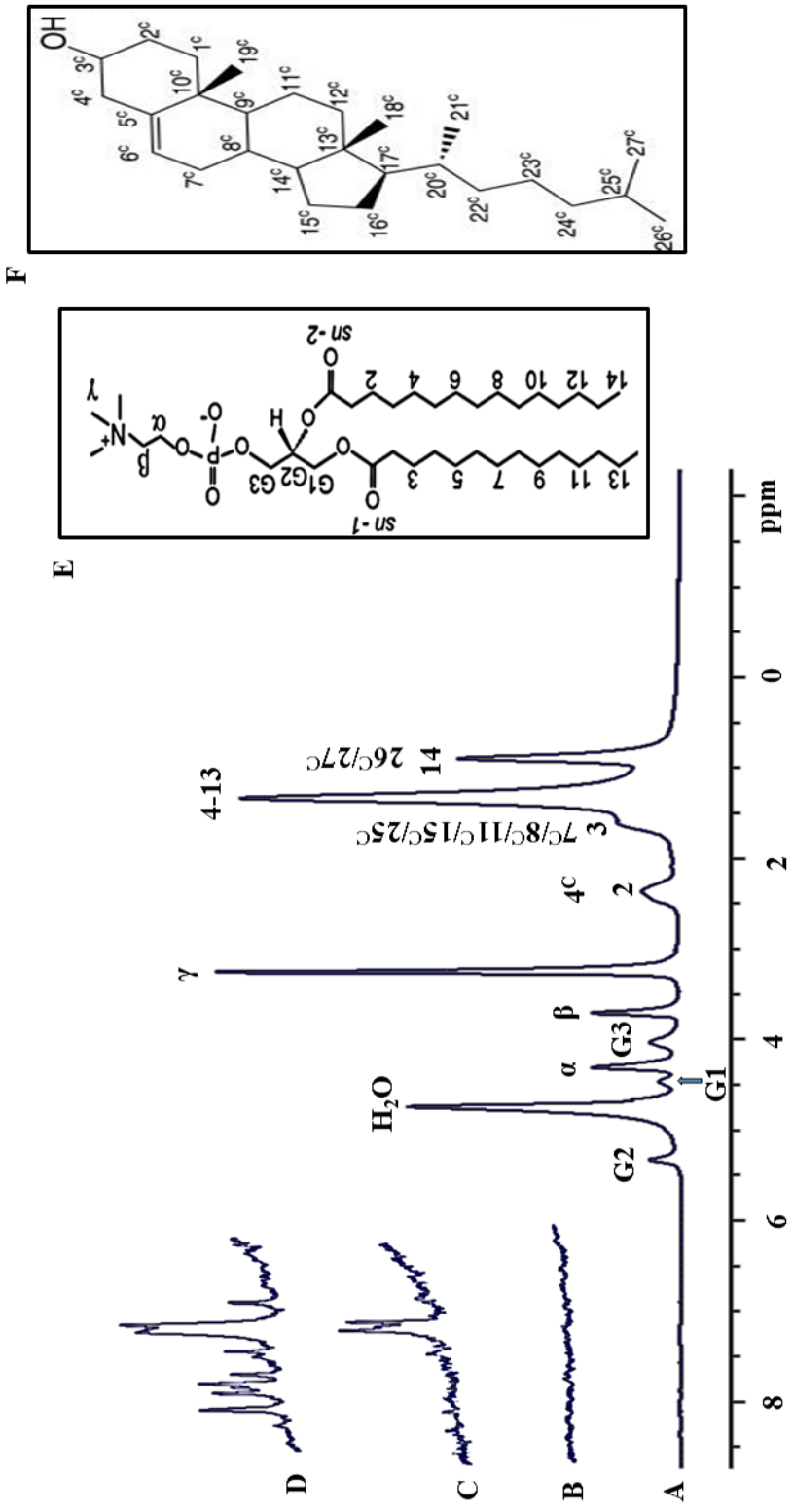

Figure 3.4.4 ^{1}H MAS NMR spectra of DMPC and cholesterol with amyloid peptide. (A) Assigned peaks of DMPC + Cholesterol; (B) DMPC + Cholesterol and $A\beta_{25\text{-}35}$ (C) DMPC + Cholesterol and KLVFF; (D) DMPC + Cholesterol and KLVFF plus $A\beta_{25\text{-}35}$; (E) Chemical structure of DMPC; (F) Chemical structure of Cholesterol

Table 3.4.4 DMPC and cholesterol functional groups and their chemical shifts

DMPC and cholesterol ^{1}H NMR Chemical Shifts	DMPC and cholesterol functional groups
0.91ppm	14 and $26^{c}/27^{c}$
1.33ppm	4-13
1.62ppm	3 and $7^{c}/8^{c}/11^{c}/15^{c}/25^{c}$
2.38ppm	2 and 4^{c}
3.26ppm	γ
3.71ppm	β
4.02ppm	G3
4.31ppm	α
4.47ppm	G1
5.33ppm	G2

3.4.5 ^{1}H MAS-NMR NOESY of DMPC lipid and amyloid peptide

The ^{1}H MAS NOESY (2D) SSNMR was used to determine the location of the amyloid peptide in the phospholipid bilayers. The co-dissolved sample of DMPC and $A\beta_{25-35}$ plus KLVFF was used to prepare lipid vesicles. This spectrum was collected at 256 increments and 128 scans per increment with 500msec mixing time at 303K and spinning speed of 10kHz. Further the spectrum was analysed to assign the different phospholipid groups of DMPC and their possible bindings with KLVFF or $A\beta_{25-35}$.

The NOESY spectrum of sample DMPC and $A\beta_{25-35}$ plus KLVFF produce diagonal peak resonances and cross peak resonances. DMPC diagonal peaks and cross peaks resonance appeared between 0 to 6ppm (Figure 3.4.5B). The amyloid peptide diagonal peaks and lipid-peptide cross peak resonances appeared between 7 and 8ppm (Figure 3.4.5A). Both the resonances are plotted in the indirect dimension (Figure 3.4.5). The cross peak provides an indication of the proximity of two peaks. The spectrum shows that the cross peaks between amyloid peptide and lipid are much weaker than the lipid diagonal and cross peaks.

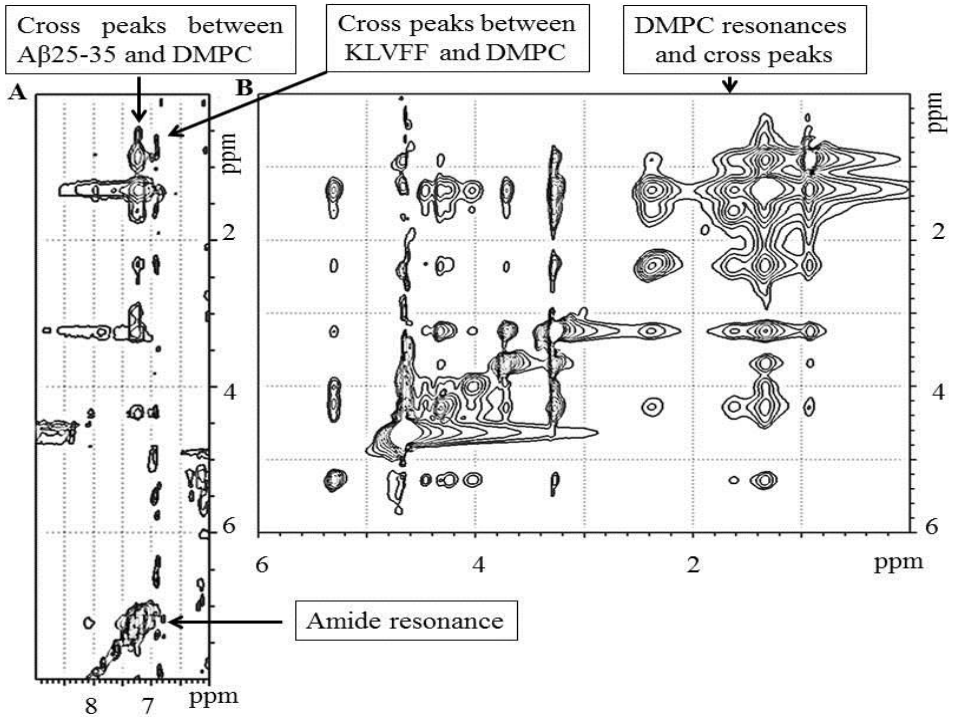

Figure 3.4.5 ^{1}H MAS NMR NOESY DMPC lipid and amyloid peptide. (A) Cross peaks between DMPC and $A\beta_{25\text{-}35}$ /KLVFF; (B) DMPC diagonal peaks with cross peaks between lipid groups.

The DMPC diagonal peaks volume and DMPC-amyloid peptide cross peaks volume were measured using CCPN software (CcpNmr Analysis, version 2.0.2). The cross-relaxation rate was applied to plot the location probability versus DMPC functional groups for amyloid peptides. The calculation and interpretation of cross-relaxation rate is described in sections 3.1.5 and 3.3.6, respectively.

Table 3.4.5 Diagonal peak volumes and Cross peak volumes of DMPC and amyloid peptides

DMPC lipid functional groups	DMPC diagonal peak volume	DMPC-$A\beta_{25-35}$ cross peak volume	DMPC- KLVFF cross peak volume
C14	6.733e+08	47826	350722
C4-13	1.951e+09	342720	146656
C3	6.456e+07	73812	252108
C2	5.405e+07	19734	140690
G1	1.515e+07		
G2	3.693e+07		25982
G3	3.657e+07	46948	49314
α	1.675e+08	70822	145466
β	2.353e+08	33980	71778
γ	1.559e+09	109952	352136

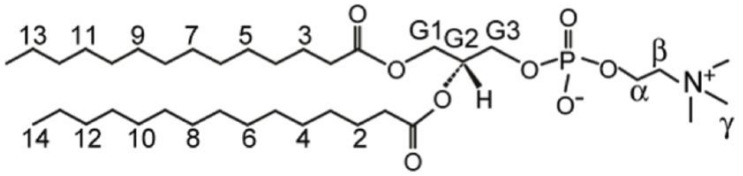

Figure 3.4.5.1 Chemical structure of DMPC

The cross relaxation rate data suggest that $A\beta_{25-35}$ and beta breaker peptides have weak interaction with the head group (α, β and γ) regions of DMPC. The DMPC tail positions C2 and C3 near the glycerol region show the strongest interaction with KLVFF (Figure 3.4.5.2). The DMPC tail positions C4-13 and C14 illustrate the weakest interaction with $A\beta_{25-35}$ and KLVFF. The cross relaxation rate at glycerol region of DMPC suggests that KLVFF interacts at positions G2 and G3 whereas $A\beta_{25-35}$ interacts only at positions G3. The strongest interaction between $A\beta_{25-35}$ and DMPC occurs at glycerol position G3 and lipid tail position C3. The data suggests that $A\beta_{25-35}$ and KLVFF may enter into the top of the lipid chain region.

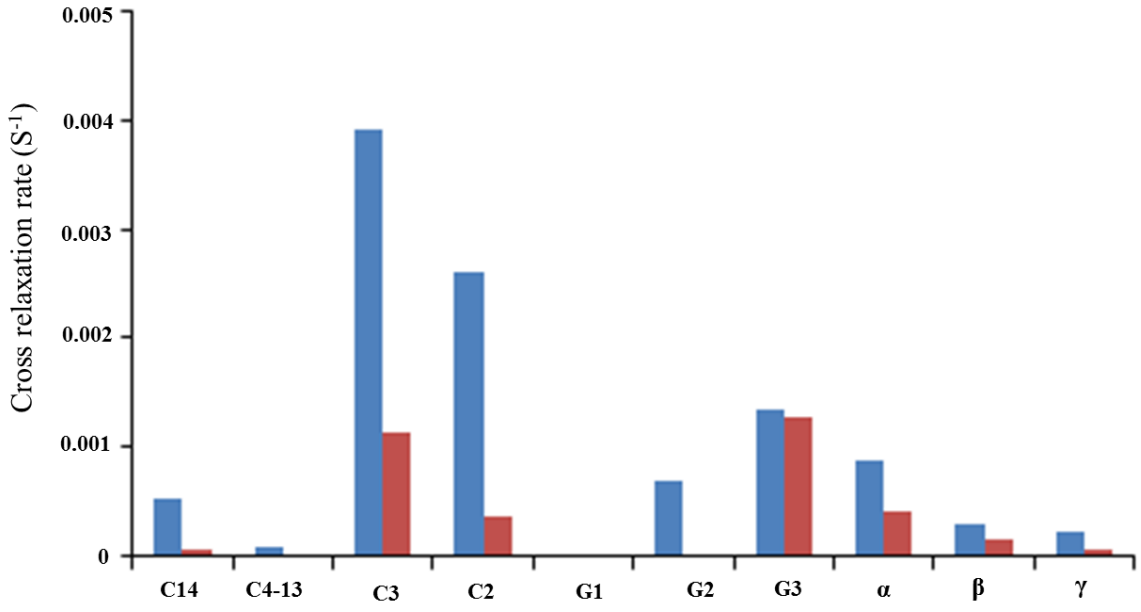

Figure 3.4.5.2 Cross relaxation rate between DMPC lipid groups and $A\beta_{25-35}$ plus KLVFF derived from a MAS-NOESY measurement. Red bars represent ^{1}H signals from $A\beta_{25-35}$ and blue bars are from KLVFF. The heights of the bars are proportional to the strength of the interaction between a particular lipid group and the $A\beta_{25-35}$ or KLVFF.

3.4.6 ^{1}H MAS-NMR NOESY of DMPC-d_{54} with cholesterol plus amyloid peptide

The location of the amyloid peptides in the deuterated phospholipid bilayers with cholesterol was determined by ^{1}H MAS NOESY SSNMR. The experimental setup is described in section 3.3. The co-dissolved sample containing DMPC-d_{54} with cholesterol and $A\beta_{25\text{-}35}$ plus beta KLVFF was used to determine NOESY spectrum at 256 increments and 128 scans per increment with 500msec mixing time. The NOESY spectrum was obtained at 10kHz MAS speed and 303K. The diagonal and cross peaks of cholesterol molecules appeared between 0 and 6ppm. The cross peaks between cholesterol molecules and amyloid peptides did not appear at the NOESY spectrum (Figure 3.4.6). The NOSEY spectrum suggests that cholesterol molecules may not interact with amyloid peptides in the lipid bilayers.

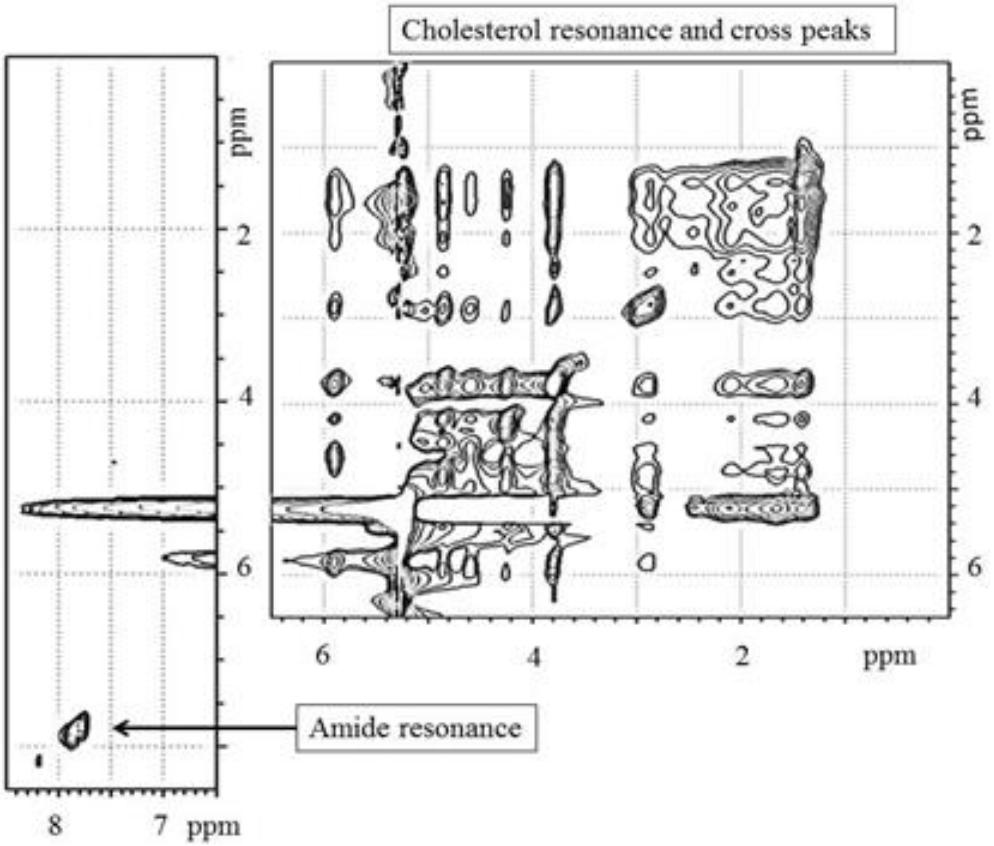

Figure 3.4.6 ^{1}H MAS NOSEY spectrum of cholesterol with DMPC-d_{54} and $A\beta_{25\text{-}35}$ plus KLVFF. No cross peaks were observed between cholesterol and amyloid peptides.

3.4.7 ^{1}H MAS-NMR NOESY of DMPC plus cholesterol and amyloid peptides

The ^{1}H MAS NOESY (2D) SSNMR was employed to determine the location of the amyloid peptides in the phospholipid plus cholesterol vesicles using co-dissolved samples of DMPC with cholesterol and $A\beta_{25-35}$ plus KLVFF. The NOSEY spectrum was collected at 256 increments and 128 scans per increment with 500msec mixing time at 310K and spinning speed 10kHz.

The NOESY spectrum of sample containing DMPC with cholesterol and $A\beta_{25-35}$ plus KLVFF produces diagonal peaks resonance and cross peaks resonance. DMPC with cholesterol diagonal peaks and cross peaks resonance appeared between 0 to 6ppm (Figure 3.4.7B). The amyloid peptide diagonal peaks and lipid- peptide cross peaks resonance appeared between 7 and 8ppm (Figure 3.4.7A).

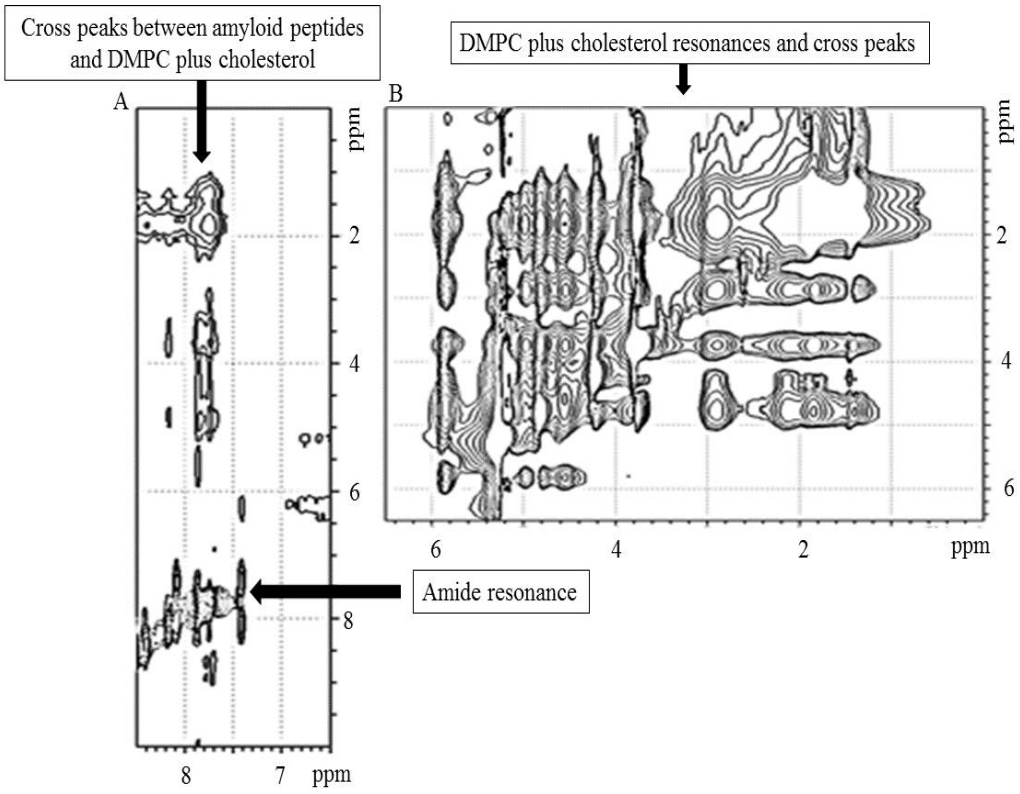

Figure 3.4.7 ^{1}H MAS NMR NOESY spectra of cross peak between lipid plus cholesterol interactions with amyloid beta. (A) Cross peaks between DMPC plus cholesterol and $A\beta_{25-35}$ plus KLVFF; (B) DMPC plus cholesterol diagonal peaks with cross peaks between lipid and cholesterol groups.

Table 3.4.7 Diagonal peaks volume and Cross peaks volume of DMPC plus cholesterol and amyloid peptides

DMPC and cholesterol functional groups	lipid diagonal peak volume	lipid-$A\beta_{25-35}$ cross peak volume	DMPC-KLVFF cross peak volume
C14 and $26^c/27^c$	2.624e+08	102811.5	333105
C4-13	6.745e+08	186223	609886
C3 and $7^c/8^c/11^c/15^c/25^c$	2.729e+07	45706	168263
C2 and 4^c	7.996e+06	1883	22478
G1			
G2			
G3	1.148e+07	28589.5	41808
α	8.940e+06	22474	98323
β	6.870e+06	17895	18958.5
γ	5.117e+08	74983	156559

The DMPC plus cholesterol diagonal peaks volume and DMPC plus cholesterol and amyloid peptides cross peaks volume were measured using CCPN software (CcpNmr Analysis, version 2.0.2). The cross-relaxation rate was applied to plot the location probability versus DMPC plus cholesterol functional groups for amyloid peptides. The calculation and interpretation of cross-relaxation rate is described in section 3.3.6 and 3.1.5.

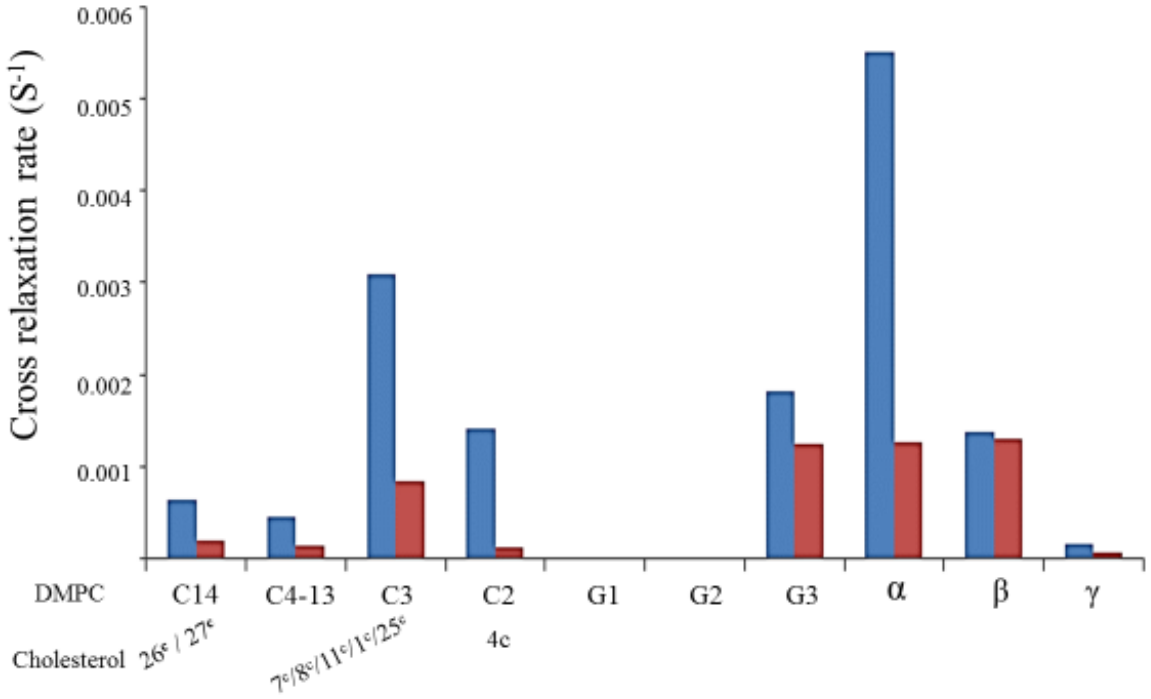

Figure 3.4.8 Cross relaxation rates between DMPC plus cholesterol and Aβ25-35 plus KLVFF derived from a MAS-NOESY measurement. Red bars represent ^{1}H signals from Aβ25-35 and blue bars are from KLVFF. The heights of the bars are proportional to the strength of the interaction between a particular lipid group and the amyloid peptides.

The cross relaxation rate data suggest that Aβ25-35 and KLVFF comprise the weakest interaction with the head group γ position of DMPC. The DMPC lipid head position β shows strong interaction with Aβ25-35 and KLVFF. α position of DMPC lipid head group indicates the strongest interaction with KLVFF in comparison to Aβ25-35 (Figure 3.4.8).

The DMPC lipid tail position C14 plus cholesterol positions $26^{c}/27^{c}$ and DMPC lipid tail positions C4-13 show weak interaction with Aβ25-35 and KLVFF (Figure 3.4.8). The DMPC tail positions C3/C2 and cholesterol positions $7^{c}/8^{c}/11^{c}/15^{c}/25^{c}$ /4^{c} indicate strong interaction with KLVFF and weak interaction with Aβ25-35 (Figure 3.4.8).

The cross relaxation rate plot suggests that the glycerol regions of DMPC position G1 and G2 do not interact with either Aβ25-35 or KLVFF but glycerol position G3 interacts with Aβ25-35 and KLVFF. The cross relaxation rate of sample DMPC with cholesterol and Aβ25-35 plus

KLVFF also suggests that cholesterol molecules may push the amyloid peptide towards head of the lipid because strong lipid peptide interactions are observed in lipid at positions G3, β and α.

3.5 Discussion

Amyloid beta (Aβ) accumulation and fibril formation on neurons are important pathological causes of AD[48]. Numerous evidences suggest that amyloidosis occur due to interaction between amyloid peptides and plasma membrane. The islet amyloid polypeptide (IAPP; causing amyloidosis of the pancreas), adopts an α-helix conformation, immediately after contact with lipid bilayers and transforms into β-sheet after prolonged incubation, which was observed by circular dischroism and fluorescence spectroscopy[54]. Engel *et al* (2006) reported that the monomeric form of IAPP can insert into the lipid monolayers whereas fibrillar form cannot[49]. ^{31}P solid state NMR data suggested that low concentration of IAPP might produce an intermediate species (between α-helix and amyloid fibres), capable of interacting with phospholipid bilayers[50]. Circular dischroism (CD) spectroscopy experiments also suggested that some sequences of IAPP along with whole fragment are also capable of developing amyloid fibrillation with phospholipid bilayers[51, 52].

Similarly, it is widely believed that in AD, the direct contact between peptide Aβ and neuronal membrane can promote toxicity on neurons. It is reported that the preservation of Aβ peptide in monomeric form in the membrane may obstruct the amyloid fibril formation and accumulation. Similar to IAPP, the membranous contact of Aβ sequences such as $A\beta_{25\text{-}35}$, $A\beta_{1\text{-}40}$ etc. together with $A\beta_{1\text{-}42}$ (complete sequence of Aβ) in oligomeric form and intermediate species (protofibrils) may cause amyloid accumulation and fibril formation demonstrated by various techniques such as CD, NMR, and patch clamp etc.[49-55]. However, the interaction mechanism between Aβ and lipid bilayer is still unclear.

The aim of this study was to examine the interactions between lipid bilayers and amyloid peptide using ^{1}H MAS SS NMR. TBL and DMPC lipid bilayer vesicles were used as mimics of biological membrane systems because of resemblance with biological membranes. The role of cholesterol during amyloid beta attachment to the membrane was also examined using deuterated DMPC containing cholesterol (20% w/w) lipid vesicles. The experimental setups

were achieved at 303K because at this temperature DMPC acyl chains are found in fluid phase state. Lipid fluid phase state is important to amplify the interaction with other molecules present in the membrane. DMPC phase transition occurs at 296.85K and DMPC plus cholesterol phase transition occurs at ~303.15K[53].

Amyloid beta fragment, $A\beta_{25-35}$ was used and dissolved in solvent HFIP. In HFIP, $A\beta_{25-35}$ retains its monomeric soluble α-helix conformation. $A\beta_{25-35}$ signifies the smallest toxic segment of Aβ peptide. It exhibits large β-sheet aggregated conformation and maintains the toxicity levels as compared to full length amyloid peptide[56]. The misfolding and aggregation of Aβ peptide at an early stage is hindered by β-sheet breaker peptide that is competent to block the growth of beta-sheet of Aβ peptide[48]. In this study, KLVFF was used to examine the interaction mechanism between lipid bilayers and amyloid peptide.

TBL vesicles model was discarded because of some contaminants found in the stocks, which was a manufacturing defect. Three sets of co-dissolved samples containing DMPC, cholesterol, $A\beta_{25-35}$ and KLVFF were prepared to examine the interaction between phospholipid bilayers and amyloid peptide using ^{1}H MAS SS NMR. The first set containing four different types of samples (DMPC, DMPC + $A\beta_{25-35}$, DMPC + KLVFF and DMPC + $A\beta_{25-35}$, DMPC + $A\beta_{25-35}$ + KLVFF) was used to investigate the amyloid peptide interaction with phospholipid bilayers. To examine the interaction between amyloid beta and cholesterol, a second set of samples (DMPC-d_{54} + cholesterol, DMPC-d_{54} + cholesterol + $A\beta_{25-35}$, DMPC-d_{54} + cholesterol + KLVFF and DMPC-d_{54} + cholesterol + $A\beta_{25-35}$ + KLVFF) was used. In the third set, the samples (DMPC +cholesterol, DMPC + cholesterol + $A\beta_{25-35}$, DMPC + cholesterol + KLVFF and DMPC + cholesterol + $A\beta_{25-35}$ + KLVFF) were prepared to investigate the interaction of amyloid beta with lipid bilayers containing phospholipid and cholesterol.

The lipid peaks were unaffected by $A\beta_{25-35}$ as shown in figures 3.4.2B, 3.4.3B and 3.4.4B. The spectra suggest that $A\beta_{25-35}$ polymerises into a fibrous structure in contact with lipid bilayer. The amyloid fibres are too large and non-mobile in the lipid bilayers and hence amide peaks are not observed between 6.5 and 8.5ppm of ^{1}H NMR spectra. The peak at aromatic region between 7 and 7.5ppm was attributed to the phenylalanine of KLVFF as shown in Figures

3.4.2.C, 3.4.3C and 3.4.4C. The spectra suggest that KLVFF in the phospholipid bilayer is in a monomeric form. It also suggests that KLVFF does not acquire a fibrillar conformation with phospholipid bilayers.

In the presence of KLVFF, $A\beta_{25-35}$ peaks appeared between 7.5 and 8.5ppm in the amide regions along with the peaks of KLVFF and lipids as shown in Figures 3.4.2 D, 3.4.3D and 3.4.4D. These amide peaks of $A\beta_{25-35}$ suggest that KLVFF inhibits the polymerisation and fibrillation of $A\beta_{25-35}$ and provides mobility to the $A\beta_{25-35}$ with lipids. The mobile molecules of $A\beta_{25-35}$ suggest that they may exist as monomeric form in the lipid bilayers. The spectrum of sample containing DMPC with cholesterol and $A\beta_{25-35}$ plus KLVFF show four prominent peaks of $A\beta_{25-35}$ at amide regions between 8 and 8.5 ppm (Figure 3.4.4D), which were different from the peaks of the samples containing DMPC and $A\beta_{25-35}$ plus KLVFF or DMPC-d54 with cholesterol and $A\beta_{25-35}$ plus KLVFF. The reasons of these peaks are unknown and it is a matter of further investigation.

The 2D NOESY experiments were performed to analyse the location of peptides in the lipid bilayers. The cross-relaxation rate is applied to evaluate the orientation of peptide particles in the lipid bilayers. The result of the sample containing DMPC and $A\beta_{25-35}$ with KLVFF suggested that $A\beta_{25-35}$ strongly interact with the first two carbon atoms (C2 and C3) of acyl chain near the glycerol and the weakest interactions occur at the end of acyl chain and head group near the membrane surface (Figure 3.4.5.2). The result also suggests that amyloid peptides may locate in the membrane at the centre of the phospholipid bilayers. 2D NOESY spectrum of sample containing DMPC-d_{54} plus cholesterol with $A\beta_{25-35}$ and KLVFF suggested that cholesterol molecules may form direct contact with $A\beta_{25-35}$ and KLVFF in the phospholipid bilayers (Figure 3.4.6). The cross relaxation rate of sample containing DMPC plus cholesterol and $A\beta_{25-35}$ with KLVFF suggested that the weakest interactions between lipids and amyloid peptide occur at the end of acyl chain plus cholesterol molecules and head group (γ) near the membranous surface (Figure 3.4.8). However, the strong interactions between DMPC plus cholesterol and amyloid peptides occur at the glycerol (G3)-head group (α and β) interface and acyl chain near glycerol (Figure 3.4.8). The cross relaxation rate plot suggests that cholesterol molecules might push the amyloid peptides towards the head region of phospholipids as shown in Figure 3.5C.

Vitiello *et al* (2009) observed that cholesterol has a great influence on beta breaker peptide (iAβ5) and DOPC bilayer interactions using electron spin resonance[54]. They reported that beta breaker peptide (iAβ5) is partly located in the DOPC bilayers and cholesterol may modulate and drive the positioning of the beta breaker peptide (iAβ5) at the membrane interface[54]. The data of DMPC plus cholesterol with KLVFF of this study also suggest that cholesterol may influence the positioning of KLVFF by forcing it towards head region, which is clearly seen at α position (Figure 3.4.8).

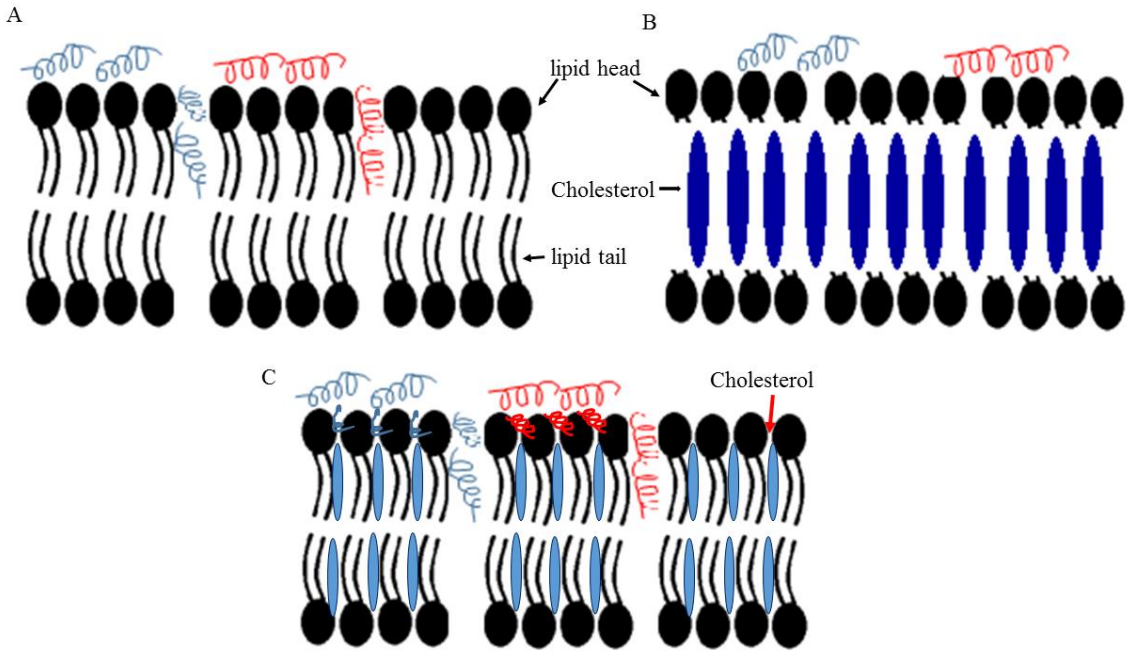

Figure 3.5 Model of lipid bilayers and peptide interaction based on ^{1}H MAS 1D and 2D (NOESY) spectra. (A) DMPC bilayers interaction with $A\beta_{25\text{-}35}$ (red) and KLVFF (blue). Both the peptides enter into phospholipid bilayers; (B) The sample of DMPC-d_{54} with cholesterol and $A\beta_{25\text{-}35}$ plus KLVFF sample. NMR signals of deuterated acyl chains of DMPC tails regions are not obtained under ^{1}H NMR, therefore lipid tails are not drawn in the diagram. Cholesterol molecules do not interact with amyloid peptide molecules and DMPC head groups interact with amyloid peptides; (C) The sample of DMPC with cholesterol containing $A\beta_{25\text{-}35}$ plus KLVFF shows that amyloid peptides interact and may enter into phospholipid bilayers and cholesterol molecules push the peptides towards the head region of phospholipids.

In conclusion, KLVFF may hinder the fibril formation of $A\beta_{25\text{-}35}$ in the lipid bilayers. KLVFF keeps $A\beta_{25\text{-}35}$ in its monomeric mobile form, which may be important to investigate the amyloid beta interaction with lipid bilayers. The amyloid peptides may enter into the membrane at the end of the lipid bilayers and may form pore like structure or puncture the cell membrane and

cause further cellular toxicity. The cholesterol has no influence to interact amyloid peptides but it may modulate and force the peptide molecules towards the membrane surface.

3.6 References

1 J.M. Berg, J.L. Tymoczko and L. Stryer, *Biochemistry*, 5th ed., W. H. Freeman and Company, New York, 2001.

2 B. Albert, D. Bray, J. Lewis, M. Raff, K. Roberts and J.D. Watson, *Molecular Biology of the Cell*, 3rd ed., Garland Publishing, New York, 1994.

3 S. Li, F. Eghiaian, C. Sieben, A. Herrmann and I.A.T. Schaap, *Biophysical Journal*, 2011, **100**, 637-645.

4 S.J. Singer and G.L. Nicolson, *Science*, 1972, **175**, 720-731.

5 G.M. Copper, *The Cell a Molecular Approach*, 2nd ed., Boston university, Sunderland, 2000.

6 M. Vestergaard, T. Hamada and M. Takagi, *Biotechnology and Bioengineering*, 2008, **99**, 753-763.

7 Q. Lin and E. London, *PLOS One*, 2014, **9**, e87903

8 P. Cao, A. Abedini, H. Wang, L-H. Tu, X. Zhang, A.M. Schmidt and D.P. Raleigh, *PNAS*, 2013, **110**, 19279-19284.

9 G.V. Meer, D.R. Voelker and G.W. Feigenson, *Nat Rev Mol Cell Biol*., 2008, **9**, 112–124.

10 J.E. Vance, *Journal of Lipid Research*, 2008, **49**, 1377-1387.

11 M. Podbielskal, S.B. Levery and E.L. Hoganl, *Clin Lipidol*., 2011, **6**, 159-179.

12 J. Huang and G.W. Feigenson, *Biophysical Journal*, 1999, **76**, 2142-2157.

13 M.R. Ali, K.H. Cheng and J. Huang, *Biochemistry*, 2006, **45**, 12629-12638.

14 V.A. Frolov, A.V. Shnyrova and J. Zimmerberg, *Cold Spring Harb Perspect Biol.* 2011, **3**, a004747.

15 S. Zhang, *Nature Biotechnology*, 2003, **21**, 1171-1178.

16 E. Strandberg, D. Tiltak, S. Ehni, P. Wadhwani and A.S. Ulrich, *Biochimica et Biophysica Acta*, 2012, **1818**, 1764-1776.

17 R. Winter and C. Jeworrek, *Soft Matter*, 2009, **5**, 3157-3173.

18 S. Lee, G. Xu, T.R. Jay, S. Bhatta, K.W. Kim, S. Jung, G.E. Landreth, R.M. Ransohoff and B.T. Lamb, *J. Neurosci*., 2014, **34**,12538-12546.

19 K. Matsuzaki, *Int. J. Alzheimers Dis.*, 2011, **2011**, 1-7.

20 J. Bieschke, Q. Zhang, D.A. Bosco, R.A. Lerner, E.T. Powers, P. Wentworth and J.W. Kelly, *Acc. Chem. Res.*, 2006, **39**, 611-619.

21 I.V.J. Murray, L. Liu, H. Komatsu, K. Uryu, G. Xiao,J.A. Lawson and P.H. Axelsen, *J. Biol Chem*., 2007, **282**, 9335-9345.

22 I.V.J. Murray, M.E. Sindoni and P.H. Axelsen, *Biochemistry*, 2005, **44**, 12606-12613.

23 D.G. Smith, R. Cappai and K.J. Barnham, *Biochimica et Biophysica Acta*, 2007, **1768**, 1976-1990.

24 J.A. McLaurin and A. Chakrabartty, *J. Biol. Chem.*, 1996, **271**, 26482-26489.

25 J.J. Kremer, M.M. Pallitto, D.J. Sklansky and R.M. Murphy, *Biochemistry*, 2000**,** **39**, 10309-10318.

26 A. Kakio, S.-I. Nishimoto, K. Yanagisawa, Y. Kozutsumii and K. Matsuzaki, *The Journal of Biological Chemistry*, 2001, **276**, 24985-24990.

27 S.-R. Ji, Y. Wu and S.-F. Sui, *J. Biol. Chem.*, 2002, **277**, 6273-6279.

28 E. Terzi, G.H. lzemann and J. Seelig, *Biochemistry*, 1997, **36**, 14845-14852.

29 S. Micelli, D. Meleleo, V. Picciarelli and E. Gallucci, *Biophysical Journal*, 2004, **86**, 2231-2237.

30 M. Bokvist, F. Lindstrom, A. Watts and G. Grobner, *J. Mol. Biol.*, 2004, **335**, 1039-1049.

31 H. Dies, L. Toppozini, M.C. Rheinstadter, *PLoS ONE*, 2014, **9**, e99124.

32 S. Dante, T. Hauss and N.A. Dencher, *Biophysical Journal*, 2002, **83**, 2610-2616.

33 S. Dante, T. Hauss and N.A. Dencher, *Eur Biophys J.*, 2006, **35**, 523-531.

34 M.D.M. Martinez-Senac, J. Villalain and J.C. Gomez-Fernandez, *Eur. J. Biochem*., 1999, **265**, 744-753.

35 A. Alia, S. Ganapathy and H.J.M. deGroot, *Photosynth Res*., 2009, **102**, 415-425

36 K. Gawrisch, N.V. Eldho and Polozov IV, *Chem Phy Lipids*, 2002, **116**, 135-151.

37 H.A. Scheidt and D. Huster, *Acta Pharmacol Sin*., 2008, **29**, 35-49.

38 Brain total lipid extract

www.avantilipids.com/index.php?option=com_content&view=article&id=408&Iemid=124&catnumber=131101. In (20-10-2014)

39 D. Huster, K. Arnold and K. Gawrisch, *J. Phys. Chem. B.*, 1999, **103**, 243-251.

40 D. Huster, A. Vogel, C. Katzka, H.A. Scheidt, H. Binder, S. Dante, T. Gutberlet, O. Zschornig, H.Waldmann and K. Arnold, *J. Am. Chem. Soc*., 2003, **125**, 4070-4079.

41 J.J. Lopez and M. Lorch, *J. Biol. Chem.*, 2008, **283**, 7813-7822.

42 A.S. Reddy, D.T. Warshaviak and M. Chachisvilis, *Biochim Biophys Acta*, 2012, **1818**, 2271-2281.

43 D.E. Warschawski, A.A. Arnold, M. Beaugrand, A. Gravel, É. Chartrand and I Marcotte, *Biochimica et Biophysica Acta*, 2011, **1808**, 1957-1974.

44 A.P. Serroa, R. Galantea, A. Kozicaa, P. Paradisoa, A.M.P.S. Goncalves da Silva, K.V. Luzyanina, A.C. Fernandesa and B. Saramago, *Colloids and Surfaces B. Biointerfaces*, 2014, **116**, 63-71.

45 Y. Kusumoto, A. Lomakin, D.B. Teplo, and G.B. Benedek, *Proc. Natl. Acad. Sci. USA*, 1998, **95**, 12277–12282.

46 H.-L. Chu and S.-Y. Lin, *Biophysical Chemistry*, 2001, **89**, 173-180.

47 K. Nomura, M. Lintuluoto and K. Morigaki, *J. Phys. Chem. B.*, 2011, **115**, 14991-15001.

48 C. Soto, E.M. Sigurdsson, L. Morelli, R.A. Kumar, E.M. Castaño and B. Frangione, *Nat Med*., 1998, **4**, 822-826.

49 M.F.M. Engel, H.A. Yigittop, R.C. Elgersma, D.T.S. Rijkers, R.M.J. Liskamp, B. de Kruijff, J.W.M. Hoppener and J.A. Killian, *J. Mol. Biol*., 2006, **356**, 783-789.

50 J.R. Brender, U.H.N. Dürr, D. Heyl, M.B. Budarapu and A. Ramamoorthy, *Biochimica et Biophysica Acta*, 2007, **1768**, 2026-2029.

51 J.R. Brender, E.L. Lee, M.A. Cavitt, A. Gafni, D.G. Steel, and A. Ramamoorthy, *J. Am. Chem. Soc.*, 2008, **130**, 6424-6429.

52 N. Arispe, E. Rojas and H.B. Pollard, *Proc. Nati. Acad. Sci. USA*, 1993, **90**, 567-571.

53 J.G. Paiva, P. Paradiso, A.P. Serro, A. Fernandes and B. Saramago, *Colloids and Surfaces B: Biointerfaces*, 2012, **95**, 65-74.

54 S.A. Jayasinghe and R. Langen, *Biochemistry*, 2005, **44**, 12113-12119.

55 M. Vestergaard, T. Hamada and M. Takagi, *Biotechnology and Bioengineering*, 2008, **99**, 753-763.

56 C.J. Pike, A.J. Walencewicz-Wasserman, J. Kosmoski, D.H. Cribbs, C.G. Glabe and C.W. Cotman, *J Neurochem.*, 1995, **64**, 253-265.

Chapter 4
Amyloid beta peptides and lipid phase behaviour: studied by ^{2}H NMR

4.1 Introduction

The lipids in membranes are mainly composed of glycerophospholipids, sphingolipids (sphingomyelin) and sterols (cholesterol)[1, 2]. The acyl chains of sphingolipids are saturated whereas acyl chains of glycerophospholipids are composed of saturated (sn-1) and unsaturated (sn-2) fatty acids[3-5]. The typical lipid composition of biological membranes is glycerophospholipids (40-60%), cholesterol (30-40%) and sphingolipids (10-20%)[6, 7]. The lipid components of outer and inner monolayers of a bilayer (also called leaflets) are not symmetrical[8-10]. The phosphatidylcholine (PC) and sphingomyelin (SM) are enriched in the outer monolayer of lipid bilayer, whereas phosphatidylethanolamine (PE), phosphatidylserine (PS), phosphatidylglycerol (PG), and phosphatidylinositol (PI) are enriched in or limited to, the inner monolayer of lipid bilayer[11]. The transverse distributional pattern of cholesterol molecules in lipid bilayers are not well established[12]. However, it is assumed that cholesterol molecules may be equally dispersed in the leaflets of lipid bilayers because cholesterol molecules have a fast flip-flop rate between outer and inner leaflets of bilayers[13-15]. Some data also suggest that cholesterol molecules show more affinity towards PC and SM than PS and PE molecules; hence it is possible that the presence of cholesterol may be more in the outer leaflet than inner leaflet of lipid bilayer[16]. These lipid molecules are self-arranged into various forms such as micellar, lamellar and hexagonal phase during aqueous contact that will affect bilayer fluidity (discussed in section 3.1.2.2).

Lipid molecules of lamellar phase (characteristic of eukaryotic membrane) may exist in many sub-phases, which may depend upon many factors, including lipid composition, structure and temperature[17, 18]. For example, when a liposome/planar bilayer is heated (from low to higher temperature) its phase changes from a highly ordered state (non-mobile) to a fluid state (mobile)[17, 19]. During the phase transition, thermal energy is absorbed over a course of temperature and the midpoint of this temperature range is the melting temperature (T_m) of the lipid bilayers[17]. High T_m value gives more stable and tightly packed lipid bilayers phase. T_m values also depend upon the composition and structure of acyl chains[20]. Lipid acyl chains with short or unsaturated fatty acids undergo phase transition at lower temperatures contrasting with the lipid acyl chains containing long or saturated fatty acids which undergo phase transition at higher temperature. The reasons behind this phenomenon are that the lipids with short chains have smaller cross sectional area and the molecules of unsaturated fatty acid chains interact with each other via less stable van der Waal forces[17, 21, 22]. Cholesterol is one of the main determining factors to maintain the bilayers fluidity. Cholesterol molecules may control the

random fluidity of the head group of lipid bilayers at the outer side, whereas at inner side, it may help to provide minor fluidity[17].

4.1.1 Lipid phase behaviour

Lipid bilayers without cholesterol molecules mainly adopt crystalline or solid phase (L_c), gel phase (L_β) and liquid-crystalline or liquid-disordered (L_d) or (L_α) phase [7, 20]. At very low temperature or hydration, lipid bilayers may adopt L_c phase. In Lc phase: (i) the fatty acid acyl chains are very rigid; (ii) the hydrophobic area is very compact, (iii) no movement occurs across the chain region. In the lamellar crystalline phase, a clear demarcation between outer and inner monolayer may be observed as shown in figure 4.1.1.

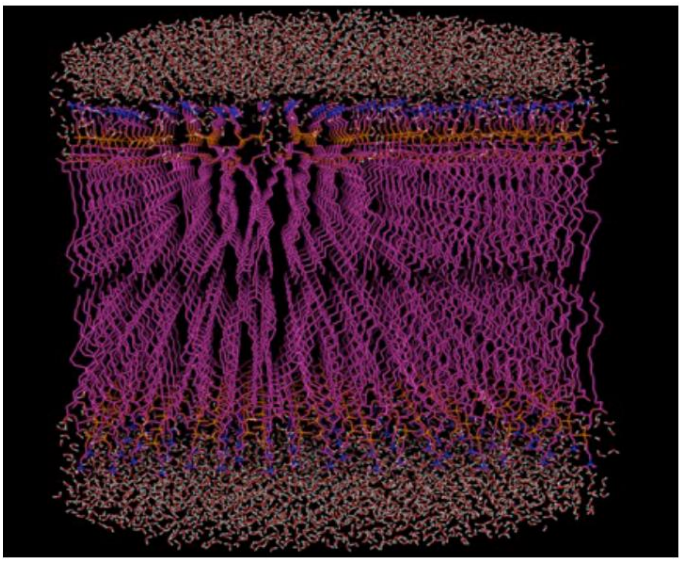

Figure 4.1.1 Schematic diagram of crystalline phase. At very low temperature the lipid bilayers adopts a crystalline phase. In the crystalline phase, chains are very rigid.

When the Lc of lipid bilayers are heated, it transforms into a gel phase. In the gel phase, (i) the acyl chain hydrocarbon molecules are closely packed and stiff, (ii) the rotation of lipid molecules is hindered, (iii) lateral diffusion are extremely restricted [23]. In other words, the gel phase exhibits a high order parameter[24]. The order parameter is a measure of structure and

dynamics of lipid molecules at different sections along the length of bilayers[26]

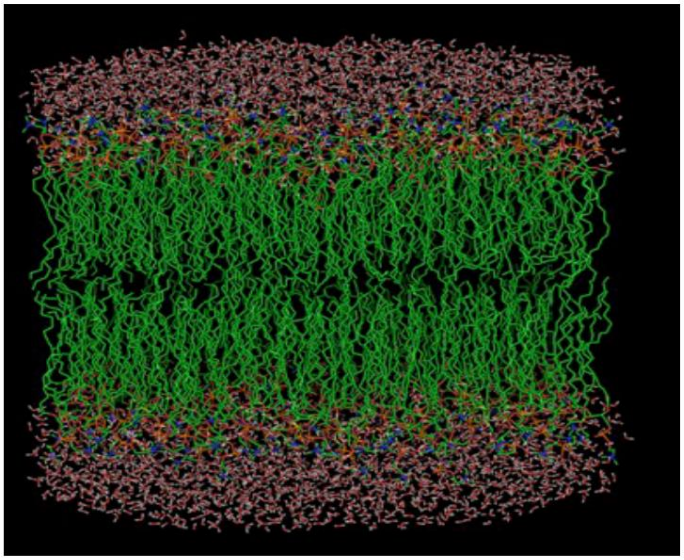

Figure 4.1.2 Schematic diagram of gel phase. In gel phase, lipid chains are very stiff and hindered lateral diffusion occurs.

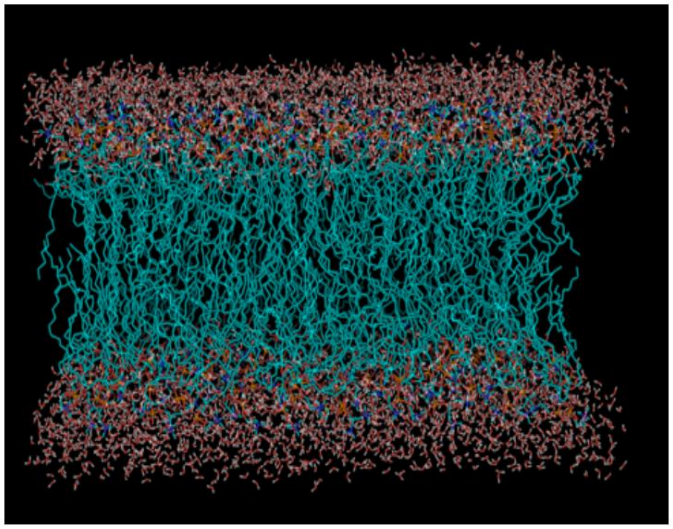

Figure 4.1.3 Schematic diagram of liquid disordered behaviour. At very high temperature, lipid bilayers acquires liquid disordered phase. In liquid disordered phase, the lipid chains are highly mobile and possess very rapid lateral diffusion.

At high temperature, the lipid bilayers may adopt the L_d phase. In the L_d phase: (i) the hydrocarbon molecules of the acyl chain possess high lateral and trans-bilayer diffusion, (ii)

increased cross section area of the hydrophobic region, (iii) each lipid molecule possesses rapid rotation around its own axis and possesses low order parameter, as compared to the gel phae[7].

The addition of cholesterol molecules into phospholipid bilayers in the L_d phase enhance the stiffness of the acyl chain region and also decrease the rate of cellular permeability. Cholesterols may slow down the rate of lateral and rotational diffusion. In other words, cholesterol molecules create a condition for lipid bilayers that possesses an intermediate state between L_d and gel phase (Figure 4.1.4). This intermediate state is referred as liquid ordered (L_o) or liquid crystalline ordered phase[25].

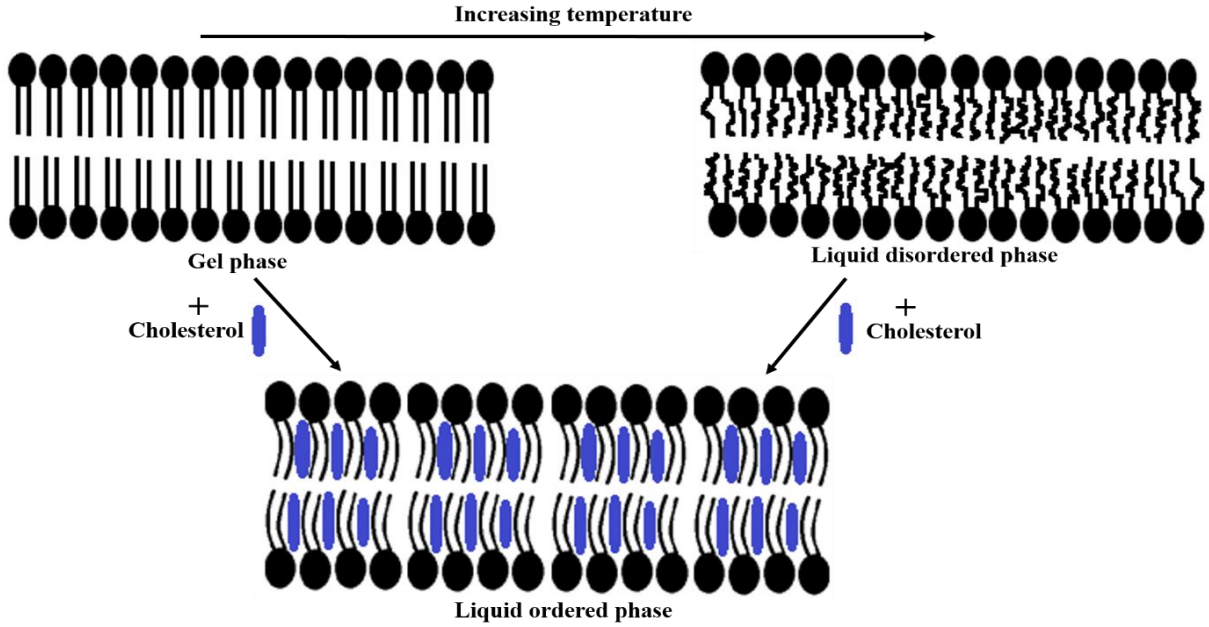

Figure 4.1.4 Schematic diagram of Liquid ordered phase. Liquid ordered phase (high order parameter and increased lipid dynamics) is the intermediate stage between gel and liquid disordered phase with cholesterol molecules and this is the characteristics of biological membrane.

4.1.2 Solid state deuterium NMR spectroscopy

Deuterium (^2H) NMR is commonly used to analyse the arrangement and dynamics of solid molecules, liquid crystals, and lipid membranes[27]. In recent times, ^2H NMR has been utilized to examine the membrane signalling molecules and molecular biology studies such as DNA fibres[28].

4.1.2.1 Principle of deuterium NMR

Deuterium is also known as heavy hydrogen and it is one of the stable isotopes of hydrogen. The deuterium nucleus is called a deuteron and it contains one proton and one neutron. Deuterium generally yields broad signals and its line width normally differs between a few hertz and a few kilohertz. Deuterium has spin 1 and also possesses an electric quadrupole moment along with a nuclear magnetic moment. ^{2}H NMR generates a single large coupling and it is happened due to the dominance of electric quadrupolar (sequence of configurations of electric charge or current which exist in ideal form) interaction over the nuclei of $^{2}H/\ ^{1}H$ magnetic dipolar coupling and chemical shifts of ^{2}H nucleus[28] The anisotropic nuclear electric field gradient produce Pake pattern (a superposition of pake doublets for non-crystalline samples) [29]. In other words, two spin -1/2 or spin-1of static powder system generate pake pattern at high-field NMR. The 2H NMR spectra may be de-paked using computational programs to show the quadrupolar splitting of each resonance[29] (Figure 4.1.2.1).

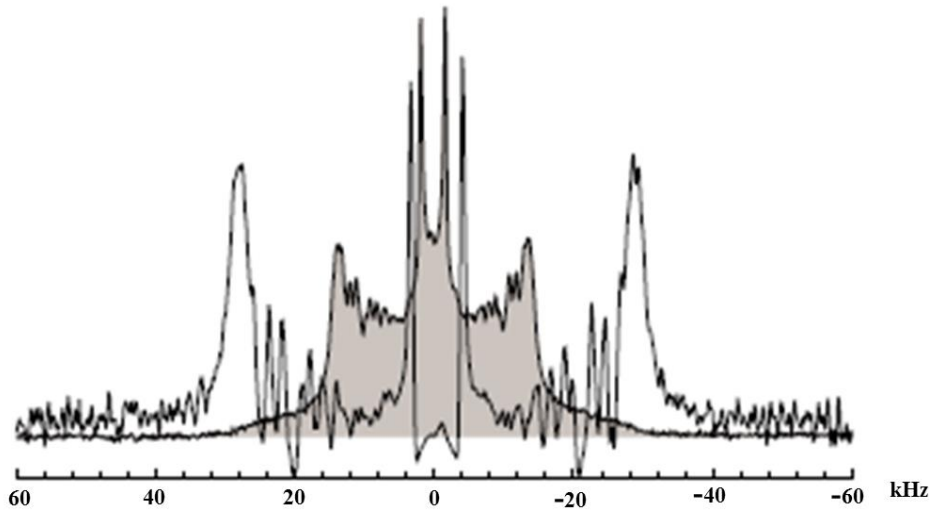

Figure 4.1.2.1 A de-paked spectra of DMPC-d_{54} shows quadrupolar splitting of the resonance[29].

4.1.3 Moments analysis

The first moment, M_1, is defined as the directly proportional to the average quadrupolar splitting ($|\Delta\nu_Q|$) and the average order parameter ($|S_{CD}|$)[30, 31] Lipid phase behaviour may be calculated and analysed by moments analysis, a method used to define the distribution of quadrupolar splittings ($\Delta\nu_Q$) and order parameters (S_{CD}) of the spectrum of ^{2}H NMR. In other words, moment analysis is used to determine the spectrum width and the mobility of the lipids.

The broader spectrum suggests that more immobile lipid whereas a narrow spectrum suggests more mobile lipids. A high spectral moment signifies the gel phase with broader spectrum whereas a low moment analysis signifies L_d or L_o phase (Figure 4.3). The spectrum of L_d or L_o phase appears sharp and narrow. L_o phase spectrum possesses central methyl splitting (described in section 4.1.4). These distribution patterns may specify the phase state of lipid molecules where the lipid phase transitions and lipid phase coexistences happen.

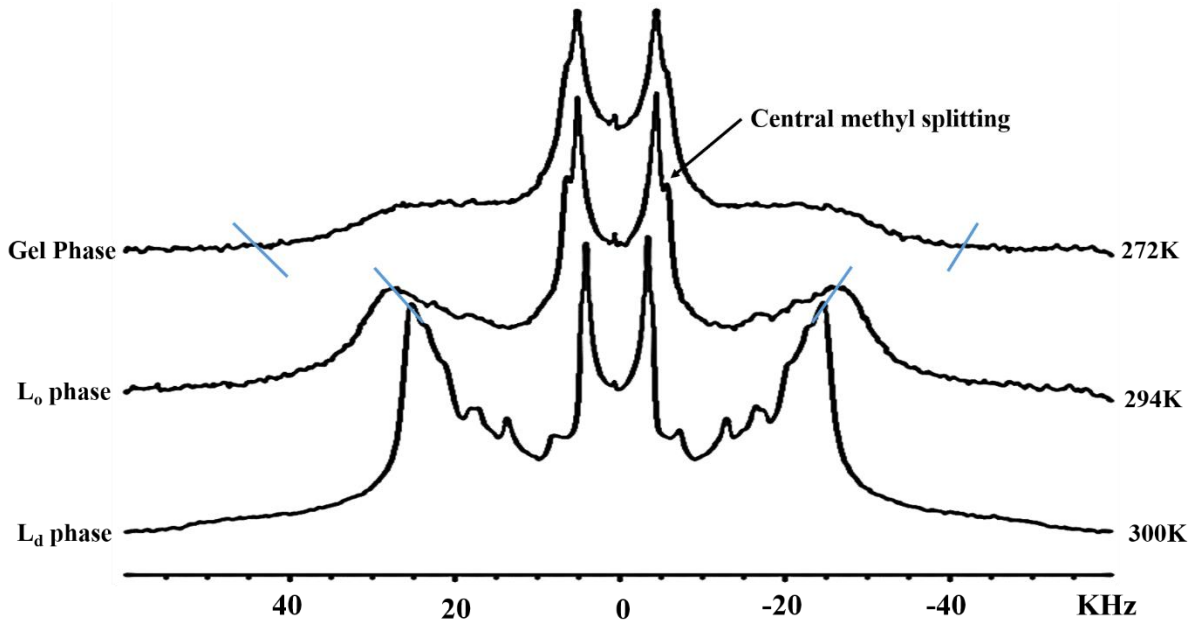

Figure 4.1.3 A typical ^{2}H NMR spectrum of DMPC-d_{54}. Gel phase shows broader spectrum at low temperature and the peaks are not well resolved. L_d and L_o phase appears at high temperature with narrow spectra and well resolved peaks. Central methyl splitting appears at L_o phase. Blue lines signify the line width of spectrum.

4.1.4 Central Terminal Methyl splitting

In L_o phase, the one lipid acyl tail is slightly deeper than other and thus terminal methyl groups of lipid tails may exist in unequal distribution (Figure 4.1.2.4). This unequal methyl group distribution gives rise the central terminal methyl (CTM) splitting. CTM plots also deliver a suggestion of the existence of the liquid ordered phase or its coexistence with either the gel phase or liquid disordered phase.

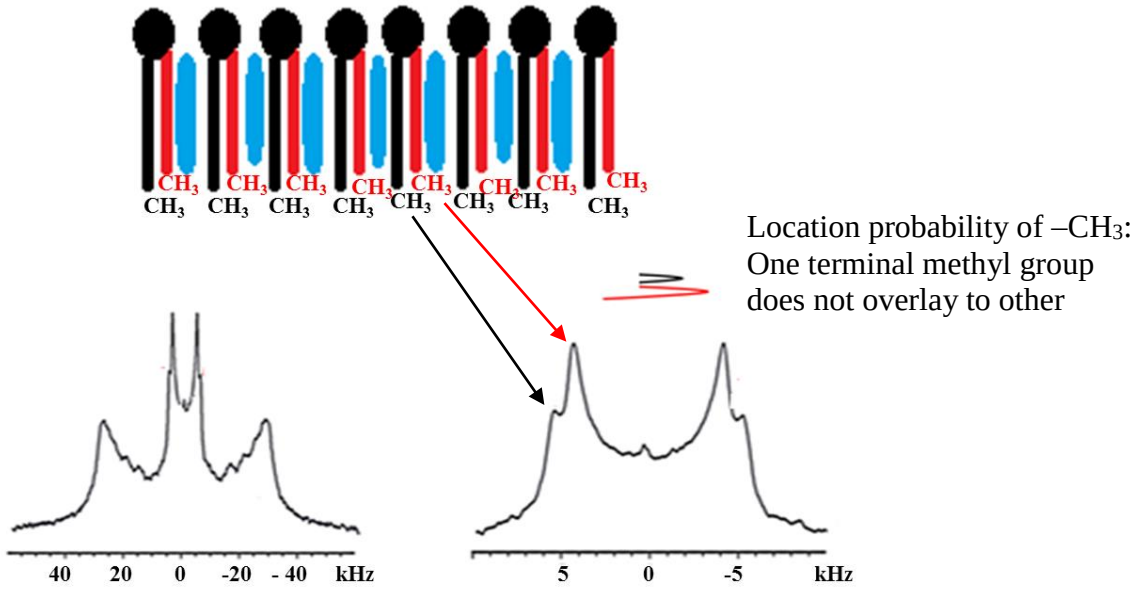

Figure 4.1.4 Schematic diagram of lipid molecules in L_o phase with CTM. In Lo phase, one acyl tail (black) is slightly deeper than other tail (red). The terminal methyl groups do not overlap with each other. The ^2H NMR spectra show a central terminal methyl splitting.

4.1.5 Aims

The aim of the study was to investigate the interactions and effects of $A\beta_{25-35}$ and KLVFF on the phase behaviour of liposomes containing DMPC-d_{54} and cholesterol using ^2H NMR spectroscopy.

4.2 Materials

1,2-dimyristoyl-d54-*sn*-glycero-3-phosphocholine **(**DMPC-d_{54}) solvated in chloroform, were purchased from Avanti Polar Lipids (Alabaster, AL, USA). $A\beta_{25-35}$ was purchased from Cambridge Biosciences (Cambridge, UK). Tris (hydroxymethyl) aminomethane (TRIS), ethylene diamine tetra acetic acid (EDTA), magnesium chloride ($MgCl_2$), hexafluoroisopropanol (HFIP) and cholesterol (laboratory grade) were purchased from Sigma-Aldrich (UK).

4.3 Methods

4.3.1 Sample preparation

TRIS buffer was prepared at concentration of 10mM TRIS, 10mM $MgCl_2$ and 0.5mM EDTA at pH7.8. The buffer was then filtered with 0.45μm syringe filter and stored at 4^{o}C. Chloroform was evaporated from chloroform dissolved DMPC-d_{54} (5ml) under vacuum using a rotary evaporator, and after evaporation of chloroform, the lipid cake was obtained. The lipid cake was suspended in 1ml of doubly distilled water and frozen at -80°C for an hour and then lyophilized overnight under high vacuum using freeze dyer to remove any trace of chloroform.

Samples of DMPC-d_{54}/$A\beta_{25-35}$, DMPC-d_{54}/cholesterol, DMPC-d_{54}/cholesterol/$A\beta_{25-35}$, DMPC-d_{54}/KLVFF, DMPC-d_{54}/cholesterol/KLVFF, DMPC-d_{54}/$A\beta_{25}$-35/KLVFF, and DMPC-d_{54}/cholesterol/$A\beta_{25-35}$/KLVFF were prepared at molar ratio of 9:1, 8:2, 8:2:1, 9:1, 8:2:1, 9:1:1, 8:2:1:1, respectively. The peptide or beta breaker peptide was co-dissolved with phospholipid/cholesterol.

4.3.2 ^{2}H NMR measurements

^{2}H NMR quadrupole echo experiments were conducted with a spectral width of 100kHz, a recycle delay of 1s, an echo delay of 30μs, an acquisition time of 10ms, $\pi/2$ pulse of 5.5μs, and scanned between 2k and 4k. All samples were firstly heated at 332K and then cooling down to 272K prior to temperature scans between 272K and 322K (with the help of thermocouple in the probe head) at 2K intervals.

NMR data were processed using Topsin version 1.3 (Bruker Instruments, Karlsruhe, Germany). ^{2}H NMR spectra were de-Paked, and first spectral moments were calculated using

NMR-Depaker software version 1.0 RC1. The de-Paking procedure was accomplished by the fast Fourier transform-based fast deconvolution algorithm.

4.4 Result

4.4.1 ^{2}H NMR spectra of DMPC-d_{54}

To examine the DMPC phase behaviour, chain deuterated lipids (DMPC-d_{54}) were used. The sample was examined under ^{2}H NMR as it generates a wide spectrum. The wide spectrum of lipid acyl chain regions show different splitting patterns at different temperatures, which is very important to analyse the phase behaviour of lipids. The sample of DMPC-d_{54} was prepared and measured according to the protocol described in section 4.3.1 and section 4.3.2.

The ^{2}H NMR spectra of DMPC-d_{54} show wide splitting with unresolved peaks between 272K and 292K (Figure 4.4.1A&C). The wide splitting and unresolved peaks suggest that the tails of DMPC-d_{54} are very rigid and immobile at low temperature, which is the characteristic of gel phase as shown in figure 4.4.1A&C. The spectra show narrow splitting with well resolved peaks between 294K and 322K (Figure 4.4.1A&C). The narrow spectra and sharp peaks, which is the feature of fluid lamellar phase or L_d phase suggest that the acyl chain of DMPC-d_{54} may be less rigid and mobile. The central terminal methyl peaks of spectra which represent the lipid tail methyl region, show the well resolved and sharp peaks at high temperature (294K onwards), this indicates fluid lamellar phase (Figure 4.4.1B&D). On the other hand, at low temperature (292K and below) the terminal methyl peaks resolution are blunt, which signifies the gel phase (Figure 4.3.1.1B&D). The data suggest that gel phase to L_d phase transition occurs from 292K to 294K (Figure 4.4.1) because the splitting becomes narrower and peaks resolution improves with the increase of temperature.

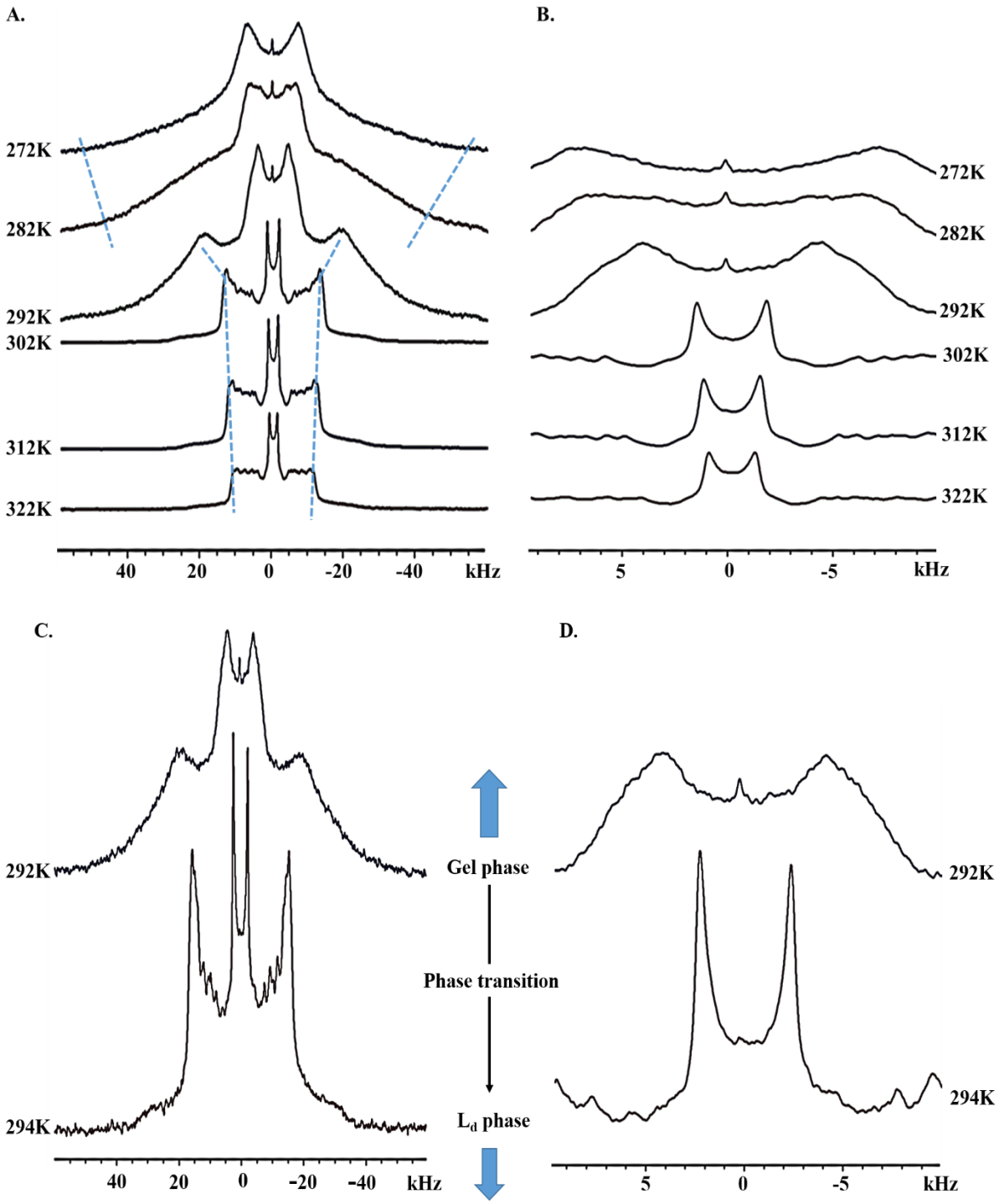

Figure 4.4.1 ^{2}H NMR spectra of DMPC-d$_{54}$ (A) Temperature ranging from 272K to 322K at 10K intervals, representing the wide splitting with unresolved peaks at low temperature and narrow splitting with well resolved peaks at high temperature; (B) Central terminal methyl peaks (272K to 322K) at 10K interval, sharp methyl peaks represent fluid lamellar phase and blunt peaks indicate gel phase; (C) The phase transition occurs from gel to liquid disordered phase between 292K and 294K; (D) Central terminal methyl peak of phase transition of DMPC-d54. Blue dotted lines signify the line width of spectra.

4.4.2 ^{2}H NMR spectra of DMPC-d_{54} plus Aβ_{25-35}

To examine the effect of Aβ_{25-35} on lipid phase behaviour, the co-dissolved sample DMPC-d_{54} and Aβ_{25-35}, was prepared according to protocol described in section 4.3.1. The ^{2}H NMR spectra suggest that the broad splitting and unresolved peaks appear between 272K and 286K whereas narrow splitting and sharp peaks appear between 288K and 322K as shown in figure 4.4.2A&C. The central terminal methyl peaks spectra show the sharp peaks at high temperature (288K onwards) and blunt methyl peaks appear at low temperature (286K and below) as shown in Figure 4.4.2B&D. The data suggest that Aβ_{25-35} is able to reduce the phase transition temperature from gel (286K) to L_d phase (288K) in comparison to DMPC-d_{54} alone. The data also suggest, at low temperature (272K-286K), Aβ_{25-35} provides more rigidity and less mobility to the acyl tail region of DMPC-d_{54} whereas at temperature between 288K and 322K, it gives less rigidity and more mobility.

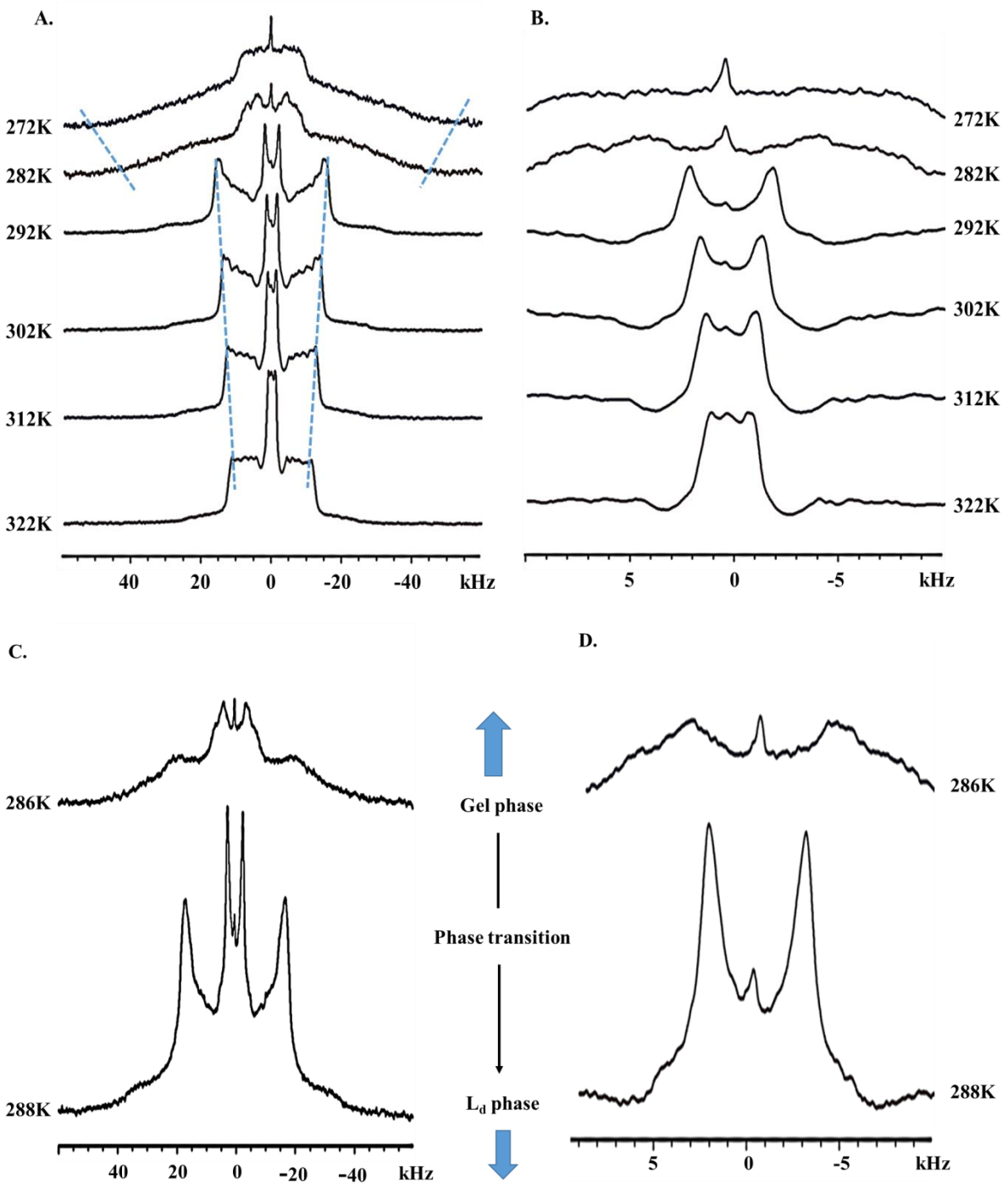

Figure 4.4.2 ^{2}H NMR spectra of DMPC-d$_{54}$ plus Aβ$_{25-35}$. (A) Temperature ranging from 272K to 322K at 10K interval. The broader splitting and unresolved peaks occur at low temperature. The narrow splitting with well resolved peaks at high temperature; (B) Central terminal methyl peaks between 272K and 322K at 10K interval; (C) The phase transition occurs from gel to liquid disordered phase between 286K and 288K; (D) Central terminal methyl peaks of phase transition occurs from gel (286K) to Ld phase (288K). Blue dotted lines signify the line width of spectra.

4.4.3 ^{2}H NMR spectra of DMPC-d_{54} plus KLVFF

To examine the effect of KLVFF on lipid phase behaviour, the co-dissolved sample DMPC-d_{54} and KLVFF was measured according to section 4.2.2.2. The spectra of DMPC-d_{54} plus KLVFF suggest that the broad splitting with unresolved peaks appear between 272K and 286K while the narrow splitting with sharp peaks are observed between 288K and 322K as shown in Figure 4.4.3A&C. The sharp methyl terminal peaks appear at high temperature (288K onwards) and blunt methyl peaks appear at low temperature (286K and below) as shown in Figure 4.4.3B&D. The data suggest that KLVFF has almost similar ability of $A\beta_{25-35}$ to reduce phase transition temperature from gel to L_d phase in contrast to DMPC-d_{54} alone.

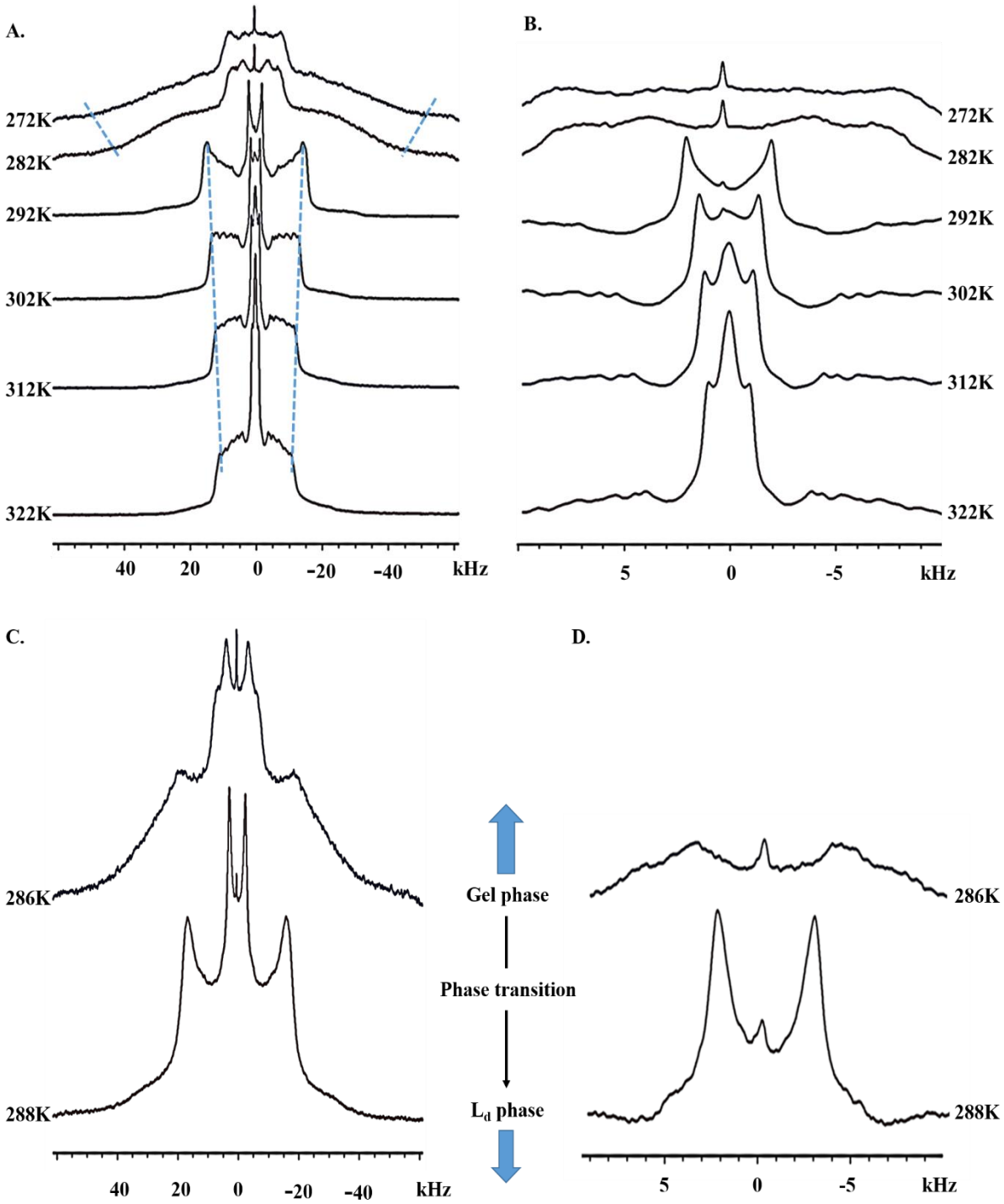

Figure 4.4.3 ^{2}H NMR spectra of DMPC-d$_{54}$ plus KLVFF (A) Temperature ranging from 272 K to 322 K at interval of 10K; (B) Central terminal methyl peaks between 272K and 322K at 10K interval; (C) The phase transition occurs from gel to liquid disordered phase between 286K and 288K; (D) Central terminal methyl peak of phase transition of DMPC-d54 plus KLVFF. Blue dotted lines signify the line width of spectra.

4.4.4 ^{2}H NMR spectra of DMPC-d_{54} plus Aβ_{25-35} with KLVFF

To examine the effect of Aβ_{25-35} plus KLVFF on lipid phase behaviour, the co-dissolved sample DMPC-d_{54} and Aβ_{25-35} plus KLVFF, was prepared and measured according to protocol described in section 4.3.1 and 4.3.2, respectively. The broad splitting and unresolved peaks appear between 272K and 290K and the narrow splitting and sharp peaks appear between 292K and 322K as shown in Figure 4.4.4A&C. The central terminal methyl peaks spectra show the sharp peaks at high temperature (292K onwards) and blunt methyl peaks appear at low temperature (290K and below) as shown in figure 4.4.4B&D. The ^{2}H NMR spectra suggest that DMPC-d_{54} with Aβ_{25-35} plus KLVFF has ability to increase the phase transition temperature from gel to L_d phase in comparison to DMPC-d_{54} with Aβ_{25-35} or KLVFF. The data suggest that KLVFF may obstruct the amyloid fibrillation in DMPC-d_{54} sample. The gel and L_d phase of DMPC-d_{54} plus Aβ_{25-35} with KLVFF are almost similar to DMPC-d_{54} alone.

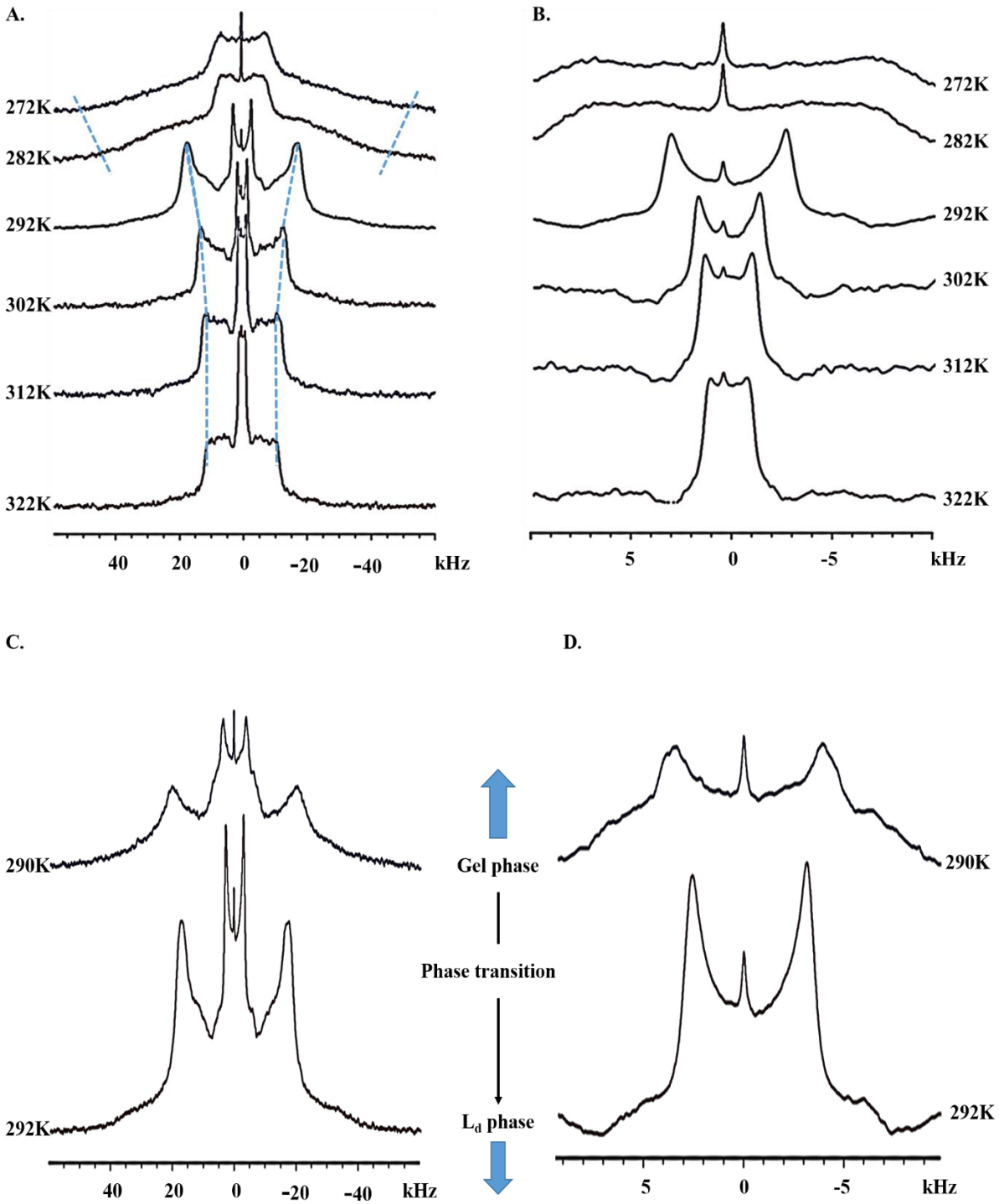

Figure 4.4.4 ^{2}H NMR spectra of DMPC-d$_{54}$ plus Aβ$_{25-35}$ with KLVFF. (A) Temperature ranging from 272K to 322K at interval of 10K; (B) Central terminal methyl peaks between 272K and 322K at 10K interval; (C) The phase transition occurs from gel to liquid disordered phase between 290K and 292K; (D) Central terminal methyl peaks of phase transition occurs from gel (290K) to Ld phase (292K). Blue dotted lines signify the line width of spectra.

4.4.5 ^{2}H NMR spectra of DMPC-d_{54} with cholesterol

The ^{2}H NMR spectra of the sample of DMPC-d_{54} with cholesterol show a mixed [gel and L_o] phase at 272K due to the occurrence of methyl splitting and broad spectrum with unresolved peaks as shown in figure 4.4.5. The spectra shows mixed [L_o + L_d] phase between 274K and 300K due to the emergence of well resolved peaks and shoulders with central terminal methyl peaks splitting (Figure 4.4.5C&D). At 302K and above, the spectra show narrow splitting without central terminal methyl splitting (Figure 4.4.5B&D), which indicates the presence of L_d phase (Figure 4.4.5A).

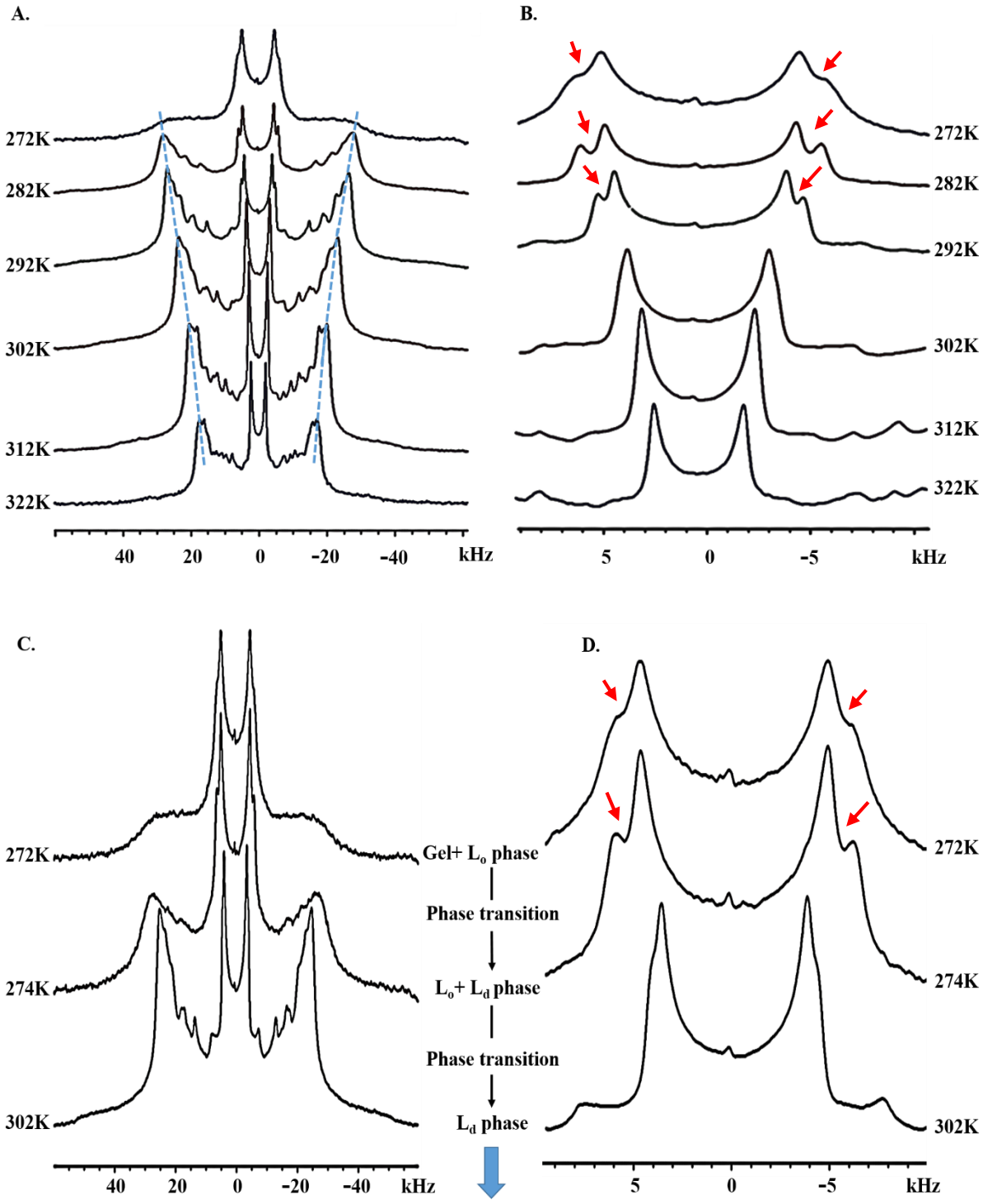

Figure 4.4.5 ^{2}H NMR spectra of DMPC-d$_{54}$ with cholesterol. (A) Temperature ranging from 272K to 322K at interval of 10K; (B) Central terminal methyl peaks between 272K and 322K at 10K interval; (C) The phase transition occurs at 272K (gel+L_o phase), 274K (L_o+L_d phase) and 302K (L_d phase); (D) Central terminal methyl peaks of phase transitions. Blue dotted lines signify the line width of spectra. Red arrows indicate the central terminal methyl splitting.

4.4.6 ^{2}H NMR spectra of DMPC-d_{54} with cholesterol plus Aβ_{25-35}

To examine the effect of Aβ_{25-35} on lipid phase behaviour in presence of cholesterol, the co-dissolved sample DMPC-d_{54} with cholesterol plus Aβ_{25-35}, was prepared and measured according to protocol described in section 4.3.1 and 4.3.2, respectively. The ^{2}H NMR spectra show a mixed [gel and L_o] phase at 272K because of the presence of methyl splitting and broad spectrum with unresolved peaks as shown in Figure 4.4.6. The spectra show mixed [L_o+ L_d] phase between 274K and 294K because of the emergence of well resolved peaks and shoulders and the splitting of central terminal methyl peaks (Figure 4.4.6C&D). At 296K and above, the spectra show narrow splitting without central terminal methyl peak splitting (Figure 4.4.6B&D), which indicates the presence of L_d phase (Figure 4.3.6A). The spectra also suggest that Aβ_{25-35} reduces the mixed [L_o+L_d] phase (294K) and L_d phase (296K) in comparison to DMPC-d_{54} with cholesterol, where the mixed [L_o+L_d] phase occurs at 300K and L_d phase emerges at 302K.

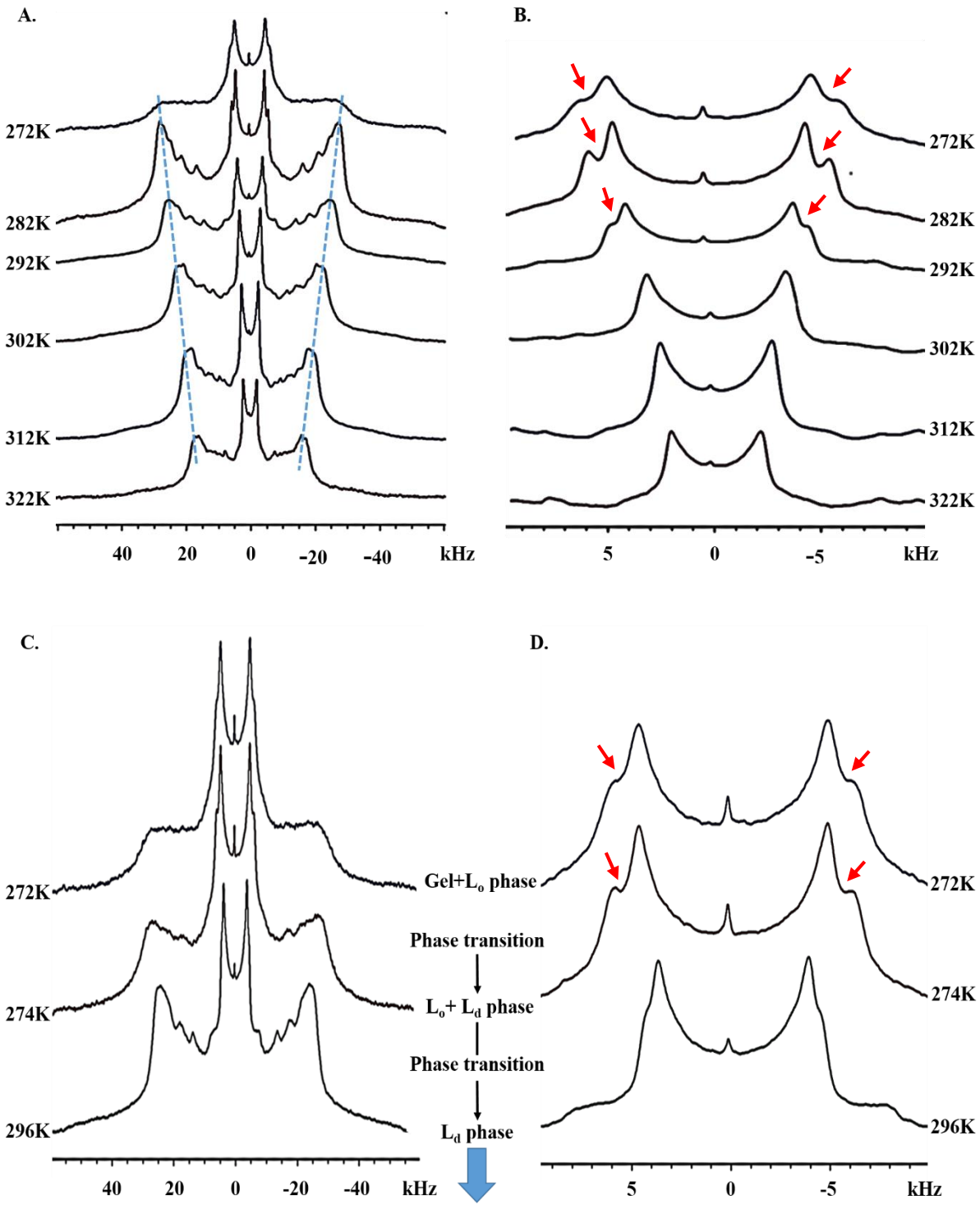

Figure 4.4.6 ^{2}H NMR spectra of DMPC-d$_{54}$ with cholesterol plus Aβ$_{25-35}$. (A) Temperature ranging from 272K to 322K at interval of 10K; (B) Central terminal methyl peaks between 272K and 322K at 10K interval; (C) The phase transition occurs at 272K (gel+ L_o phase), 274K (L_o+ L_d phase) and 296K (L_d phase); (D) Central terminal methyl peaks of phase transitions. Blue dotted lines signify the line width of spectra. Red arrows indicate the central terminal methyl splitting.

4.4.7 ^{2}H NMR spectra of DMPC-d_{54} with cholesterol plus KLVFF

To examine the effect of KLVFF on lipid phase behaviour in the presence of cholesterol, the co-dissolved sample DMPC-d_{54} with cholesterol plus KLVFF, was prepared and measured according to protocol described in section 4.3.1 and 4.3.2, respectively. The ^{2}H NMR spectra show a mixed [gel+L_o] phase at 272K due to the appearance of methyl splitting and broad spectrum with unresolved peaks as shown in Figure 4.4.7. The spectra shows mixed [L_o+L_d] phase between 274K and 304K because of the emergence of well resolved peaks and shoulders and the splitting of central terminal methyl peaks (Figure 4.4.7C&D). At 306K and above, the spectra show narrow splitting and absence of central terminal methyl peak splitting (Figure 4.4.7B&D), which indicates the L_d phase (Figure 4.4.7A). The spectra also suggest that KLVFF increases the mixed [L_o+L_d] phase (304K) and L_d phase (306K) in comparison to DMPC-d_{54} with cholesterol, where the mixed [L_o+L_d] phase occurs at 300K and L_d phase emerges at 302K.

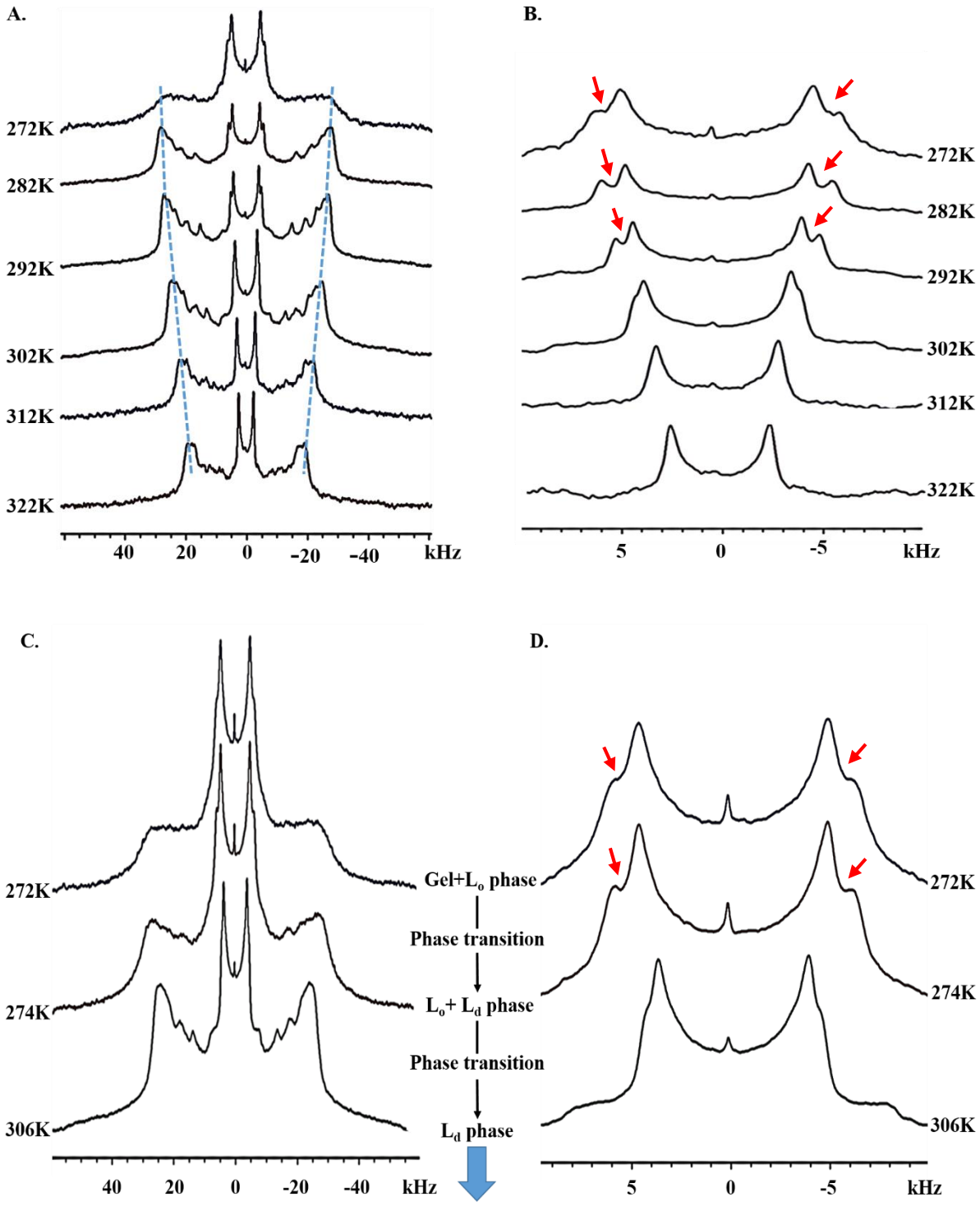

Figure 4.4.7 ^{2}H NMR spectra of DMPC-d$_{54}$ with cholesterol plus KLVFF. (A) Temperature ranging from 272K to 322K at interval of 10K; (B) Central terminal methyl peaks between 272K and 322K at 10K interval; (C) The phase transition occurs at 272K (gel+L_o phase), 274K (L_o+L_d phase) and 306K (L_d phase); (D) Central terminal methyl peaks of phase transitions. Blue dotted lines signify the line width of spectra. Red arrows indicate the central terminal methyl splitting.

4.4.8 ^{2}H NMR spectra of DMPC-d_{54} with cholesterol and beta breaker peptide (KLVFF) plus Aβ_{25-35}

To examine the effect of Aβ_{25-35} plus KLVFF on lipid phase behaviour in presence of cholesterol, the co-dissolved sample DMPC-d_{54} with cholesterol and Aβ_{25-35} plus KLVFF, was prepared and measured according to protocol described in section 4.3.1 and 4.3.2, respectively. The ^{2}H NMR spectra shows mixed [L_o+L_d] phase between 272K and 316K because of the emergence of well resolved peaks and shoulders and the splitting of central terminal methyl peaks (Figure 4.4.8C&D). At 318K and above, the spectra show narrow splitting without central terminal methyl peak splitting (Figure 4.4.8B&D), this indicates the L_d phase (Figure 4.4.8A&C). The spectra also suggest that Aβ_{25-35} plus KLVFF increases the mixed [L_o+L_d] phase (316K) and L_d phase (318K) in comparison to DMPC-d_{54} with cholesterol, where the mixed [L_o + L_d] phase occurs at 300K and L_d phase emerges at 302K.

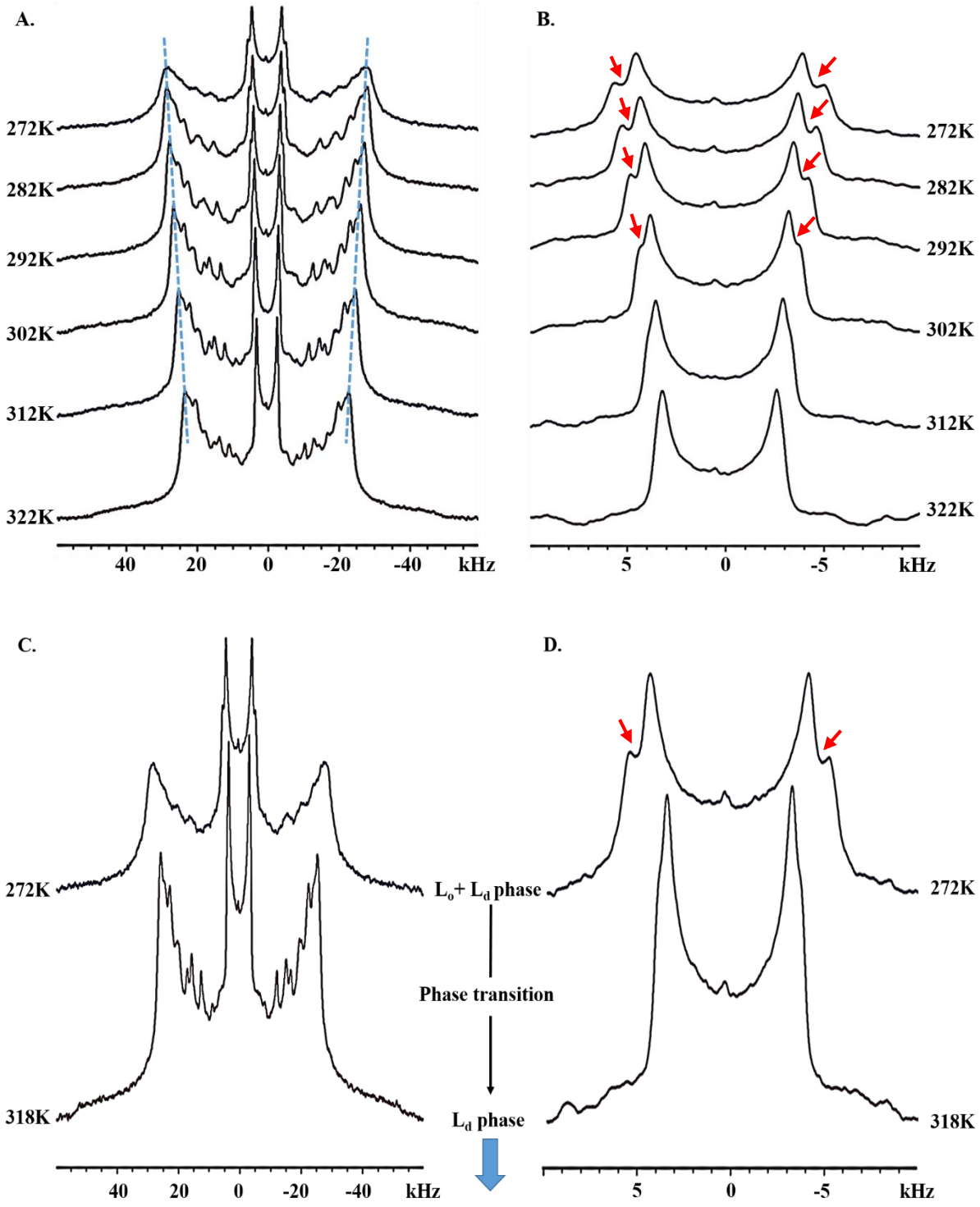

Figure 4.4.8 ^{2}H NMR spectra of DMPC-d$_{54}$ with cholesterol and Aβ$_{25-35}$ plus KLVFF. (A) Temperature ranging from 272K to 322K at interval of 10K; (B) Central terminal methyl peaks between 272K and 322K at 10K interval; (C) The phase transition occurs at 272K (L_o+L_d phase) and 318K (L_d phase); (D) Central terminal methyl peaks of phase transitions. Blue dotted lines signify the line width of spectra. Red arrows indicate the central terminal methyl splitting.

4.4.9 First Moments (M_1) analysis of DMPC-d54 and DMPC-d_{54} with $A\beta_{25-35}$ /KLVFF

M1 data obtained from ^2H NMR spectra of samples DMPC-d54 (purple diamonds), DMPC-d54 plus $A\beta_{25-35}$ (green squares), DMPC-d_{54} plus KLVFF (brown squares) and DMPC-d54 plus $A\beta_{25-35}$ with KLVFF (red triangles) are plotted in figure 4.4.9. The M_1 analysis plot of DMPC-d_{54} suggests that the lipid exists in gel phase at low temperature below 294K. The slope from 274K to 282K represents the presence of pre-fluid lamellar phase commonly known as ripple phase[32]. In ripple phase molecules of lipid are bent at an angle to the normal axis of lipid bilayers[32]. A steep slope emerges between 292K and 294K and this sharp decrease in gradient may attribute the fluid lamellar or L_d phase which emerges from 294K.

The M_1 plots of DMPC-d_{54} plus $A\beta_{25-35}$ and DMPC-d_{54} plus KLVFF show two regions. First region appears between 272K and 286K, which represents the gel phase and the second region emerges between 288K and 320K, which represents fluid lamellar or L_d phase. The M_1 plots of DMPC-d54 plus $A\beta_{25-35}$ / KLVFF also suggest that $A\beta_{25-35}$ or KLVFF decrease the phase transition temperature from gel to L_d phase in comparison to DMPC-d_{54} alone.

The M_1 plot of DMPC-d_{54} plus $A\beta_{25-35}$ with KLVFF suggests a sudden decrease in gradient between 290K and 292K. This sudden decrease indicates that lipid goes from gel to L_d phase transition. Gel phase occurs between 272K and 290K and L_d phase emerges between 292K and 320K. The plot also suggests that KLVFF may increase the phase transition temperature between gel and L_d phase in comparison to DMPC-d_{54} plus $A\beta_{25-35}$ / KLVFF.

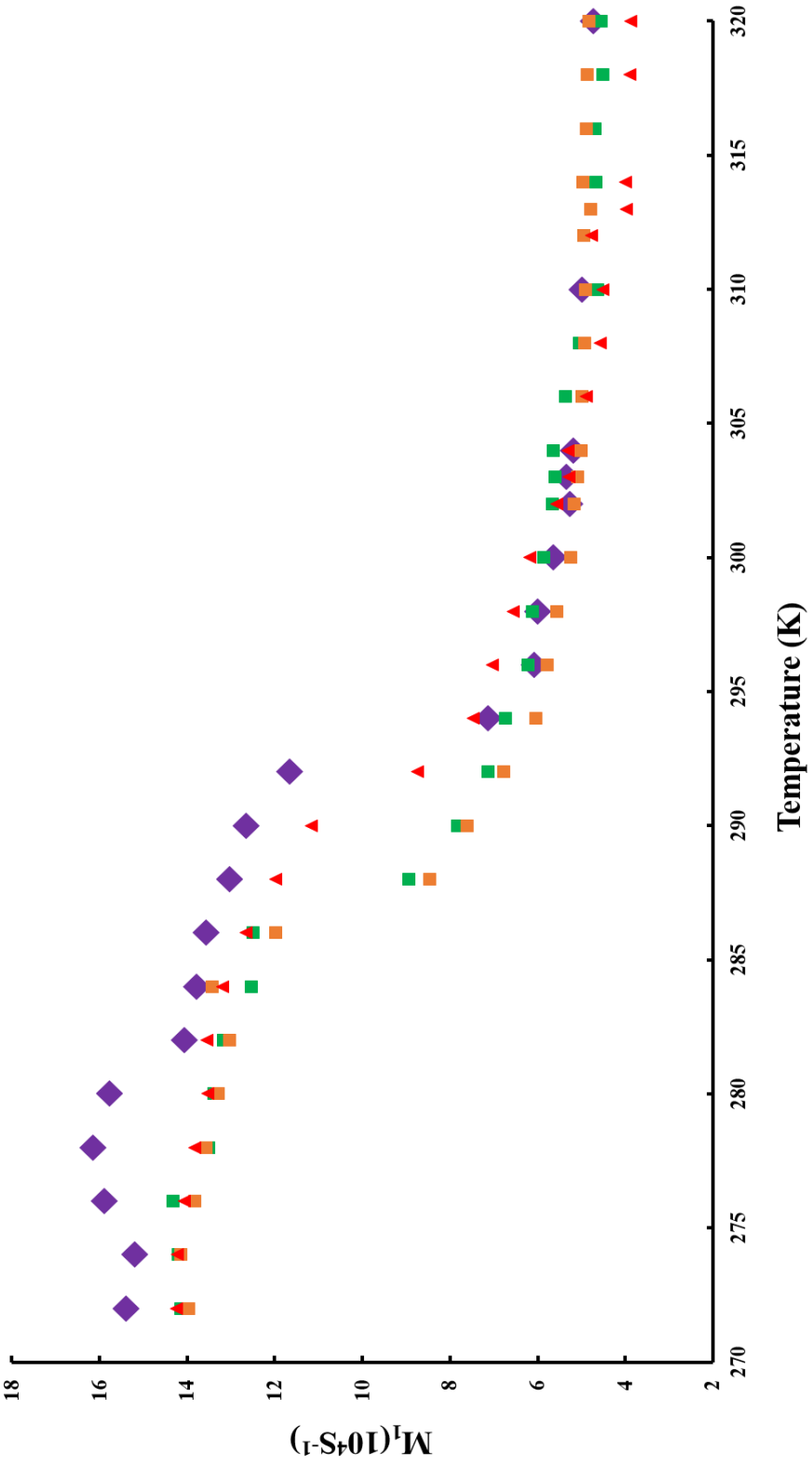

Figure 4.4.9 First moment (M_1) analysis of DMPC-d_{54} (purple diamonds), of DMPC-d_{54} plus $A\beta_{25-35}$ (green squares), DMPC-d_{54} plus KLVFF (brown squares) and DMPC-d_{54} plus $A\beta_{25-35}$ with KLVFF (red triangles)

4.4.10 First Moments (M_1) analysis of DMPC-d_{54} plus cholesterol and DMPC-d_{54} plus cholesterol with Aβ_{25-35}/KLVFF

The temperature dependence of DMPC-d_{54} plus cholesterol or DMPC-d_{54} plus cholesterol with Aβ25-35/KLVFF was evaluated by M_1 analysis based on ^{2}H NMR spectra. The ^{2}H NMR spectra of cholesterol containing samples show central terminal methyl splitting, which represent the L_o phase. Hence there is no sudden phase transition observed between gel L_o and L_d phase and this suggest that all of them may co-exist. The M_1 plots of DMPC-d_{54} plus cholesterol or DMPC-d_{54} plus cholesterol with Aβ_{25-35}/KLVFF show a smooth curve. It may be distinguished into three different gradients, probably describing three phases or phase coexistence, which is based on methyl splitting and ^{2}H NMR spectra. The M_1 plots and central terminal methyl splitting of DMPC-d_{54} plus cholesterol suggests three different phase regions: mixed [gel+L_o] phase occurs from 272K to 274K; [L_o+L_d] phase coexistence from 274K to 300K; and L_d phase from 302K onwards as shown in Figure 4.4.10A.

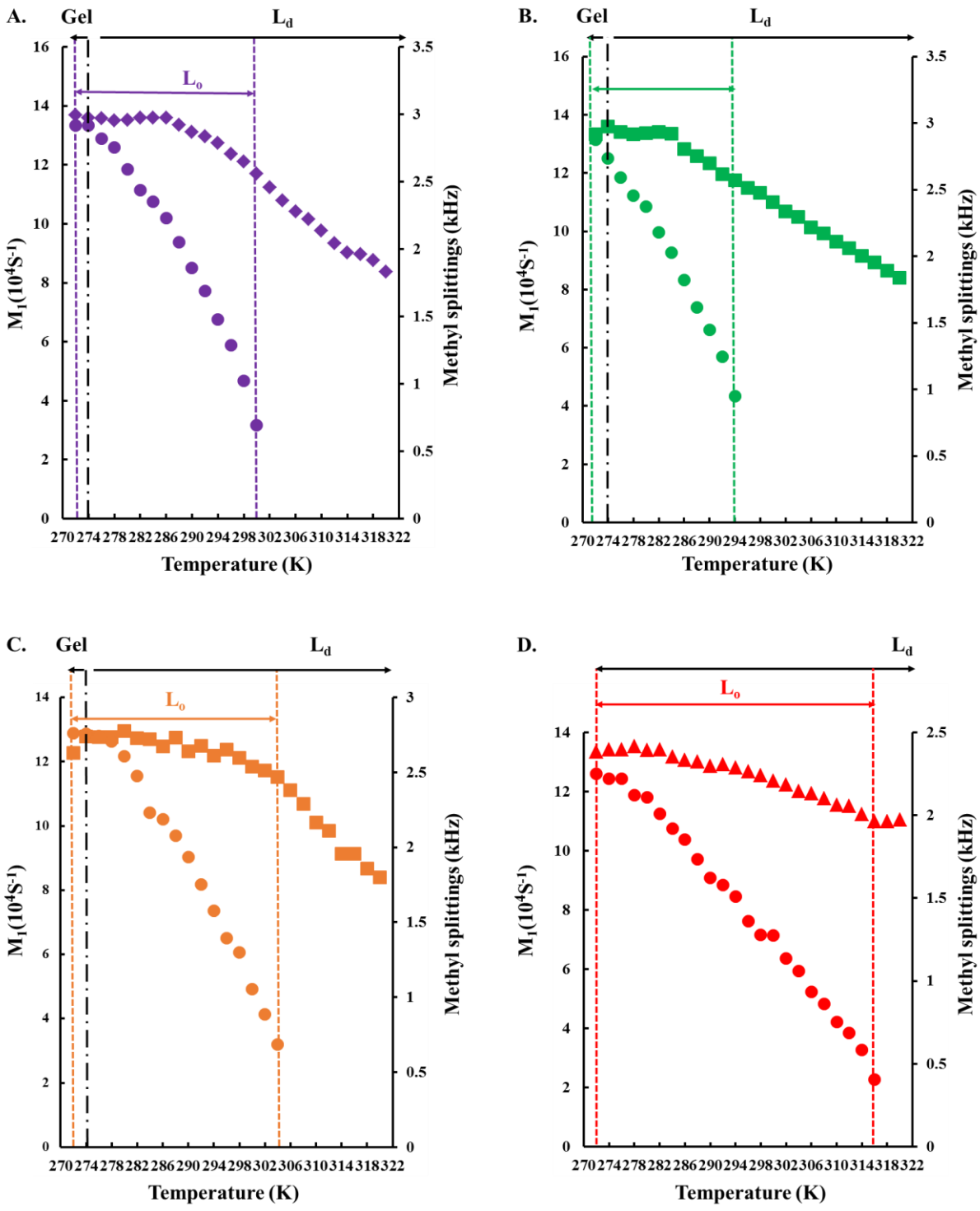

Figure 4.4.10 First moment (M_1) analysis of (A) DMPC-d_{54} plus cholesterol; (B) DMPC-d_{54} plus cholesterol with $A\beta_{25\text{-}35}$; (C) DMPC-d_{54} plus cholesterol with KLVFF; (D) DMPC-d_{54} plus cholesterol with $A\beta_{25\text{-}35}$ plus KLVFF. Filled circles represent the methyl splitting and filled rectangles, diamonds and triangles indicate the M_1 movement.

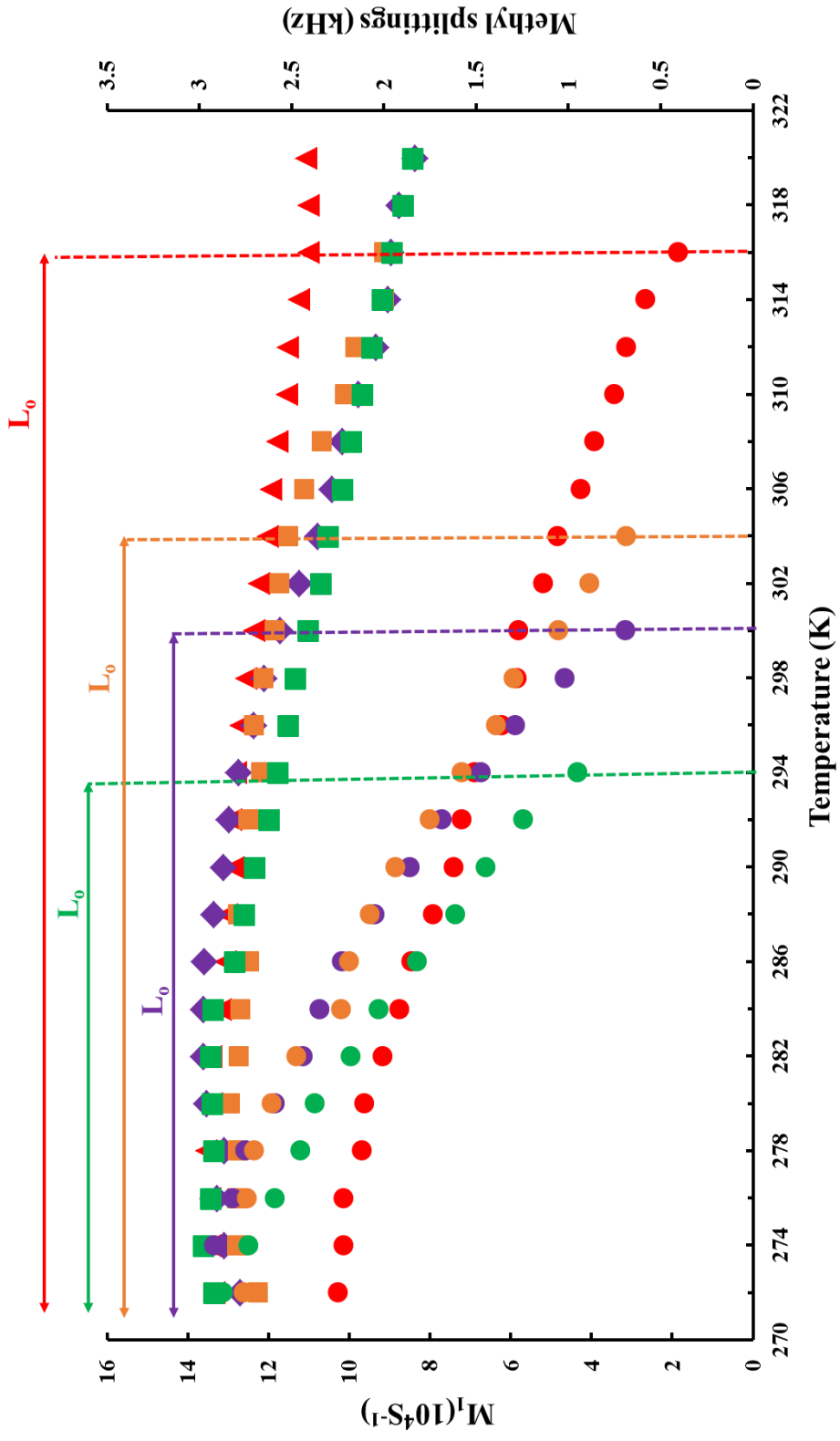

Figure 4.4.11 Comparison of first moment (M_1) analysis of DMPC-d_{54} plus cholesterol (purple), DMPC-d_{54} plus cholesterol with A$\beta_{25\text{-}35}$(green), DMPC-d_{54} plus cholesterol with KLVFF (brown) and DMPC-d_{54} plus cholesterol with A$\beta_{25\text{-}35}$ plus KLVFF(red). Filled circles represent the methyl splitting and filled rectangles, diamonds and triangles indicate the M_1 movement.

The M_1 plot of DMPC-d_{54} plus cholesterol with $A\beta_{25-35}$ suggests that the mixed [gel+L_o] occurs from 272K to 274K; [L_o+L_d] phase exists between 274K to 294K; and L_d from 294K onwards as shown in Figure 4.4.10B. The data suggest that $A\beta_{25-35}$ reduces the phase transitions temperature from mixed [gel+L_o] to [L_o+L_d] phase and from mixed [L_o+L_d] phase to L_d in comparison to DMPC-d_{54} plus cholesterol. The M_1 plot of DMPC-d_{54} plus cholesterol with KLVFF suggests that the mixed [gel+L_o] appears between 272K to 274K; mixed [L_o+L_d] phase occurs between 274K to 304K; and L_d from 306K onwards as shown in Figure 4.4.10C. The data suggest that KLVFF increases the phase transitions temperature from mixed [gel+L_o] to mixed [L_o+L_d] phase and from mixed [L_o+L_d] phase to L_d in comparison to DMPC-d54 plus cholesterol. The M_1 plot of DMPC-d_{54} plus cholesterol and KLVFF with $A\beta_{25-35}$ suggests that the mixed [L_o+L_d] phase occurs between 272K to 316K; and L_d from 318K onwards as shown in Figure 4.4.10D. The data suggest that KLVFF with $A\beta_{25-35}$ increases the phase transitions from mixed [L_o+L_d] phase to L_d in comparison to DMPC-d_{54} plus cholesterol.

4.5 Discussion

The effect of Aβ on membrane fluidity has been investigated. It is reported that Aβ may disrupt the cellular functions such as cellular transport, signalling and enzymatic activity using various techniques such as patch clamp and calcium-assay[33-35]. However, the mechanism and role of beta amyloid peptide on lipid bilayer fluidity is still controversial. The aim of this study was to investigate the effect of Aβ on lipid acyl chain and its order parameter using DMPC-d_{54} lipid vesicles, $A\beta_{25-35}$ and KLVFF under ^2H NMR.

DMPC-d_{54} retains the gel phase until 292K and it adopts L_d phase from 294K and above temperatures. The addition of $A\beta_{25-35}$ or KLVFF to the lipid bilayers shows a significant effect on the phase behaviour. $A\beta_{25-35}$ and KLVFF both reduce the phase transition temperature from gel to L_d phase in comparison to DMPC-d_{54}. However, DMPC-d_{54} plus $A\beta_{25-35}$ with KLVFF increases the phase transition temperature from gel to L_d phase in comparison to DMPC-d_{54} plus $A\beta_{25-35}$ or KLVFF. The relative location, orientation and physical state of amyloid peptide molecules in the lipid bilayers may affect the phase transitions. The physical state of $A\beta_{25-35}$ may be in the form of insoluble fibres (based on chapter 2 data), which may locate on the surface of lipid head groups (base on chapter 3 data). The KLVFF show high interaction at lipid tail acyl group near the glycerol region (as described in section 3.4.5) that may cause more stiffness to the lipid molecules. Hence, it may reduce the temperature of phase transitions. The soluble form of $A\beta_{25-35}$ ($A\beta_{25-35}$ plus KLVFF) may enter into lipid bilayers (as described in chapter 2 and 3) and cause same level of lipid order as DMPC-d_{54} molecules.

The M_1 plots of DMPC-d_{54} plus $A\beta_{25-35}$/KLVFF/ $A\beta_{25-35}$ plus KLVFF show an overlap between 272K and 280K, suggest that the peptide molecules may not exhibit any effects on the lipid phase behaviour. The M_1 analysis of DMPC-d_{54} sample suggest that it may adopt ripple phase between 274K to 282K but this phase is not observed in DMPC-d_{54} plus $A\beta_{25-35}$/KLVFF/ $A\beta_{25-35}$ plus KLVFF because the peptide molecules may hinder the ripple phase. At temperature (282K-284K and above 294K), the M_1 plots of samples (DMPC-d_{54} and DMPC-d_{54} plus $A\beta_{25-35}$/KLVFF/ $A\beta_{25-35}$ plus KLVFF) show an alignment or overlapping which suggest that all the samples possess same lipid order as DMPC-d_{54} alone. The data also suggest that the peptides may not exhibit any effects on lipid bilayers at this temperature range. At high temperature (312K and above), the M_1 plot of $A\beta_{25-35}$ plus KLVFF with DMPC-d_{54} shows high lipid order

than DMPC-d_{54} or DMPC-d_{54} with Aβ_{25-35} or KLVFF. The data suggest that peptide species and quantities may also increase the lipid order at high temperature, which needs further investigation.

The addition of cholesterol is expected to encourage L_o phase, and this is observed as central terminal methyl splitting in the ^2H NMR spectra of sample DMPC-d_{54}/cholesterol (Figure 4.4.5). The M_1 plot of DMPC-d_{54} with cholesterol suggests three sets of phase transition, which are mixed [gel+L_o] phase (272K), mixed [L_o+L_d] phase (274K-300K) and L_d phase (302K onwards). The temperatures of phase transition are based on visual analysis of spectra. These are only approximate temperature values because of unclear phase transitions occurring in presence of cholesterol. However, M_1 data may not be used to determine the start point of mixed [gel+L_o] phase. The central terminal methyl splitting data provide a start temperature (272K) and end temperature (300K), which gives the presence of L_o phase. Since the start temperature of L_d phase is very similar to the temperature found in M_1 plot (274K). Hence, the existence of mixed [L_o+L_d] phase between 274K and 300K is assumed. The exact lipid phase transition temperatures of samples may be analysed further by using techniques such as X-ray scattering which provide further evidences by the measurement of bilayer thickness etc.

The addition of Aβ_{25-35} or KLVFF to DMPC-d_{54} plus cholesterol also shows significant effects on the phase behaviour. The M_1 and central terminal methyl splitting indicate that Aβ_{25-35} decreases phase transition temperature whereas KLVFF/ KLVFF plus Aβ_{25-35} increases the phase transition temperature from mixed[L_o+L_d] to L_d phase in comparison to DMPC-d_{54}+cholesterol alone. The insoluble form of Aβ_{25-35} locating on the surface of phospholipid or cholesterol molecules (as discussed in chapter 2 and 3) may reduce the temperature of lipid phase behaviour. The physical state and location of KLVFF and KLVFF plus Aβ_{25-35} molecules in the bilayer with cholesterol may increase high lipid order at temperature above than 304K and 316K, respectively. The cholesterol molecules may push KLVFF and KLVFF plus Aβ_{25-35} towards head region (as discussed in chapter 3). It may be one of the reasons that KLVFF and KLVFF plus Aβ_{25-35} molecules may possess long temperature range of L_o phase. The M_1 plots of samples (DMPC-d_{54}+cholesterol and DMPC-d_{54}+cholestrol with Aβ_{25-35}/KLVFF/KLVF plus Aβ_{25-35}) show an overlap at low temperature range (272K-284K) and high temperature range (300K-3004K), suggest that all samples may have similar lipid order

as DMPC-d_{54}+cholesterol alone. The data also suggest that $A\beta_{25-35}$/KLVFF/KLVFF plus $A\beta_{25-35}$ may not exhibit any effect on lipid bilayers with cholesterol.

Table 4.1 List of DMPC-d_{54}/ $A\beta_{25-35}$ / KLVFF phase transition

Lipid/ lipid plus peptide	Phase transitions
DMPC-d_{54}	Gel(272K) - ripple phase(274K - 282K) - gel phase (≤ 292K)- L_d phase (≥294K)
DMPC-d_{54}+ $A\beta_{25-35}$	Gel(≤ 286K) - L_d phase (≥288K)
DMPC-d_{54}+ KLVFF	Gel(≤ 286K) - L_d phase (≥288K)
DMPC-d_{54}+ $A\beta_{25-35}$+KLVFF	Gel(≤ 290K) - L_d phase (≥292K)
DMPC-d_{54}+Cholesterol	Gel+L_o(≤ 274K) – [L_o + L_d]phase (≤300K)- L_d phase (> 300K)
DMPC-d_{54}+Cholesterol+ $A\beta_{25-35}$	Gel+L_o(≤ 274K) – [L_o + L_d]phase (≤294K)- L_d phase (> 294K)
DMPC-d_{54}+Cholesterol+ KLVFF	Gel+L_o(≤ 274K) – [L_o + L_d]phase (≤ 304K)- L_d phase (> 304K)
DMPC-d_{54}+Cholesterol+ $A\beta_{25-35}$+KLVFF	[L_o + L_d]phase (≤ 316K)- L_d phase (> 316K)

Simons *et al* (1998) examined the effect on cholesterol on the production of Aβ using hippocampal neurons. They found that depletion of cholesterol level (70%) completely inhibited the production of Aβ[36]. Ehehalt *et a*l (2003) reported that cholesterol levels may affect the production of Aβ in Neuro2a cells[37]. Umeda *et al* (2010) reported that production of Aβ may reduce the cholesterol level in Neuro2a cells due to increase efflux[38]. Cecchi *et al* (2008) suggested that increased level of membranous cholesterol may protect the toxicity of Aβ in human neuroblastoma cells[39]. The role of cholesterol in amyloidosis is still controversial and real mechanism unknown. Hence, in this study, the mechanism of cholesterol with amyloid peptide in lipid phase behaviour was investigated. The data suggest that cholesterol may increase the temperature length of mixed [Lo+Ld] phase in the presence of soluble Aβ. The long temperature boundary of mixed [Lo+Ld] of soluble Aβ in presence of cholesterol may prevent the aggregation of amyloid peptide and this may resemble the biological model data of Cecchi *et al* (2008). But it may need further investigation to examine the toxicity level and aggregation of amyloid peptide in presence of cholesterol

In conclusion, the amyloid beta, $A\beta_{25-35}$ (insoluble form) can reduce the phase transitions temperature with or without cholesterol in DMPC-d_{54} bilayers. KLVFF may reduce phase transition temperature in DMPC-D_{54} and increase the phase transition temperature in presence of cholesterol. At both low and high temperatures, the peptides (KLVFF/$A\beta_{25-35}$/ KLVFF plus $A\beta_{25-35}$) may not exhibit any effects in lipid bilayers with or without cholesterol. The cholesterol molecules may modulate the KLVFF in the lipid bilayers. The data may be important to understand the mechanism and effect of amyloid beta during lipid phase transitions.

4.6 References

1 B. Ramstedt and J.P. Slotte, *Biochimica et Biophysica Acta*, 2006, **1758**, 1945-1956.

2 B. Westerlund and J.P. Slotte, *Biochimica et Biophysica Acta*, 2009, **1788**, 194-201.

3 R.F.M. de Almeida, A. Fedorov and M. Prieto, *Biophysical Journal*, 2003, **85**, 2406-2416.

4 R.E. Brown, *Journal of Cell Science*, 1998, **111**, 1-9.

5 H. Martinez-Seara, T. Rog, M. Karttunen, I. Vattulainen and R. Reigada, *J. Phys. Chem. B.*, 2009, **113**, 8347-8356.

6 N.E. Ziołkowska, R. Christiano and T.C. Walther, *Trends in Cell Biology*, 2012, **22**, 151-158.

7 T.P.W. McMullen, R.N.A.H. Lewis and R.N. McElhaney, *Current Opinion in Colloid and Interface Science*, 2004, **8**, 459–468.

8 P.F. Devaux and R. Morris, *Traffic*, 2004, **5**, 241-246.

9 V. Kiessling, C. Wan and L.K. Tamm, *Biochimica et Biophysica Acta*, 2009, **1788**, 64-71.

10 L.A. Clifton, M.W.A. Skoda, E.L. Daulton, A.V. Hughes, A.P.Le Brun, J.H. Lakey and S.A. Holt, *J R Soc Interface*, 2013, **10**(89), 1-11.

11 C.M. Pfefferkorn, Z. Jiang and J.C. Lee, *Biochim Biophys Acta.*, 2012, **1818**(2), 162-171.

12 J. Huang, *Methods Enzymol*. 2009, **455**, 329-364.

13 K. Simons and W.L.C. Vaz, *Annu. Rev. Biophys. Biomol. Struc.*, 2004. **33**, 269-295.

14 J.C.M. Holthuis, T. Pomorski, R.J. Raggers, H. Sprong and G.V. Meer, *Physiological Reviews*, 2001, **81**, 1689-1723.

15 G.V. Meer, D.R. Voelker and G.W. Feigenson, *Nat Rev Mol Cell Biol*., 2008, **9**(2), 112-124.

16 S. Vijayaraghavalu, C. Peetla, S. Lu and V. Labhasetwar, *Mol Pharm*., 2012, **9**(9), 2730-2742.

17 H. Lodish, A. Berk, L. Zipursky, P. Matsudaira, D. Baltimore, J. Darnell, *Molecular Cell Biology*, 4 ed., W. H. Freeman and Company: New York, 2000.

18 M.C. Mansilla, L.E. Cybulski, D. Albanesi and D. de Mendoza, *Journal of Bacteriology*, 2004, **186**, 6681-6688.

19 A.V Popova and D.K Hincha, *BMC Biophysics*, 2011, **4**, 1-11.

20 E. London and D.A. Brown, *Biochimica et Biophysica Acta*, 2000, **1508**, 182-195.

21 P.J. Quinn and C. Wolf, *Biochimica et Biophysica Acta*, 2009, **1788**, 33-46.

22 M.O. Eze, *Biochemical Education*, 1991, **19**(4), 2004-2008.

23 A. Raudino, M.G.Sarpietro, and M. Pannuzzo, *J Pharm Bioallied Sci*., 2011, **3**(1), 15-38.

24 F. Schmid1, S. Dolezel, O. Lenz, S. Meinhardt, *Journal of Physics Conference Series*, 2014, **487,** 1-13.

25 L.S. Vermeer, B.L. de Groot, V. Reat, A. Milon and J. Czaplicki, -*Eur Biophys J*, 2007, **36**, 919-931.1

26 P.B. Moore, CF. Lopez and M.L. Klein, *Biophysical Journal*, 2001, **81**, 2484-2494.

27 B. Hoff, E. Strandberg, A.S. Ulrich, D.P. Tieleman and C. Posten, *Biophysical Journal*, 2005, **88**, 1818-1827.

28 M.F. Brown, S. Lope-piedrafita, G.V. Martinez and I. Petrache, *Modern Magnetic Resonance*, 2006, **3**, 1-12.

29 M.-A. Sani, D.K. Weber, F. Delaglio, F. Separovic and J.D. Gehman**,** *PeerJ*, 2013, **1**, e30.

30 J.H. Davis, *Biophys*., 1979, **27**, 339-358.

31 T. Barlets, R.S. Lankalapalli, R. Bittman, K. Beyer and M.F. Brown, *J. Am. Chem. Soc*., 2008, **130**, 14521-14532.

32 S.L. Veatch and S.L. Keller, *Biochem. Biophys. Acts*, 2005, **1746**, 172-185.

33 N. Arispe, E. Rojas and H.B. Pollard, *Proc. Nati. Acad. Sci. USA*, 1993, **90**, 567-571.

34 H. Hartmann, A. Eckert and W.E. Muller, *Biochem Biophys Res Commun.*, 1994, **200**(3), 1185-92.

35 W.G. Wood, G.P. Eckert, U. Igbavboa and W.E. Muller, *Biochimica et Biophysica Acta*, 2003, **1610**, 281-290.

36 M. Simons, P. Keller, B. De Strooper, K. Beyreuther, C. G. Dotti, and K. Simons, *Proceedings of the National Academy of Sciences of the United States of America*, 1998, **95** (11) 6460-6464.

37 R. Ehehalt, P. Keller, C. Haass, C. Thiele, and K. Simons, *Journal of Cell Biology*, 2003, **160**,113-123

38 T. Umeda, H. Mori, H. Zheng, and T. Tomiyama, *Journal of Neuroscience Research*, 2010, **88**, 1985-1994.

39 C. Cecchi, F. D. Nichino, M. Zampagni, C. Bernacchioni, E. Evangelisti, A. Pensalfini, G. Liguri, A. Gliozzi, M. Stefani and A. Relini, *Journal of Cellular and Molecular Medicine*, 2008, **12**, 1990-2002.

Chapter 5
Summary

The aim of this project was to investigate the interaction of amyloid beta peptide and lipid bilayers. The amyloid beta and lipid bilayers interaction was examined under NMR spectroscopic methods using DMPC/ DMPC-d_{54} bilayers with or without cholesterol, $A\beta_{25-35}$ and beta breaker peptide, KLVFF. The overall results of this research showed that $A\beta_{25-35}$ in soluble state may interact with phospholipid bilayers. However, $A\beta_{25-35}$ in soluble state may not interact with cholesterol.

Generally, $A\beta_{25-35}$ may adopt non-soluble fibrous structure immediately after the aqueous contact and this form does not produce NMR signals due to its large fibrous structure. After addition of KLVFF, $A\beta_{25-35}$ produces sharp peaks of its residues. The data suggest that KLVFF may hinder the $A\beta_{25-35}$ non-soluble structure. It has been previously reported that KLVFF may be able to break the H-bonding of β-sheet structure of $A\beta_{1-42}$ between 16-20 residues (homology sequence of KLVFF) and thus inhibit the formation of fibrous structure. Based on amyloid beta structure models and the results of this study, KLVFF may also inhibit the fibrous structure of $A\beta_{25-35}$ in two possible ways; (i) by breaking the H-bond of β-sheet structure residues from 32 to 35, (ii) Val(18) and Phe(20) of KLVFF may interact with Ala(27) and Asn(30) of $A\beta_{25-35}$, respectively. MTT-assay data suggest that without KLVFF, $A\beta_{25-35}$ may exhibit the toxic effect on PC12 cell lines.

$A\beta_{25-35}$ has ability to adopt non-soluble structure after contact with lipid environment. The non-soluble structure are large and non-mobile thus it does not generate NMR signals. NOSEY cross-relaxation rate show that $A\beta_{25-35}$ in presence of KLVFF may enter into the bilayers. The soluble form of $A\beta_{25-35}$ may interact predominantly with the phospholipid chain near glycerol region whereas it may not directly interact with cholesterol. The data also suggest that the cholesterol molecules may push the soluble $A\beta_{25-35}$ towards the head region.

The lipid phase behaviour analysis of DMPC-d54 bilayers containing $A\beta_{25-35}$ with or without cholesterol showed that $A\beta_{25-35}$ may cause a significant change to phase behaviour by lowering phase transition temperature. This may happen due to the formation of amyloid non-soluble structure on the surface of lipid bilayers or it may not enter into the lipid bilayers. The $A\beta_{25-35}$ with KLVFF may exhibit almost the same temperature of phase transition as DMPC-d_{54}

bilayers. In presence of cholesterol, $A\beta_{25-35}$ with KLVFF may also cause a significant change in phase transition by raising temperature of phase transition and elongating ranges of phase transition. The data suggest that cholesterol may accelerate the lipid order parameter or it may also push the $A\beta_{25-35}$ (soluble form) towards the surface of lipid bilayers.